Comprehensive Digital Archiving Techniques through High-resolution Imaging System with Line Sensor

Peng WANG

2022

Doctoral Dissertation for the Degree of Doctor of Engineering

Comprehensive Digital Archiving Techniques through High-resolution Imaging System with Line Sensor

by

Peng WANG

Department of Mechanical Engineering and Science

Graduate School of Engineering

Kyoto University

Kyoto, Japan

2022

Abstract

Digital archiving is a storage method or repository of digital material that an individual or organization desire to keep for a longer period of time. With the rapid development of imaging technology, this method is no longer limited to a few scenarios such as library and archives department, but also applied to digital preservation and conservation such as digital archiving of cultural heritage. High resolution imaging technology can provide high quality recording of the object, which enables diverse applications of such high quality images. In this study, attention was paid to taking advantage of the high resolution imaging system to extract as much information as possible, so that the digital archiving of precious artifacts can be more detailed and stereoscopic. This means that the improvement is not only in the visual aspects of the image, but more in providing comprehensive information, including accurate shapes, faithful colors, etc. As the start point of the whole process of digital archiving, image acquisition is the most crucial aspect. To some degree, it is meaningless to conduct any post-processing without a good quality image at first. Hence, emphasis is given to the development and implementation of all image acquisition systems presented in this dissertation.

The first half of this dissertation discussed the basic concept of the development and implementation of high resolution imaging system using a linear sensor-based camera. The current achievements of digital archiving for general applications and scenarios were introduced at first. After that, the reason for developing a comprehensive digital archiving system was clarified, which is also the benefit of using one system to acquire multi-layer information of an object. As mentioned, image acquisition is an important process of digital archiving, so the selection of the imaging related components, including the type of sensor, optical lens, light source and the image processing just after the image acquisition, also need to be considered very carefully. In terms of the imaging mechanism and structure feature, an area sensor-based camera can capture the whole image of the object in one shot, while a linear sensor based-camera can acquire only one image line of the object in one shot. To build up a two-dimensional image of the object, either the camera or object is moved perpendicular to the line of pixels. This might seem like a complicated way to image an object compared with “area sensor-based cameras” that take two-dimensional images. However, for line sensor-based camera, typical sensor resolutions of 512, 1k, 2k, 4k, 8k, and 12k are available for the image acquisition. Moreover, a line sensor-based camera has higher detail of expressiveness and higher spatial resolving capability than an area sensor-based one, which makes it more suitable for resolving fine details of an object. Considering the high fidelity of colorimetric property is required in some applications, the white LED with high efficiency and low heat dissipation are applied as the illumination of the system. And a pre-processing method for eliminating uneven illumination distribution is developed as well. The working mechanism and the prototype of the imaging system introduced here are the base of all the systems presented in later chapters, which can be named as high resolution imaging system using linear imagers. Despite of the objectives of each system or method, the basic concept of imaging mechanism is identical.

The second half of this dissertation is related to the application of high resolution imaging system with linear imager. Three applications with three different objectives were presented and discussed in detail. The first one is ‘spectral reflectance estimation using rotating multi-filter scanning system’. In this application, to develop a more efficient multispectral imaging

system, a concept of rotating filter scanning system is proposed. Compared to the conventional method that needs several scans to acquire relevant multispectral images, the proposed method can acquire the multispectral images with only one scan. Through a series of image processing, the processed images can be used in the estimation of spectral reflectance. An indirect method (learning sample based method) was employed in spectral reflectance estimation. To find the most proper filter combination, a simulation was conducted to optimize the filter selection, so that the accuracy of spectral reflectance estimation can be maximized as much as possible. Based on the experimental results, the accuracy of the estimated spectral reflectance by the proposed method is comparable to the results acquired by the conventional method, especially when efficiency issue is considered.

The second one is ‘color reproduction of glass plate using filter coefficient’. In this application, a method for color reproduction of old glass dry plates digitized by a linear sensor camera is proposed. A high-resolution scanner based on linear sensor camera was developed for digitizing glass plates, which is beneficial for high-quality color reproduction. The color reproduction uses filter coefficient calculated from color information of multiband filters. An approach for the calculation of filter coefficient used for color reproduction is addressed in detail. The method was applied to the digitization and color reproduction of a wall painting belonging to World Cultural Heritage Horyuji Kondo, Japan. A verification experiment is conducted to evaluate the accuracy of color reproduction results. Experimental results show that the proposed method is capable of high-quality color reproduction of image details, and there is merit to using this high-resolution digitization techniques for cultural heritage.

The last one is ‘2.5D surface structure reconstruction method using imaging system with linear sensor'. In this application, a line-sensor camera based photometric stereo method for high-resolution 2.5D surface shape reconstruction is proposed. Compared to using an area sensor-based camera, a line sensor-based one can acquire higher resolution images with less geometric distortion, which can yield more accurate depth map results. A technique for estimating the lighting direction based on such system is addressed in detail for high resolution surface shape reconstruction with improved efficiency. Experimental results yielded reconstructed depth maps comparable with the accuracy of conventional method like a laser ranger. In addition to surface reconstruction, the images acquired are colorimetrically accurate. This means that the method can produce both stereoscopic and spectroscopic information for digitizing cultural heritage with textured surfaces.

The results demonstrated the capability and practicality of the imaging system according to the objectives of each application and showed how effectively to take advantage of the acquired high resolution images by each proposed imaging system. The spectroscopic attributes, faithful color reproduction and 2.5 dimensional data provide more layers of information for digital archiving, which make the recording of precious artifacts more detailed and stereoscopic. This implies the possibility and potential that the results can be widely used in various scenarios, such as education, museum exhibition, etc.

Acknowledgements

First and foremost, I would like to express my sincere gratitude to my supervisors, Prof. Ari Ide-Ektessabi and Prof. Masahiro Hasuo, for their exact guidance and excellent supervision throughout all my career of Ph.D. course. The encouragements and supports are invaluable and significant to me whether in life or academics.

I would like to sincerely thank Dr. Jay Arre Toque, a former member of the Advanced Imaging Laboratory, for his patient direction, heartwarming advice, careful reviewing of all my manuscripts for publication, and great patience and help in my study and experiments throughout the whole duration of my Ph.D. course.

I would also like to thank the other members or former members of the laboratory, especially to Mr. Pengchang Zhang, Mr. Tomoyuki Takeda, Mr. Ryo Ogino, Mr. Takuya Yamaguchi, Mr. Daichi Tsunemichi. I am so grateful for your patience and help in my experiments and daily life.

My sincere appreciation should also go to Ms. Terumi Akasaka and Ms. Mie Kado. I thank you for your kind support and help in every aspect of my daily life, and great patience and help on my Japanese learning.

I would like to thank all my friends in China and Japan who give me spiritual even material support and constant encouragement.

Finally, I would like to express my deepest gratitude to my family: my father, my mother, my grandparents, for their unconditional love, caring and sacrifice for educating and preparing me for my future. Without your support, understanding and encouragement, I would never have the opportunity to come here and accomplish my study.

Inadvertently, for those whom I failed to mention, I would like to apologize, for it is quite impossible to remember all those who offered help and assistance along the way. Nonetheless, I would like to say my sincerest thanks to you.

Table of Contents

Chapter 1

General Introduction

1.1 Digital Archiving and Imaging Technology

Digital archiving has a pivotal role in some target fields such as library, archives department, museum and art gallery, etc. It has been used to maintain the archives of significant items and greatest accomplishments of human history for a long time. The concept and definition of digital archives has been evolved over time, which was referred to either those collection of born-digital records based on activities of people and organization, or the websites that provide access to collections of digitized materials. However, digital heritage and digital collection, such kind of concept have been appeared to make it more diverse[1,2]. Imaging technology, on the other hand, is a key point to bring digital archiving to a higher level. The advances in imaging technology and computing have made it possible to use various method to accomplish digital archiving which was not realistic in the past. So, a huge number of relevant applications based on different intentions have been developed. These applications include but not limited to record appearance, color, and shape of a target object[3-9].

In the past, the most basic task of digital archiving was to digitally archive objects in a convenient and efficient way, so that to make them easy to be accessed and managed[10]. On most occasions, the objects are digitized as a form of image. However, the demands for more precise result of digital archiving have been increased over time. This is not only due to the technological advancement of imaging devices that capable of providing higher quality image, but also the demand of public for high quality archived image. A high quality image refers to an image with high resolution and accurate color, which can benefit for improving visual experience and detail expressiveness. But these improvements are limited to subjective visual perception and aesthetic perspective. And now, numerous methods and applications are dedicated to how to improve image quality further and make use of these images to acquire more information from them. For example, analytical imaging, which is defined as the use of image processing to extract useful information from images by quantifying the interaction between matter and electromagnetic radiation. The applications based on this method have been employed in various fields such as remote sensing, medical imaging, biological imaging and cultural heritage imaging, etc[11,12,13]. The last one that would be mentioned many times in this dissertation, can be used in cultural investigation including material identification, evaluation of painting degradation, cultural heritage conservation. The mentioned usage for cultural heritage implies the feasibility that the digital archives can be presented with not only the images but also multi-level information such as material attributes[14,15]. If an imaging system that is capable of acquiring multiple information is used in digital archiving, the archived results will contain both of the images and the information obtained from corresponding applications.

Since the useful information is extracted from image to fulfil the requirements of applications, the depth and breadth of an application depends on the sophistication of its corresponding imaging system. The three including image acquisition, image processing and data analysis, is

one of the common procedures to determine how an imaging system is used in relevant applications[16]. As the three steps mentioned in order, image acquisition is the first and the most crucial step of all. This step will affect whether the next image processing can be proceeded smoothly, then affect the feasibility and reliability of data analysis. There are two types of image acquisition systems namely, area sensor camera-based image acquisition systems and line sensor camera-based image acquisition systems. The former ones are widely used in commercial imaging products, which cover all lines from high end to low end. Digital single lens reflex camera (DSLR) is a typical product for the high-end line, while mobile phone with camera is an example for the low-end line. Area sensor-based image acquisition system has been widely used in the digital archiving nowadays, and this technique can accomplish the image acquisition work easily and efficiently. Such imaging system offers fairly uniform light distribution, relatively high resolution and relatively accurate color rendering as well. In terms of the imaging mechanism and structure feature, a line sensor-based imaging system has higher detail expressiveness and higher spatial resolving capability than an area sensor-based one, which makes it more suitable for resolving fine details of precious target objects such as cultural heritage[17,18]. In addition, a line sensor- based camera is a better choice for recording color of target objects with higher color fidelity. The most crucial point is that the line sensor-based camera has a less geometrical optic problem for imaging and no issue of pixel interpolation[17,18].

The other two steps are based on the acquired image itself to determine how to process the image and the analysis of related data. So, the initial point of the three steps is how to use image, or what kind of image is needed for application. The first intention comes to mind naturally is visualization, which is one of the conventional applications. But such usage for artistic expression can no longer satisfy the demands in modern times. As the applications based on analytical imaging mentioned in previous, the useful data extracted from images can be used in many different fields. If we summarize and arrange this data, all of them can be categorized into spectral, colorimetric and spatial in nature[19,20].

Multispectral images, generally, can be defined as a series images recording the electromagnetic spectral information at each pixel position of a target object. Such kind of image is widely employed in various applications, such as remote sensing, quality inspection, medical, and digital archiving. An RGB color image can be considered as a typical and simple example of the multispectral image, which contains three channels R, G, B, respectively. If it is observed in some particular software, the image to corresponding channel would show its specific component in grayscale. Compared with this simple example of multispectral images acquired by conventional imaging method, multispectral images contain more spectral information which have higher resolution of spectrum and contain more than three spectral channels. The spectral information included in the multispectral images are very useful in analysis of materials, since materials produce spectral signatures. It is based on a fact found in physics that when an object is irradiated by an electromagnetic source, it behaves in a way that can be predicted and quantified[21]. In other words, spectral reflectance data is an identity card of a material, and this can be used for material analysis easily. In addition, metamerism, a phenomenon where happens to the image acquired in conventional color imaging with different illumination conditions, can be eliminated by using multispectral image instead. Conventionally, for obtaining multispectral images, the method that placing one or a set of selected spectral filters in front of the imaging device offers flexibility and variety of spectral channels can be used. Or some cameras are prebuilt with a specially designed sensor module

for multispectral imaging. But no matter which method is used, the acquisition of a series of multispectral images needs several-time scan, and more time is needed for finding corresponding position. This means that the image acquisition could be more efficient and easier to use.

A variety of technology have been applied to digital archiving. Photography is one of the leading techniques which provides a new frontier to the field of archiving. However, due to the limitation of the technique development in the old days, there was no electronic photosensitive element to form an image digitally yet, then a medium for storing the archived image is needed. The usage of films and glass-based gelatin plates are typical examples for this, but these old techniques can not satisfy the demands for digital archiving today[22]. As mentioned in previous, digital archiving has been widely used in museums. Inevitably, some precious artworks and cultural heritage were archived using those old techniques. In some exceptional scenarios, for an instance, Horyuji Kondo wall painting, which belongs to UNESCO World Heritage Site under the name Buddhist Monuments in the Horyuji Area, was photographed onto a one-to-one scale glass dry plate 85 years ago (1935)[22]. A calamitous fire that broke out later in 1949 which resulted in the severe damage to the wall paintings. It means that these glass-based dry plates are the only documentation material that recorded the original appearance of the wall painting during that time, but no color included. Although the color image of the wall painting can be reproduced using the glass dry plates by a traditional technique with the negative-positive process, the reproducing process which is known as collotype printing is very subjective. Even the retained glass dry plates are digitized by modern imaging technique, the acquired images cannot be directly used to reproduce the color of the wall painting properly. Hence, more attention needs to be paid to find a proper way reproduce the original color of the wall painting. It is more like a process to building a bridge between old technology and new technology. A well-implemented image acquisition system can ensure the image acquisition of the object in high quality. On the other hand, to ensure the reproduced color of the wall painting is systematical and faithful, a color reproduction method can be based on the remaining documentation materials. The method must take advantage of the retained resources and should be verified properly.

3D reconstruction has been gaining increasing interests and demands in digital archiving and many other fields. The digital archival in 3D can produce more stereoscopic information and more vividly visual effects. Various related applications and methods have been developed around the world in the past few decades[23,24]. Generally, laser-based methods and image-based methods are two leading technologies widely used in the 3D reconstruction. The former approach can obtain or measure the dimension of objects with high accuracy but no image color data, low efficiency and high cost, while the latter one is more economical and comes with image color information but a comparatively low accuracy of dimension measurement. Both have merits and drawbacks for corresponding applications, and the practicality of both are also gradually being improved with the development of computing technology. Considering the development trend of digital archiving applications, image-based methods are obviously better choice for providing images and stereoscopic information at the same time. Moreover, various high-precision image acquisition systems and methods have been developed for 2D objects, which can be digitized with high resolution and exceptional color reproduction. However, digital archiving remains a challenging problem for researchers. Especially, when we try to scan a 2.5D object that has complex texture or uneven surface, it is not easy to acquire a result

combined with good-quality image and object's surface shape. In an on-the-site digitization environment, an applicable and efficient imaging system that can acquire high-resolution image with surface information would be very helpful to inspect the quality of digitization work and provide more useful information to related researchers.

1.2 Motivation

The above section has described the early definition of digital archiving and the changes that have occurred over time. Meanwhile, it also pointed out the importance of image acquisition methods according to actual application requirements. As so far, most of the existing image acquisition systems used for digital archiving are using area sensor-based camera. In terms of the imaging mechanism and structure feature, a line sensor-based image acquisition system has less geometrical problem and no issue of pixel interpolation. Since line sensor-based camera has higher detail expressiveness and higher spatial resolving capability, it is more suitable for resolving fine details of the target objects appeared in digital archiving[17]. In addition, it is a better choice for recording color with higher fidelity.

A considerable number of applications and methods has been published on ‘how to utilize and extract useful information from images’, including spectral, colorimetric and spatial information. These studies have greatly facilitated the development of digital archiving. However, this does not ensure that these technologies can be applied to all scenarios properly. As the issue described in previous, the way to acquire multispectral images can be further optimized to become more efficient. And this is under the premise of not affecting the subsequent image processing and data analysis results. The issue of reconstructing the color of the wall painting is an exceptional case, but the problem that encountered in dealing with the objects archived with old techniques is not rare. In the old days, there were not a few objects that use early photography techniques for archiving. These old materials, especially glass dry plates, should be taken seriously. 3D reconstruction related technologies have been well-studied and widely used for digital archiving, but in some subdivisions, there is still space for improvement. Especially, when we try to scan a 2.5D object that has complex texture or uneven surface, it is not easy to acquire a result combined with good-quality image and object's surface shape. Since the 2D images can be acquired by line sensor-based imaging system in high resolution, if surface shape information can be obtained from these images, the results of the digital archiving would be more stereoscopic.

Based on the above, the purpose of this study is to develop a comprehensive imaging system for digital archiving using linear imagers. In terms of the intention of actual applications, the system is capable of acquiring high resolution images, obtaining spectral information, reproducing high fidelity color and reconstructing accurate depth map (2.5D surface shape) results. The results of digital archiving acquired by the system should be faithful and can be used for further applications other than the basic task of digital archiving, such as material analysis, education, exhibition and 2.5D printing for replica.

1.3 Development of Comprehensive Digital Archiving System

As emphasized in previous, image acquisition is the most crucial step of the three steps to develop an imaging system. Since the merits of using line sensor-based camera described in previous, an image acquisition prototype based on line sensor camera is developed and implemented in this study. It is a flat-bed scanner that mainly consists of a line sensor-based camera module, a stepping motor for driving the object stage, a white LED light source for illumination which is well designed for high color fidelity and minimum light irradiation, and a scanner frame structure. Notably, this preliminary model would be the basis for image acquisition system that appear in all applications of this dissertation. In addition to image acquisition, corresponding data extraction and analysis are also two other major tasks of the three steps. In this study, the extractable data based on image processing can be divided into the following three types: spectral, color, and spatial in nature.

For the first type of information, in general, spectral information can be extracted from multispectral images or trichromatic images (i.e., RGB color images). Multispectral imaging offers new frontiers for digital archiving such as heritage preservation and historical research, especially for its capability of analysis and investigation of materials. And a number of multispectral image acquisition systems have been developed for imaging precious artworks. The method that placing one or a set of spectral filters in front of the imaging device offers flexibility and variety of spectral channels that can be used. But the acquisition of a series of multispectral image needs several times scan, and more time is needed for finding corresponding position. To develop a nondestructive and more efficient multispectral image acquisition method, a concept of rotating multi-filter scanning system is introduced in this study. This system is developed from the preliminary model mentioned above. A special multispectral image is acquired by the system using optimized selection of the filters which was simulated and tested in the experiment. This special image contains spectral information of all channels, so the image processing including separation and interpolation is used to recover the single-channel images for each channel. Since the spatial resolving power of the system is verified, the recovered multispectral images can be further used in estimation of spectral reflectance. There are three types of methods to reconstruct or estimate spectral reflectance from multispectral images namely, direct method, interpolation method, and indirect method. The first method is based on the inverse transfer function of the overall spectral sensitivity of the image acquisition system, which is a matrix multiplication of the spectral distribution of the light source, the spectral transmittances of the spectral filters and the spectral sensitivity of the camera sensor. Even it can achieve accurate result of estimation theoretically, the method itself is way more complex to deal with the measurement of spectral characteristics of the system. For the second method, the response of the image acquisition system can be interpolated to find an approximation of the corresponding spectral reflectance factor, and therefore the method is called reconstruction by interpolation. But this method requires more spectral information with more channels compared to the others. Indirect method, which is also known as learning sample-based method. It means that a learning sample is first used to build the transformation relationship between the response of the image acquisition system and spectral reflectance factor, and after that, the response of the image acquisition system of other targets can be transferred into spectral reflectance factor. Based on the discussion above, the indirect method is employed in this study, because it does not require prior knowledge of the spectral

characteristics of image acquisition system. The spectral characteristics of image acquisition system can be estimated by utilizing a learning sample. The learning sample was designed by the Advanced Imaging Technology Laboratory, Kyoto Univ., and it focuses on the pigments commonly used in Japanese artworks. This sample is also employed as a target object used in the experiment. Since the spectral reflectance data of each patch was measured as the reference, the accuracy of the estimation can be evaluated by comparing the estimated data and the reference data.

For the second type of information, color reproduction of a particular object in an exceptional case is presented in this dissertation. The object are four pieces of glass dry plates which recorded a precious wall painting with multiband filters in four colors 85 years ago (1935). These glass dry plates are the only documentation material that recorded the original appearance of the wall painting during that time, but the coating layer is now fragile and sensitive to storage conditions. A calamitous fire that broke out later in 1949 which resulted in the severe damage to the wall paintings. The color image of the wall painting can be reproduced using the glass dry plates by a traditional technique with the negative-positive process though, the recovered image can be highly affected by the procedure of this technique which is very subjective. Considering the storage condition and the concerns above, digital archiving is a better choice for the preservation of this precious cultural heritage. There are three issues that need to be carefully considered to accomplish color reproduction of the wall painting using the glass dry plates: 1) a proper method to accomplish the digitization of the glass dry plates, 2) a proper approach to take advantage of the digital images and the remaining documentation materials, 3) a scientific methos to reproduce the color of the wall painting. To address the first issue, a high-resolution flatbed scanner for digitizing large format transmissive object was designed. The scanner provides wide scanning resolution that ranges from 600-3000 dpi, and it is also capable of high-fidelity color reproduction. Notably, the scanner is also based on the preliminary model mentioned in previous but in a transmissive imaging mode with some adjustments. A monochrome camera is used to scan the glass dry plates with single channel. To obtain uniform transmitted light with the camera, we experimented on the optimum distance between the light source and the object and installed an acrylic resin panel in front of the LEDs. The panel made of acrylic resin served as a diffuser, and the light from the point light source is diffusely scattered between particles in the acrylic resin, so that the light emitted from the panel becomes diffuse light. More details related to the image acquisition is shown in Chapter 4. To address the rest two issues, much attention was paid to develop a color reproduction method utilizing the information of multiband filters, which is a solution to maximize the use of the remaining documentation materials. For high-precision color reproduction, we proposed a method for producing one color image by incorporating the color information of each filter into the multiband images. The color information of the multiband filters is based on the mathematical relationship between the spectral characteristics and different standard color spaces. The RGB information of each filter is used to calculate a parameter named as filter coefficient, which is used in color reproduction together with acquired multiband images. Additionally, a standard IT8.7/2 color chart is captured as a target object to evaluate the accuracy of color reproduction result. As a result, the proposed image acquisition method and color reproduction method complements each other, so that we can obtain high-resolution and color-accurate digital archives.

For the purpose of acquiring the third type of information, this dissertation devotes its

discussion to 2.5D surface shape reconstruction from image. Generally, laser-based methods and image-based methods are two leading technologies widely used in 3D reconstruction for many successful applications, which is also applicable to 2.5D reconstruction. The former approach can obtain or measure the dimension of objects with high accuracy but no image color data included, low efficiency and high cost, while the latter one is more economical and comes with image color information data but a comparatively low accuracy of dimension measurement. With the rapid development in imaging and computing technology, many efforts have been made to address the weakness of the latter one, which make it become more popular in practice. Considering the basic task and more stereoscopic information for digital archiving, image-based method is a better choice to satisfy both needs at the same time. Among the image-based methods, photometric stereo method and stereovision method are widely used in the field. Compared with stereovision method, whose 3D reconstruction accuracy and efficiency still cannot meet the growing requirements, the photometric stereo method is capable of extracting more details of the object surface, and its accuracy depends on the resolution of the acquired image. Since the objective is to rebuild the surface shape of a flat object with slightly textured surface, the photometric stereo method is more appropriate for this study. Based on its imaging mechanism and structure feature, a line sensor-based camera has high detail of expressiveness and high spatial resolving capability, which makes it suitable for resolving fine details of an object. The most crucial point is that the line sensor-based camera has a less geometrical optic problem for imaging. So, based on the discussion above, we employed an image acquisition system that can obtain the object surface shape and color image at the same time by photometric stereo using a line sensor-based camera. This image acquisition system is also developed based on the preliminary model mentioned in previous. In addition, a technique for estimating the light source incident angle based on such system is proposed and verified. A selected reference object can be scanned with the target object at the same time, which makes the whole process of image acquisition more efficient.

The development of this comprehensive imaging system for digital archiving begins with building a basic platform for image acquisition, then making adjustment in terms of the intended applications and applying corresponding image processing, and finally to data extraction and analysis. The preliminary model of the image acquisition system is to ensure the basic task of digital archiving, that is, obtaining high quality images. It is then utilized in three different applications to acquire the information including spectroscopic, colorimetric and spatial, which is the most useful information from images at the visible region. Relevant image processing methods are developed and implemented for extracting information and further analysis. The system developed in this study has potential to be used in a variety of scenarios for digital archiving and makes the digital archives more diverse, faithful, systematic and stereoscopic.

1.4 Dissertation Overview

The goal of this dissertation is to develop a comprehensive digital archiving system or solution that is capable of high resolution image acquisition, multispectral imaging, high color fidelity reconstruction, and 2.5D surface shape reconstruction. Numerous methods and applications have been developed though, in this dissertation, each part of the system mentioned above is

redesigned or optimized for providing more comprehensive result of digital archiving and more efficient way to accomplish digital archiving. Emphasis is also given to the subdivision in some actual applications with practical examples.

This dissertation is divided into six chapters. It concludes that the basic concept of the image acquisition system developed and implemented throughout the dissertation. The applications and methods based on this image acquisition system for acquiring the information including spectral, colorimetric, and spatial in nature are discussed in detail, respectively.

Chapter 1 introduces the concept of digital archiving and its evolution with the development of imaging technology[1,2,25,26]. In terms of the data extracted from images, the difficulties encountered in digital archiving are discussed in detail. Then, the motivation of this study is explained. The key points for developing a comprehensive digital archiving system are addressed. The dissertation overview is given at last.

Chapter 2 explains the image acquisition system used in this study. It is a line sensor-based system and the imaging mechanism explained in this chapter would be a basic concept of all image acquisition system employed in later chapters. Several crucial points of the system including image sensor, shading correction, image noise, and color evaluation, etc. are addressed.

Chapter 3 proposes a new method to acquire multispectral images. Unlike conventional methods that uses filters to obtain the images in multiple scans, a rotating filter is proposed to acquire a special image containing multispectral information, which is much more efficient way for many on-the-site applications. The special image is processed with image separation and interpolation to change into several normal images with corresponding spectral information. Since image interpolation is involved in this process, a verification is conducted to evaluate the interpolated results or the spatial resolving power of the system. The processed images are used in estimation of spectral reflectance. The main method used for estimation is based on pseudoinverse model, which is also known as an indirect method. To acquire the spectral reflectance data with high accuracy, a simulation is conducted for optimizing the filter selection and the number of acquired images. Since a specially designed learning sample with known spectral data is used in the experiment, a comparison between the estimated data and reference data is discussed in detail.

Chapter 4 presents a new color reproduction method combined with a specific application which is an exceptional but not uncommon example in digital archiving. The background of the wall painting and related glass dry plates are addressed at the beginning of this chapter. To reproduce the color of the wall painting, a high-resolution transmission type scanner based on linear sensor camera was developed for digitizing the glass dry plates, then the color reproduction uses filter coefficient calculated from color information of multiband filters. The imaging mechanism of the scanner used in this part, which is based on the concept mentioned in Chapter 2, is addressed. An approach for the calculation of filter coefficient used for color reproduction is discussed in detail. A verification experiment is conducted to evaluate the accuracy of color reproduction results. The method was applied to the digitization and color reproduction of a wall painting belonging to World Cultural Heritage Horyuji Kondo, Japan.

Chapter 5 focuses on a method of 2.5D surface reconstruction for digital archiving. It aims to develop an image-based surface shape reconstruction method, which can rebuild the surface

shape of target objects with high precision and provide more available information for related research and application such as 2.5D printing. A line-sensor camera based photometric stereo method for high-resolution 2.5D surface shape reconstruction is proposed and explained in detail. Compared to using an area sensor-based camera, a line sensor-based one can acquire higher resolution images with less geometric distortion, which can yield more accurate depth map results. A technique for estimating the lighting direction based on such system is addressed for high-resolution surface shape reconstruction with improved efficiency. To evaluate the reconstruction result of the proposed method, a laser ranger was employed as the reference for the accuracy comparison. In addition, an ancient clay tablet containing cuneiform was selected as a test case to demonstrate that it is possible to use the acquired data in various application scenarios.

Chapter 6 discusses concluding remarks and directions of future works. In this chapter, the achievements that we have made and presented in this dissertation are summarized. A line sensor camera-based imaging system is developed and applied as a basic concept to the other three applications. And a series of image processing and analysis methods are also summarized according to the relevant applications. It can be expected that the research results and achievements accomplished in this dissertation could become an effective and indispensable solution for digital archiving.

1.5 References

1) T. Koga: "A Review on Diversification of Digital Archives: Based on Comparison of Concepts between Japan and Other Countries", Research of Art·Documentation, 24, pp. 70-84 (2017)

2) T. Koga: "Overview: How to comprehend archives: A review from Japan (<Special feature>Current states of the Archives in Japan)", Information Science and Technology Association, 62, 10, pp. 408-414 (2012)

3) H. L. Shen, J. H. Xin, and S. J. Shao: " Improved Reflectance Reconstruction for Multispectral Imaging by Combining Different Techniques ", Optics Express, 15, 9, pp. 5531-5536 (2007)

4) H. L. Shen, P. Q. Cai, S. J. Shao, and J. H. Xin: "Reflectance Reconstruction for Multispectral Imaging by Adaptive Wiener Estimation", Optics Express, 15, 23, pp. 15545-15554 (2007)

5) H. L. Shen, H. G. Zhang, S. J. Shao, and J. H. Xin: "Chromaticity-based Separation of Reflection Components in a Single Image", Pattern Recognition, 41, 8, pp. 2461-2469 (2008)

6) H. L. Shen, C. W. Weng, H. J. Wan, and J. H. Xin: "Correcting Cross-media Instrument Metamerism for Reflectance Estimation in Multispectral Imaging", Journal of the Optical Society of America A, 28, 4, 511-516 (2011)

7) Y. Cheng, H. L. Shen, and X. Du: "Robust Surface Reconstruction from Gradient Fields",

Electronics Letters, 48, 7, pp. 375-376 (2012)

8) T. Q. Han, Y. Cheng, H. L. Shen, and X. Du: “Robust Photometric Stereo using Structural Light Sources”, Journal of Electronic Imaging, 23, 3, article 033004 (2014)

9) H. L. Shen, T. Q. Han, and C. Li: “Efficient Photometric Stereo using Kernel Regression”, IEEE Transactions on Image Processing (TIP), 26, 1, pp. 439-451 (2017)

10) The University of Edinburgh: “Digital Archives and Preservation > What is the Digital Archive service?”, https://www.ed.ac.uk/information-services/library-museum-gallery/crc/digital-archives-and-preservation/what-is-the-university-s-digital-archive-service, accessed 01/10/2021

11) P. D. Heermann and N Khazenie: “Classification of Multispectral Remote Sensing Data using a Back-propagation Neural Network”, IEEE Transection on Geoscience and Remote Sensing, 30, 1, pp. 81-88 (1992)

12) K. M. Pohl, J. Fisher, J. J. Levitt, M. E. Shenton, R. Kikinis, W. Eric L. Grimson, and W. M. Wells: “A Unifying Approach to Registration, Segmentation, and Intensity Correction”, Medical Image Computing and Computer-Assisted Intervention – MICCAI 2005. MICCAI 2005. Lecture Notes in Computer Science, 3749, pp. 310-318 (2005)

13) R. Bellucci, P. L. Carcagni, A. D. Patrib, R. Fontanc, C. Frosinini, M. C. Gambino, M. Greco, M. Mastroianni, M. Materazzi, E. Pampaloni, L. Pezzati, R. Piccolo and P. Poggi: “Integration of Image Data from 2D and 3D Optical Techniques for Painting Conservation Applications”, The Imaging Science Journal, 55, 2, pp. 80-89 (2013)

14) I. El-Rifai, E. Hagar, M. Hend, Y. Bebars, and A. Ide-Ektessabi: "Artwork digitization and investigation a case study of the loom weaver oil painting by Hosni el-Bannani.", Mediterranean Archaeology and Archaeometry, 13, 2, pp. 21-29 (2013)

15) J. A. Toque, P. Zhang, P. Wang, and, and A. Ide-Ektessabi: “High-Resolution Multispectral Scanning for Mesoscopic Investigation of Discoloration of Traditional Japanese Pigments”, Computational Color Imaging. CCIW 2015. Lecture Notes in Computer Science, 9016, pp. 195-207 (Feb. 2015)

16) J. A. Toque: “Material Investigation through High-resolution Analytical Imaging and Spectrometry” (Doctoral Degree Thesis), Kyoto University, 2013

17) J. A. Toque, Y. Sakatoku, A. Ide-Ektessabi: "Analytical Imaging of Cultural Heritage Paintings Using Digitally Archived Images", Computer Vision and Image Analysis of Art, 7531, pp.75310N (Feb. 2010)

18) J. A. Toque, Y. Murayama, Y. Matsumoto, A. Ide-Ektessabi: "Polarized Light Scanning for Cultural Heritage Investigation", Computer Vision and Image Analysis of Art II, 7869, pp.78690N (Mar. 2011)

19) M. López-Álvarez, J. Hernández-Andrés, E. Valero, and J. Romero: "Selecting algorithms, sensors, and linear bases for optimum spectral recovery of skylight", J. Opt. Soc. Am. A 24, 942-956 (2007)

20) N. Shimano: “Optimization of Spectral Sensitivities with Gaussian Distribution Functions

for a Color Image Acquisition Device in the Presence of Noise", Optical Engineering, 45, 1, 013201 (2006)

21) J. A. Toque, Y. Sakatoku, J. Anders, Y. Murayama, and A. Ide-Ektessabi: "MULTISPECTRAL IMAGING - The Influence of Lighting Condition on Spectral Reflectance Reconstruction and Image Stitching of Traditional Japanese Paintings", Proceedings of IMAGAPP 2009 – International Conference on Imaging Theory and Applications, pp. 13-20 (2009)

22) S. Nishimura: "Photography of Cultural assets - A Century of Photographs by Benrido -", Jpn. Photographic Soc., J75, pp.489-492 (2012)

23) I. Aicardi, F. Chiabrando, A. M. Lingua, F. Noardo: "Recent Trends in Cultural Heritage 3D Survey: The Photogrammetric Computer Vision Approach", Journal of Cultural Heritage, 32, pp. 257-266 (2018)

24) M. Daneshmand, A. Helmi, E. Avots, F. Noroozi, F. Alisinanoglu, H. S. Arslan, J. Gorbova, R. E. Haamer, C. Ozcinar, G. Anbarjafari: "3D Scanning: A Comprehensive Survey", Computer Vision and Pattern Recognition (cs.CV), arXiv, 1801.08863

25) Y. Lusenet: "Tending the garden or harvesting the fields: digital preservation and the UNESCO charter on the preservation of the digital heritage", Library Trends, 56, pp.164-182 (2007)

26) C. Karp: "Digital Heritage in Digital Museums", Museum International, 66, pp.157-162 (2014)

Chapter 2

High Resolution Imaging System

2.1 Introduction

Imaging technology always plays a significant role in various fields. And increasing number of related applications have been developed and employed in such as medical analysis, remote sensing, digital archiving in recent decades[1-3]. Especially, in the field of digital archiving for cultural heritage preservation and historical research, various methods that can accurately record the information of the research object, including its shape, color, and spectral attributes. However, there is always a conflict between conservation and investigation. For instance, a conservator wants to preserve the integrity of the object by minimizing its exposure to damaging conditions such as prolonged exposure to uncontrolled humidity and temperature as well as unsafe ambient light, while an investigator could become overzealous in documenting and acquiring as much information as possible without so much regard on the integrity of the object. Therefore, there is a need for an accurate but safe technique to archive such precious object with information as much as possible and allow the investigators to have a deep sight of it. On the other hand, the demands for image quality are called from various practices. As emphasized in previous, image acquisition is significant part of any imaging system. It is meaningless to conduct any image processing technique without an image good enough. The data extracted from the images would also become unreliable. A line sensor-based imaging system and its imaging mechanism is explained in this chapter, which is also a basis of all image acquisition system employed in later chapters. Several crucial points involved in image acquisition are also addressed.

2.2 Image Sensor

2.2.1 Type of Image Sensor

In terms of the image sensor type, imaging devices can be classified into charged-coupled display (CCD) based device and complimentary metal-oxide-semiconductor (CMOS) based device. In a CCD image sensor, pixels are represented by p-doped MOS capacitors[4]. These capacitors are biased above the threshold for inversion when image acquisition begins, allowing the conversion of incoming photons into electron charges at the semiconductor-oxide interface; the CCD is then used to read out these charges and transfer the charges sequentially to voltage. CCD image sensors are widely used in professional, medical, and scientific applications where high-quality image data is required. In applications with less exacting quality demands, such as consumer and professional digital cameras, active pixel sensors (CMOS) are generally used. In a CMOS imager sensor, the charge-to-voltage conversion takes place in each pixel, which offers better responsivity but higher image noise[5-7]. However, CMOS has also made

considerable progress in recent years, which results that not only for low-cost imaging markets but also for many high performances applications including high-end digital still photography, high-definition television and even several space applications. In fact, both mainstream techniques have merits but also lacking maturity in some aspect. But in recent years, the performance gap between the two types of sensors has been narrowing and many efforts have been made to address the weaknesses of both. It is important to consider what exact application would be involved when choosing a type of image sensor and to know that not the more expensive the better.

2.2.2 Color Sensor and Monochrome Sensor

According to the mechanism of imaging, virtually every digital sensor works by capturing light in an array of photo sites, and it is similar to how a grid of buckets would store falling rain drops. When the exposure begins, each photo site is uncovered to collect incoming light. When the exposure ends, the occupancy of each photo site is read as an electrical signal, which is then quantified and stored as a numerical value in an image file.

For color sensors (generally, RGB color sensors), these work by capturing only one of several primary colors at each photo site in an alternating pattern, using a mechanism called "color filter array" (CFA)[8]. For an instance, in area sensor based-color camera, the most widespread and successful CFA has been the Bayer pattern, which uses alternating rows of red-green and green-blue filters: A necessary but undesirable side-effect of CFA's is that each pixel effectively captures only one third of incoming light, since any color not matching the pattern is filtered out. (Fig. 2.1(a)) Any red or blue light that hits a green pixel will not be recorded. The CFA also means that at any given photo site position location, one color will be measured directly and the other two will have to be inferred. This process of intelligently combining photo sites to produce full color pixels is referred to as "demosaicing" and happens during RAW image development[8]. However, this is also a factor to affect the image quality when using an area sensor based-color camera.

In the contrast to color sensor, monochrome sensors capture all incoming light at each pixel and regardless color. Each pixel therefore receives three times more light, since red, green and blue are all absorbed. (Fig. 2.1(b)) This translates into a 1-1.5 stop improvement in light sensitivity, and that is why the standard or default ISO speed of monochrome sensor is higher than color sensor. This can also improve the appearance of noise when shooting under artificial light or other color temperatures which differ substantially from daylight.

Furthermore, monochrome sensors also do not require demosaicing to create the final image-the values recorded at each photo site effectively just become the values at each pixel[9]. As a result, monochrome sensors are able to achieve a slightly higher resolution. So monochrome camera sensors are capable of higher detail expressiveness and sensitivity than would otherwise be possible with color. The features of each type of sensors mentioned above may seem to be merits and demerits though, the choice of image sensor highly depends on the intended application.

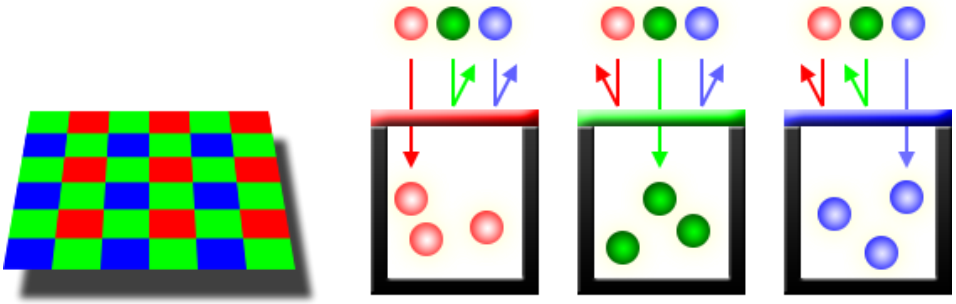

(a)

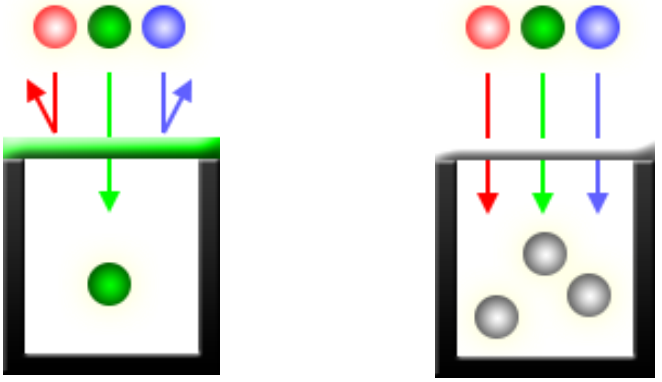

Color photosite (less light) Monochrome photosite (more light)

(b)

Fig. 2.1 Comparison of color photosite and monochrome photosite.

2.2.3 Line Sensor Based-Camera and Area Sensor Based-Camera

According to the image acquisition, scan camera can be classified into line sensor-based camera and area sensor-based camera[10,11]. A line sensor-based camera has a single line of pixels that can form an image line in fast succession. To build up a two-dimensional image of an object, either the camera or object is moved perpendicularly to the line of pixels. (Fig. 2.2(b)) This might seem like a complicated way to image an object compared with area sensor-based camera that take two-dimensional images with only one shot as shown in Fig. 2.2(a). However, for line sensor-based camera, typical sensor resolutions of 512, 1k, 2k, 4k, 8k, and 12k are available for the image acquisition. Line sensor-based camera is widely employed in applications which need to image an object with high resolution and high quality such as important documents and photos, while area sensor-based camera is well known for its widely usage in digital cameras and mobile phones, etc.

As mentioned in previous, for an area sensor-based color camera, the demosaicing process is conducted when an image is converted from the Bayer pattern to an image with full color pixels. It means that the process is to interpolate two missing color values of each image pixel. However, once the interpolation is involved in the imaging stage, the image quality would be

affected by the accuracy of the interpolation method used for it. Compared with an area sensor-based color camera, a line sensor-based one has no issue of pixel interpolation in accordance with its sensor arrangement. It has three independent image sensor arrays in three colors as shown in Fig. 2.2(b). Such constructional feature enables a line sensor-based imaging system has higher detail expressiveness and higher spatial resolving capability than an area sensor-based one, which makes it more suitable for resolving fine details of precious target objects such as cultural heritage. In addition, a line sensor- based camera is a better choice for recording color of target objects with higher color fidelity. The most crucial point is that the line sensor-based camera has a less geometrical optic problem for imaging and no issue of pixel interpolation.

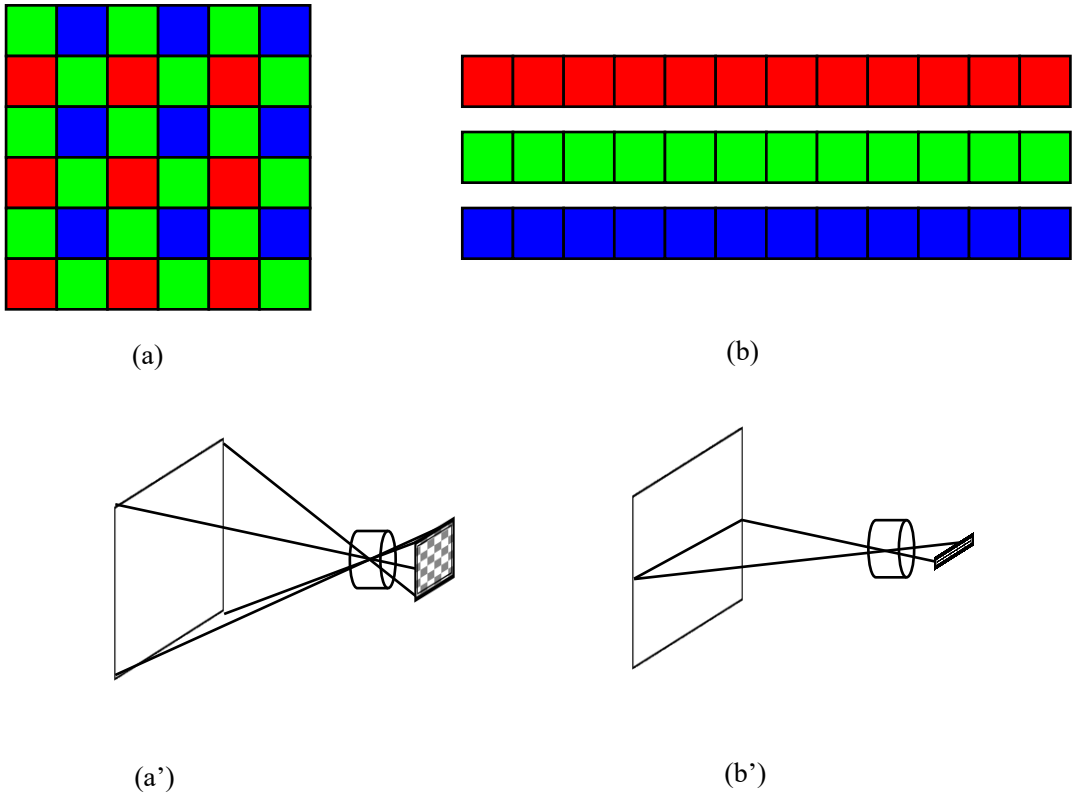

Fig 2.2 Basic concept diagram of two types of image sensor and corresponding imaging mechanism. (a) and (a') gives arrangement of pixel array in an area sensor based camera and corresponding imaging mechanism, respectively; (b) and (b') gives arrangement of pixel array in a line sensor based camera and corresponding imaging mechanism, respectively.

2.3 Line Sensor-Based High-resolution Imaging System

In Fig. 2.3, it presents a schematic representation of line sensor-based high resolution image acquisition system. The system is mainly compromised of line sensor-based camera with lens and light source. Since line sensor-based camera could only obtain one image in line shape within one capture, the whole image is obtained by sequential captures with moving the camera in the direction perpendicular to the image sensor of the camera. Such process of image acquisition using a line sensor-based camera is referred to image scanning. Therefore, a

mechanical structure for moving the camera to complete scan is usually included in the components of the system. Mechanical linear guides are commonly used to build the structure, and stepping motor is a better choice for implementing the motion of camera since it is capable of precise control of speed and position for the motion. The design of the mechanical structure makes it mechanically stable and vibration-free. In addition, this design could be very flexible to be modified according to different applications and specific requirements of image acquisition. White LED is employed as the light source used for illumination. Compared to some conventional light source commonly used in digital archiving and exhibition such as fluorescent and halogen lamps, white LED has better performance on lower energy dissipation, lower heat generation, light wight, more controllable spectra, and more durable. These merits are very important to the system and its application in digital archiving[12-14].

The proposed image acquisition system and its imaging mechanism are the preliminary model and basis for the image acquisition system that would appear in all applications in this dissertation. Depending on the application requirements, the system is capable of scanning RGB color images and monochromatic images with high resolution. In accordance with the type of target objects, the system can be adjusted to deal with both reflective and transmissive objects. For an instance, to acquire the multispectral images with the proposed method presented in the next chapter, a trichromatic camera is employed, and a specially designed combination of filters is equipped to the system. All the adjustments for the image acquisition corresponding to the intended applications would be discussed in detail in later chapters.

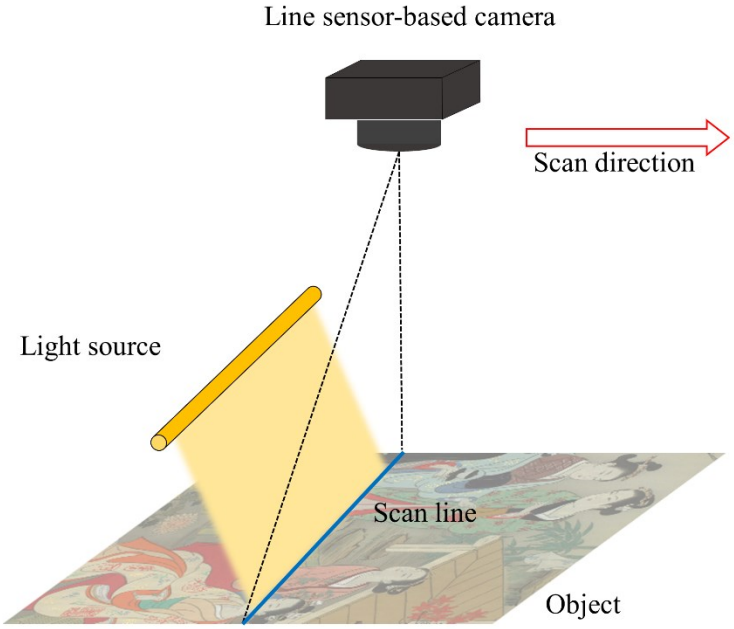

Fig 2.3 Schematic representation of line sensor-based high resolution image acquisition system

When speaking of high-resolution image or high-quality image, resolution is one of the most common criteria used to measure image clarity or quality. It is also a point where most controversy occurs. It is unreasonable to evaluate or define the precision of an imaging system

only by the level of resolution in isolation from the actual application requirements and imaging condition. In this study, this technical term refers to physical size of the smallest feature that the image system can recognize or decern. Or in other words, it can show the resolving power of the imaging system. As mentioned in previous, the image system introduced in this dissertation refers to line sensor-based scanner according to its imaging mechanism. The unit of measurement for resolution is the Dot Per Inch (dpi). For example, a resolution of 600DPI denotes that 600 pixels are used to reveal the object of physical length of one inch and thus one pixel in the image represents the information from a physical size of approximate 43 μm. The higher the resolution, the more details the image can reveal. The standard resolution setting for image acquisition by the proposed scanner ranges from 300-3000dpi. Theoretically, with all image acquisition settings in the correct order, higher resolution means more detail and finer imaging results. In terms of the intended application, the resolution can be changed beyond 3000dpi by adjusting or exchanging the lens and other relevant parameters of the scanner. As explained in the previous section, line sensor camera does not involve pixel interpolation in accordance with the arrangement of sensor elements, which is particularly beneficial when the acquired images are used for spectral reconstruction, color reduction and extraction of spatial information. The line sensor-based scanner proposed in this study has good compatibility with objects of different sizes, such as those of several meters in dimensions. Another important requirement for most applications of digital archiving is whether it is non-contact or non-destructive. For most commercial scanners, it is difficult to find a balance between high resolution, non-contact scanning requirements, and large object size. Especially, some of them designed for large objects generally require contact scanning which is highly unacceptable in some cases of digital archiving.

There is another technical term known as optical resolution, which is also used to evaluate the ability of an imaging system to reproduce object detail[25-27]. It is described as a frequency, measured in line pairs per millimeter [lp/mm]. A line pair is a pair of black and white lines in object space. For a given imaging system, lens resolution is not absolute. At a given resolution setting, the ability to observe the two lines as separate entities will be dependent on greyscale level. A system can more easily resolve a line pair if the difference in the greyscales of the line pairs between them is greater. This greyscale difference is known as contrast. Optical resolution is thus defined as a spatial frequency, given in [lp/mm], at which a specific contrast is achieved. To calculate the optical resolution of an imaging system, the exact size of the sensor element used in the device is needed. By starting with the sensor, it is easier to know the lens performance required in the system or other application requirements. The highest frequency resolvable by a sensor, the Nyquist frequency, is effectively two pixels or one line pair[26]. For a given image sensor, the maximum optical resolution of the imaging system ε based on this image sensor can be calculated by multiplying the size of the sensor element s, usually in units of microns, by 2 (to create a line pair), and then dividing that into 1000 to convert to millimeter(Eq. 2.1).

$$\varepsilon[\mathrm{lp/mm}] = \left(\frac{1}{2 \times s}\right) \times \left(\frac{1000\mu\mathrm{m}}{1\mathrm{mm}}\right) \tag{2.1}$$

Taking the image sensor used in the next experiment as an example, it is a line sensor based color camera (TLC-16K5CL), and the exact size of sensor element is 5.0μm. According to the formula shown in Eq. 2.1, the maximum optical resolution of the imaging system can be calculated as 100[lp/mm]. It indicates that, ideally, this is the maximum optical resolution

value that can be achieved with this camera, or the imaging system based on it. Each line pair would require two pixels, and one inch equals to 25.4mm, thus the maximum optical resolution can be converted to 5080dpi. As for lenses, every lens has performance limit settled by the laws of physics and the Airy disk, known as diffraction limit[28,29]. This limit indicates the theoretical maximum resolving power of the lens given in [lp/mm]. The diffraction-limited resolution[30] ξ, which is referred to the cutoff frequency of a lens, can be calculated using the F/# of lens and the wavelength of light λ as shown in the following equation:

$$\xi[\mathrm{lp/mm}] = \left(\frac{1}{\mathrm{F/\#} \times \lambda}\right) \times \left(\frac{1000\mu\mathrm{m}}{1\mathrm{mm}}\right) \tag{2.2}$$

The lens would be incapable of resolving greater frequencies if the diffraction limit is reached. For a given lens, the diffraction-limited resolution at F/16 for 500nm light (green light) can be calculated as 125[lp/mm] corresponding to 6350dpi. However, all the above are theoretical values without accounting for other factors. In real-world imaging, since the application requirements are different from one to another, the choice of lens and the setting of lens including aperture, working distance etc. would be changed correspondingly. So, as mentioned in previous, the unit of measurement for resolution used in this study is the Dot Per Inch (dpi), which presents the actual precision of an imaging system in image acquisition.

Scanning small-size object at high resolutions is not difficult for most existing high-end commercial scanners. However, for some on-the-site application scenarios in digital archiving for cultural heritage, these commercial scanners are limited by size conditions to accomplish the scanning. Even if the scanning can be done in steps, it still requires multiple image stitching, which also increase the error caused by stitching. To address the above issue, a line sensor-based scanner developed and designed in the lab is taken as an example to further investigate the quality of scanned images in terms of focus and geometric distortion specifically. To obtain a wider scanning width as much as possible, all experimental parameters were set for relatively low resolution scanning from 200-500dpi approximately. A total of four different resolution settings were tested with the same working distance. Correspondingly, four combinations of lens and extension tubes were used to achieve different resolution settings. Table 2.1 shows the four groups of experimental parameters used in this experiment. For better understanding, the unit of [µm/pixel] is used to describe that how one pixel in the image represents the information from a physical size of an object. Different lenses mainly refer to lenses with different focal lengths and aperture opening. Fundamentally, F/# is the ratio of the focal length of the lens to the effective aperture diameter, so the constant F/# can be achieved by maintaining this ratio with different focal lengths and effective aperture diameters. Based on the parameters, two set of experiments were conducted. The first set of experiment had no relative position adjustment of the object and the imaging system, while the second set experiment was adjusted with the level of the camera, the axial rotation of the camera and the position of the object with respect to the scanner.

The experimental set-up is shown in Fig. 2.4. The scanner manly consists of a camera module including a line sensor-based camera and a lens, a light source, and a scanner frame. In general, it is hardly to find such a scanner with a huge frame in commercial scanners, and this frame design is used to optimize the scanner to increase its working distance up to 1688mm. The increasement of the working distance helps the scanner obtain larger coverage of scanning width. The largest scanning width achieved in this experiment was approximately 2000 mm. Considering the limitation scanning length in vertical direction, the maximum size of the object

available for one scan with the scanner is about 2000 by 2000 mm. If the object size is even much larger than this maximum size, multiple scans can be performed in conjunction with the use of slide guides, and the scanned images can be finally stitched together to obtain a larger scan size. But as far as the current situation is concerned, it is rare for a single scan to cover a scanning range of 2000 by 2000 mm. The lowest image resolution achieved in this experiment was 200 dpi using the combination of 60mm lens and 10mm extension tube. The experimental results including shading correction, geometric distortion correction and color calibration would be discussed in later subsections.

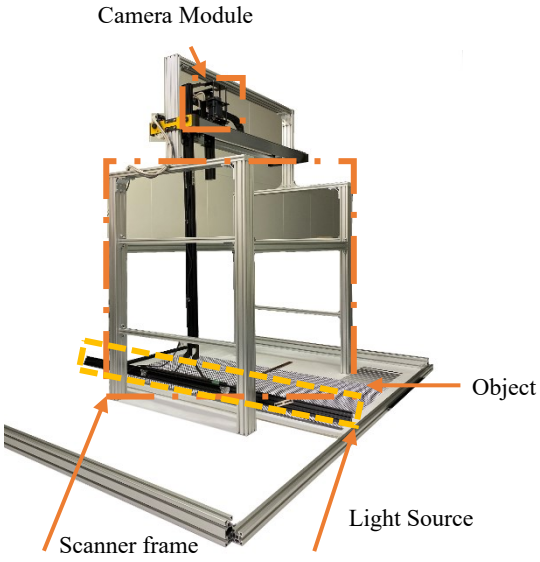

(a)

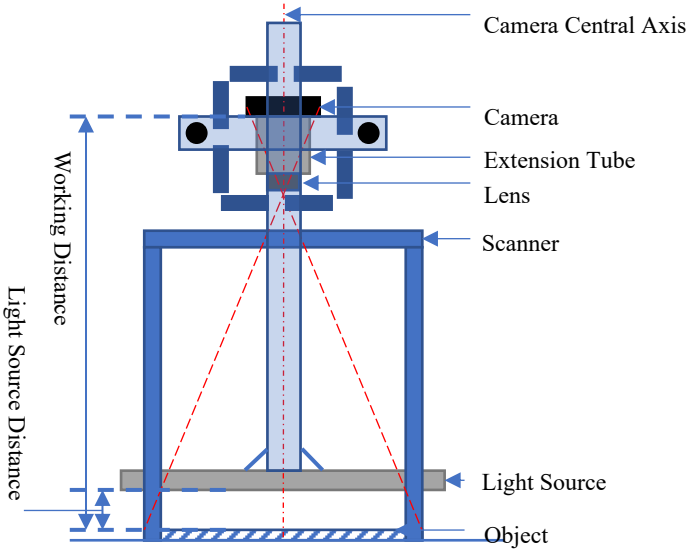

(b)

Fig 2.4 Line sensor-based scanner for image acquisition of large target object. (a) is the photograph of the actual experimental set-up; (b) shows a schematic diagram of the scanner.

Table 2.1 Four groups of experimental parameters used for different resolution settings.

Parameters	Expt. 1	Expt. 2	Expt. 3	Expt. 4
Resolution (dpi)	200	279	361	493
μm/pixel	127	91	70	51
Lens F/#	16	16	16	16
Focal Length of Lens (mm)	60	80	105	135
Effective Aperture Diameter(mm)	3.8	5	6.6	8.4
Extension Tube (mm)	10	20	50	90
Working Distance (mm)	1688	1688	1688	1688
Light Source Distance (mm)	130	130	130	130
Scanning Speed (mm/s)	5.08	3.64	2.81	2.06
CC_cycle	250000	250000	250000	250000
CC_width	10000	10000	10000	10000

2.3.1 Shading Correction

For an ideal condition, when a uniform object is captured by an imaging device with a uniformed light source, the output of each sensor element of the device should have the same value. However, the light arriving at the sensor element is not ideally uniform and even. Despite the cases that device manufactures may add some function to make the output of each sensor element same, the reason for this is partially due to the variations in the pixel-to-pixel sensitivity of the sensor, and partially due to the distortions in the optics including the artifacts from the lens and the illumination, even the weakening of light intensity. Basically, shading is defined as the unevenness of light distribution in the image. The method by which images are produced - the interaction between objects in real space, the illumination, and the camera--frequently leads to situations where the image exhibits significant shading across the field-of-view. In some cases, the image might be bright in the center and decrease in brightness as one goes to the edge of the field-of-view. In other cases, the image might be darker on the left side and lighter on the right side[15]. The shading might be caused by non-uniform illumination, non-uniform camera sensitivity, or even dirt and dust on glass (lens) surfaces. In general, this shading effect is undesirable. Eliminating it is frequently necessary for subsequent processing and especially when image analysis or image understanding is the final goal[16].

In practice, when a relatively small object is scanned with a low-resolution setting, the distribution is not so critical since the human eyes are not that sensitive to the difference in light balance. In contrast, when a relatively big object is scanned with a high-resolution setting, especially it has color surface and multi-features or texture, even small difference would be highly noticeable.

Under ideal illumination states that all relative parameters are well calibrated, the recorded brightness of the image should be same at all pixel position. But the fact is not that ideal, the shading phenomenon happens. The purpose of shading correction is to ensure image uniformity regardless of exposure. This correction can be conducted by adjusting the brightness level in reference to a white standard. The white standard needs to be taken and the target value for the white standard needs to be assumed which is usually set to a value between 220 and 240. The

relationship between the intensity of the illumination and the pixel value of the image at the position (x, y) can be described by Eq. 2.3:

$$p(x,y) = I_L(x,y) \cdot c(x,y) \tag{2.3}$$

$$c(x,y) = \begin{cases} r(x,y) \\ 10^{-OD(x,y)} \end{cases} \tag{2.4}$$

Where,

(x, y): Pixel position on the image

$p(x, y)$: Observed pixel value of the image

$I_L(x, y)$: Intensity of the lightsource

$OD(x, y)$: Optical density

$r(x, y)$: Reflectance

$10^{-OD(x,y)}$: Absorbance

Then the relationship between the light intensity and spatial distribution can be described as (Eq. 2.5):

$$p'_T(x,y) = \sigma_S \cdot p_T(x,y) \tag{2.5}$$

$$\sigma_S = \frac{S_L}{p_W(x,y)} \tag{2.6}$$

$$\Longrightarrow p'_T(x,y) = \frac{S_L}{p_W(x,y)} \cdot p_T(x,y) \tag{2.7}$$

Where,

$p_T(x, y)$: Pixel value of the target at position (x, y)

$p'_T(x, y)$: Shaded pixel value of the target at position (x, y)

$p_W(x, y)$: Pixel value of the white standard at position (x, y)

σ_S: Shading correction coefficient

S_L: Shading level

Eq. 2.5 shows that the shading in the image can be corrected by multiplying a shading correction coefficient σ_S, which based on the reference white standard acquired by the same scanning system. The S_L in Eq. 2.6 is referred to adjustable shading value, and it can be based on the maximum pixel value across the white standard or the average of the pixel value.

Fig. 2.5 shows the comparison of the images before and after shading correction. In Fig. 2.5(a), significant unevenness of the light distribution can be observed. The closer the image is to the edge in the horizontal direction, the more noticeable the shadowing phenomenon becomes. And with the increase of image resolution, this phenomenon has a tendency to gradually diminish on the images scanned in the preliminary experiment, but it still exists as shown in Fig.2.5(d). This is because the higher resolution setting has narrower scanning width, which means that

the image edge is closer to the center of the camera lens. On the other hand, the corrected images have had the shading phenomenon removed and the light distribution on the images are distributed evenly.

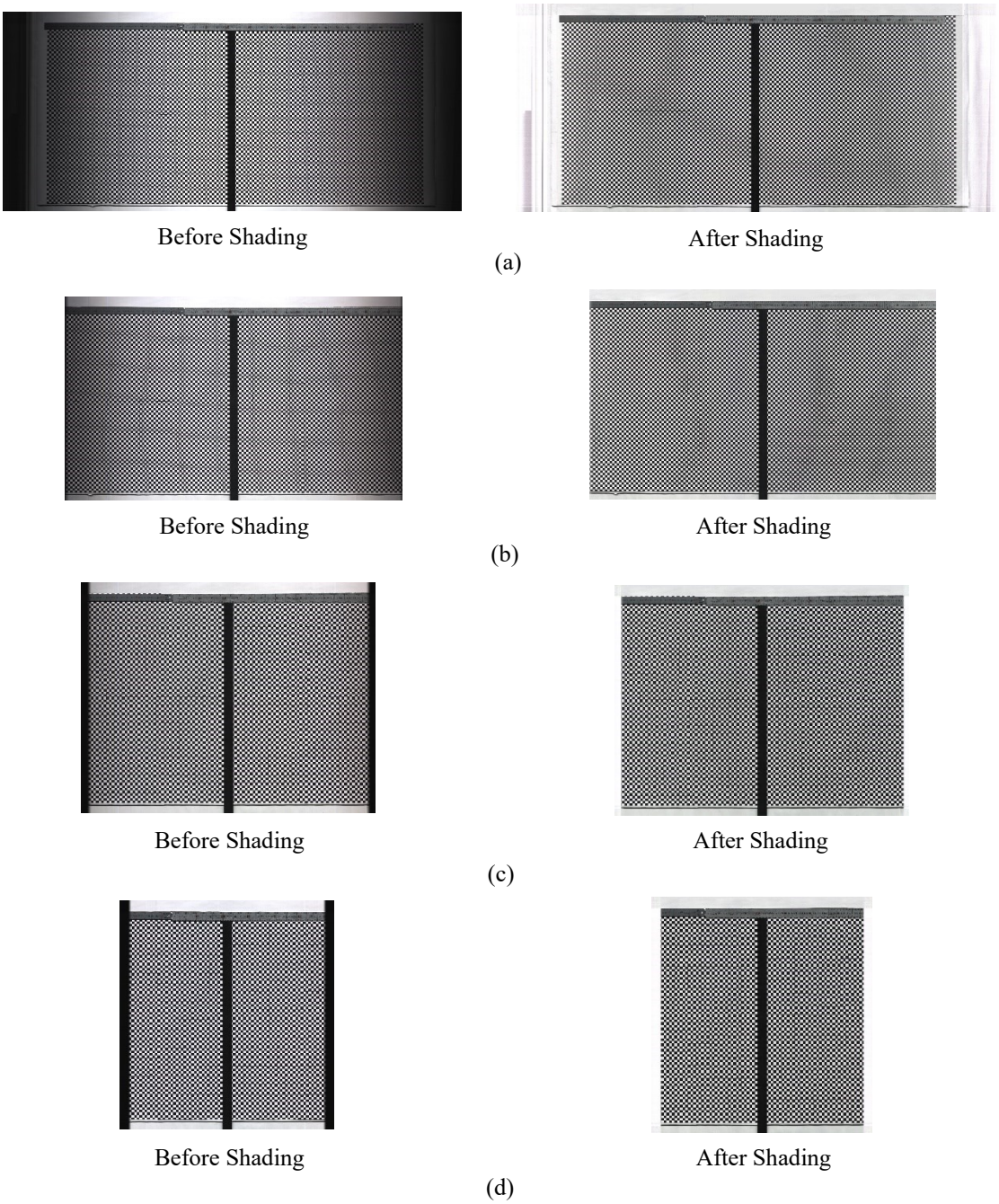

Fig 2.5 Comparison of the images scanned with different resolution settings before and after shading correction. (a) shows the images scanned with the experimental parameters 1 at 200dpi; (b) shows the images scanned with the experimental parameters 2 at 279dpi; (c) shows the images scanned with the experimental parameters 3 at 361dpi; (d) shows the images scanned with the experimental parameters 4 at 493dpi, respectively. This comparison is mainly used to show the effectiveness of the shading correction.

2.3.2 Evaluation of Geometric Distortion

Image geometric distortion usually occurs when the straight line of an image appears to be deformed or curved. This phenomenon happens to every imaging system with optical lens. It is a form of optical aberration. A test chart with a black and white checkered pattern and several scales were used for test scanning and assist in evaluating the distortion of the scanned images.

As mentioned in previous, a total of four groups of experimental parameters were tested in this experiment, which used different combinations of lens and extension tubes to achieve different resolutions. The experiment was conducted twice as two sets. The first set was a preliminary experiment without adjustment, while the second set was conducted by adjusting camera axial rotation, camera level, and the position of the object with respect to the scanner.

In the experiment, it was found that without the adjustments, significant positional distortion was found in the vertical direction of the image with range from 10.4 to 11.7mm, while the horizontal direction was minimal distortion. After adjusting camera axial rotation, camera level, and the position of the object with respect to the scanner, minimal distortion can be found on the scanned images. However, if the images after adjustment are observed very carefully, there are still some defective parts on the edge of the images. This is caused by an overly wide scan width.

To further investigate the distortion of the adjusted images, the test chart and the scales were used to assist in evaluating the distortion. The number of pixels of some selected checked pattern was counted in each 1cm in both horizontal and vertical direction of the images. Fig. 2.6 shows these selected checked pattern used as samples in the calculation. The position of these samples in the images are the central axis in the horizontal and vertical directions, and only complete checked patterns are selected.

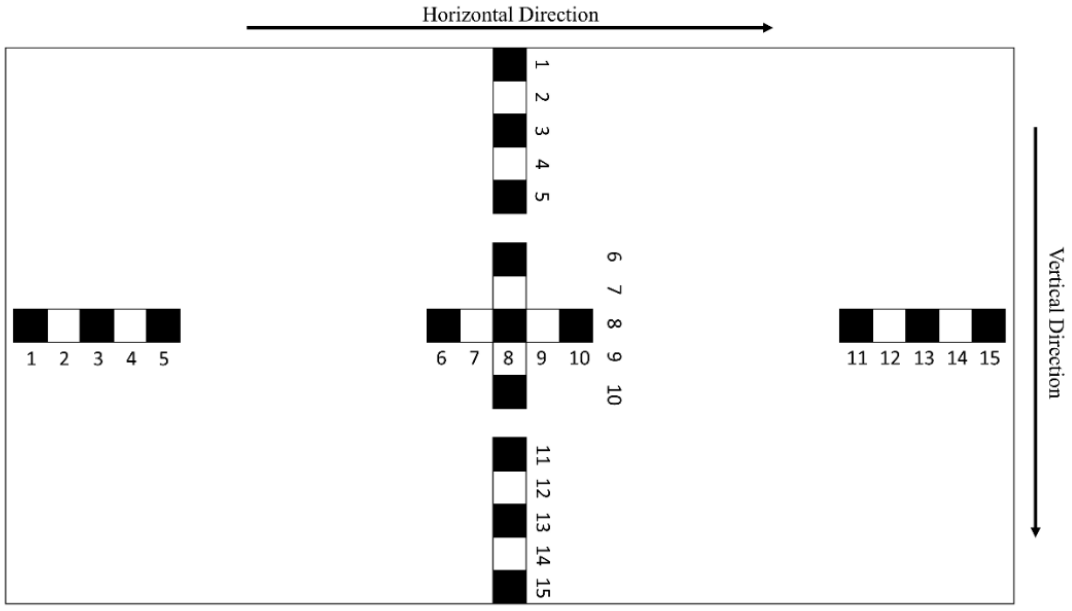

Fig 2.6 Selected checked patterns used as samples for evaluating image distortion.

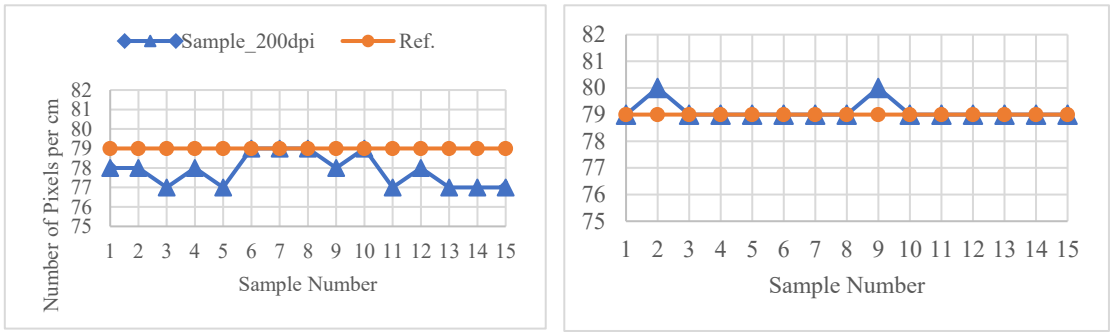

(a)

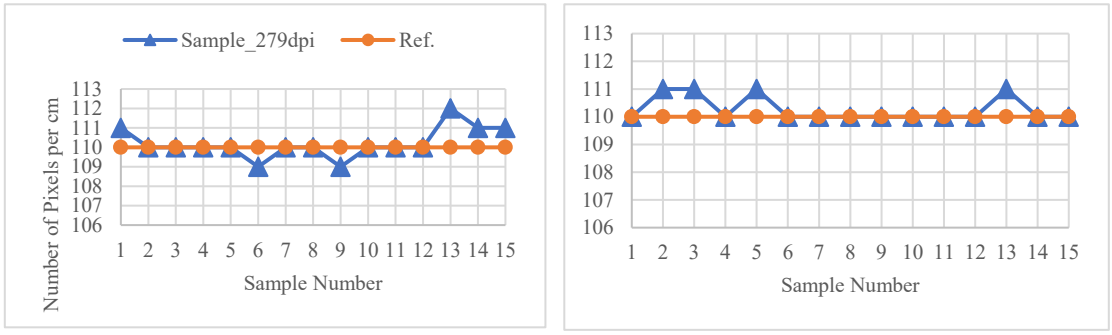

(b)

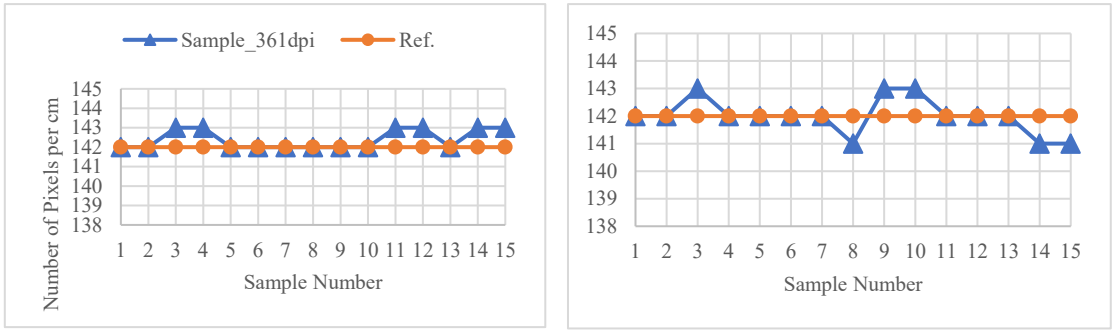

(c)

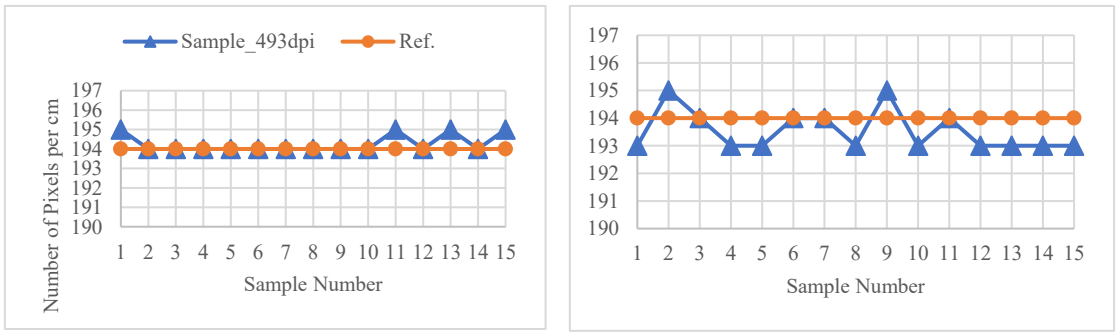

(d)

Fig 2.7 Pixel position deviation in each selected samples in different scanning resolution. The graphs on the left side are the samples in horizontal direction; The graphs on the right side are the samples in vertical direction.

Table 2.2 Comparison of RMSE of positional deviation in different resolution settings

	200DPI		**279DPI**		**361DPI**		**493DPI**	
	Pixels	μm	Pixels	μm	Pixels	μm	Pixels	μm
Horizontal	1.39	176.5	0.77	70	0.63	44.3	0.52	26.7
Vertical	0.37	46.9	0.52	47.3	0.63	44.3	0.86	44.3

Since the scanning resolution settings are already known (Table. 2.1), the theoretical numbers of pixels contained in 1cm can be easily calculated, which is used as the reference data in later calculation. The measured values are then used to calculate the root mean square error (RMSE) together with the reference data using the following equation:

$$\mathrm{RMSE} = \sqrt{\frac{\sum (x - \bar{x})^{2}}{n}} \tag{2.8}$$

where x is the measured value of each selected sample, $\bar{x}$ is the number of pixels calculated by the corresponding resolution, and n is the number of the selected samples.

The results are shown in Fig. 2.7 and Table 2.2, where the figure gives pixel position deviation of each selected sample in the image scanned with different resolution settings and the table shows the corresponding RMSE of different resolution settings. These results indicate that low resolution scanning causes more image distortion than relatively higher resolution, while the lower resolution can provide wider scanning width. The wider scanning width may cause more sever distortion at image edges in the horizontal direction. On the other hand, from the comparison of RMSE of positional deviation in different resolution settings (except 200dpi), it can be found that the image acquired by this line sensor-based scanner has minimal distortion and the error is within ±1pixel. Such errors obtained in this way at low resolution scanning are sufficient to demonstrate the performance of the line sensor-based scanner in combating image distortion.

2.3.3 Image Correspondence and Image Registration

Image correspondence is a common issue and fundamental problem in computer vision. It refers to the scenario when at least two or more images need to be corresponded from which part of one image to which part of another image. In general, these images are taken from different sensor, different viewpoints or at different time[23)]. Majority of the comprehensive imaging analysis systems require the image corresponding process or relevant procedure, which could also be an intermediate step for other exact applications such as stereo vision, structure from motion and or even a simple image stitching. There is another technical term namely, image registration[23)], very similar to this. The image registration is more focused on determining the

geometric transformation that relates identical points in two images. But both of them have one thing in common and that is to find the relationship between the two images.

The experimental results presented in the previous subsection demonstrate the accuracy of the line sensor-based scanner. This advantage can also be of great use in the image correspondence and alignment process. The usage of this would be presented and discussed in later chapters.

2.3.4 Image Noise

Image noise is an unavoidable topic in image processing. This concept involves all times of imaging techniques, such as one can be generated by film grain and can be produced by the image sensor and circuitry of a scanner or digital camera. Generally, the image noise is defined as the "unwanted signal or feature" acquired during image capture. RMS noise was used to evaluate the noise of images in this study, which can be derived from the standard deviation of the measured sensor response[6]. In terms of the ISO 15739 guideline[17], three types of noise are given as follows: fixed pattern noise σ_{fp}, temporal noise σ_{temp} and total noise σ_{total}, where the fixed pattern noise σ_{fp} is defined as the unwanted variation captured by every exposure; the temporal noise is defined as the random noise due to image sensor dark current, photon shot size, analogue processing, and quantization, which varies from one image to the next; the total noise is defined as the unwanted variations captured by a single exposure. Eq. 2.9 shows the relationship of these three types of noise, where the total noise is a sum of fixed pattern noise and temporal noise.

$$\sigma_{total}^2 = \sigma_{fp}^2 + \sigma_{temp}^2 \tag{2.9}$$

A case of image noise evaluation performed in our laboratory is taken as an example to describe its general procedure. A gray sheet with uniform optical density is commonly used to evaluate the image noise. The image of the gray sheet is acquired by an imaging system that needs to be evaluated, and the image acquisition is performed multiple times for the accuracy of the evaluation. Then, the acquired images are averaged to calculate the noise. The temporal noise is calculated by the following equations.

$$\sigma_{temp} = \sqrt{\frac{8}{7}\sigma_{diff}^2} \tag{2.10}$$

$$\sigma_{diff} = \frac{1}{8}\sum_{i=1}^{8}\sqrt{\frac{\sum_x \sum_y \left(P_{i,xy} - P_{ave,xy}\right)^2}{n}} \tag{2.11}$$

Where $P_{i,xy}$ is the pixel value of ith image, $P_{ave,xy}$ is the pixel value of the averaged image, x and y are the coordinates of the pixels on the image, and n is the number of pixels selected from image for analysis.

The fixed pattern noise is calculated by the following equations.

$$\sigma_{fp} = \sqrt{\sigma_{ave}^2 - \frac{1}{7}\sigma_{diff}^2} \tag{2.12}$$

$$\sigma_{ave} = \sqrt{\frac{\sum_x \sum_y \left(P_{ave,xy} - \bar{P}_{ave}\right)^2}{n-1}} \tag{2.13}$$

$$\bar{P}_{ave} = \frac{1}{n}\sum_x \sum_y P_{ave,xy} \tag{2.14}$$

From Eq. 2.12 to Eq. 2.14, the fix pattern noise and the temporal noise calculated above, the total noise can be obtained. What calls for special attention is that even any two types of imaging system equipped with different image sensors can achieve almost same imaging quality in terms of image noise, it is does not mean that they are equal in all aspect of imaging. Any kind of comparison should be performed in specific experimental condition in terms of the applications. What happens to the battle of CCD and CMOS is a good example to prove this.

2.3.5 Color Evaluation

The color evaluation method developed by the Advanced Imaging Technology Laboratory in Kyoto University is addressed in detail in this section. The procedure chart is shown as Fig. 2.8.

Firstly, a total of three targets are used for a scan: a target object, white standard sample, and color chart. A standard IT8.7/2 color chart is used in the evaluation[18,19]. The second step is shading correction which is used for calibrating the uneven distribution of light in horizontal direction on the image. And the pixels are extracted from the white standard sample to calculate their average RGB values. The calculated pixel value is used for color correction as the representative pixel value of the captured image.

In step 3, the RGB value obtained from previous step is converted to the XYZ color space[20]. This process can be expressed as following equation:

$$\boldsymbol{X_0} = \boldsymbol{AR} \tag{2.15}$$

where $\boldsymbol{X_0}$ is a 3 x 228 matrix of XYZ tristimulus values provided by the color chart manufacture, $\boldsymbol{A}$ is a conversion matrix from RGB to XYZ space, $\boldsymbol{R}$ is a 3 x 228 matrix of RGB values of extracted patches. Here, the XYZ tristimulus values are normalized within the range 0~1. The matrix $\boldsymbol{A}$ can be obtained if an inverse matrix of $\boldsymbol{R}$ exists, but $\boldsymbol{R}$ has no inverse matrix because it is not regular. However, this can be solved by multiplying the transpose matrix of $\boldsymbol{R}$, which makes $\boldsymbol{RR}^{\mathrm{T}}$ becomes regular and has an inverse matrix. Thus, $\boldsymbol{A}$ can be obtained by calculating the coefficient matrix of the linear multiple regression model using the Moore-Penrose generalized inverse matrix as shown in the following Eq. 2.16.

$$\boldsymbol{A} = \boldsymbol{X_0 R}^{\mathrm{T}}(\boldsymbol{RR}^{\mathrm{T}})^{-1} \tag{2.16}$$

Using the obtained matrix $\boldsymbol{A}$, the matrix $\boldsymbol{X}$ with XYZ values is estimated from RGB values as shown in Eq. 2.17 and regarded as the representative pixel values.

$$\boldsymbol{X} = \boldsymbol{AR} \tag{2.17}$$

In step 4, the XYZ values of the components in matrix $\boldsymbol{X}$ obtained in step 3 are converted to the L*a*b* space which is defined by CIE. The normalized XYZ values are divided by the white point (white standard) coordinates (0.9505,1.000,1.089) of the D65 standard light source[21], and a primary transformation called the Bradford transformation of color is performed as shown in follows:

$$\begin{aligned} X_i' &= X_i/0.9505 \\ Y_i' &= Y_i \\ Z_i' &= Z_i/1.089 \\ i &= 0,1,2,\cdots,228 \end{aligned} \tag{2.18}$$

where X_i', Y_i', Z_i' are values that are linearly transformed from the components X_i, Y_i, Z_i of the ith column of the matrix $\boldsymbol{X}$.

$$f(t) = \begin{cases} t^{1/3} & t > (6/29)^3 = 0.008856 \\ [(29/3)^3 t + 16]/116 & Otherwise \end{cases} \tag{2.19}$$

$$\begin{aligned} L_i^* &= 116 f(Y_i') - 16 \\ a_i^* &= 500\big(f(X_i') - f(Y_i')\big) \\ b_i^* &= 200(f(Y_i') - f(Z_i')) \\ \mathrm{i} &= 0,1,2,\cdots,228 \end{aligned} \tag{2.20}$$

$$\boldsymbol{L} = (\boldsymbol{L}^* \quad \boldsymbol{a}^* \quad \boldsymbol{b}^*)^{\mathrm{T}} \tag{2.21}$$

Then, for converting X_i', Y_i', Z_i' to L_i^*, a_i^*, b_i^*, $f(t)$ needs to be calculated firstly as shown in Eq. 2.19. The $f(t)$ is used in Eq. 2.20 to accomplish the conversion. Finally, a 1 x 288 matrix $\boldsymbol{L}$ is obtained, and the $\boldsymbol{L}^*, \boldsymbol{a}^*, \boldsymbol{b}^*$ consists of ith L_i^*, a_i^*, b_i^* vector, respectively.

In step 5, the matrix $\boldsymbol{L}$ and the reference data of color chart are used to minimizing the color difference, which represents the closeness of the patch colors. We introduce a matrix $\boldsymbol{L_1}$ firstly for the next step calculation:

$$\boldsymbol{L_1} = (\boldsymbol{L^*} \quad \boldsymbol{a^*} \quad \boldsymbol{b^*} \quad \boldsymbol{L^*L^*} \quad \boldsymbol{a^*a^*} \quad \boldsymbol{b^*b^*} \quad \boldsymbol{L^*a^*} \quad \boldsymbol{a^*b^*} \quad \boldsymbol{b^*L^*} \quad \boldsymbol{E})^{\mathrm{T}} \tag{2.22}$$

where the ith components of $\boldsymbol{L^*}, \boldsymbol{a^*}, \boldsymbol{b^*}, \boldsymbol{L^*L^*}, \boldsymbol{a^*a^*}, \boldsymbol{b^*b^*}, \boldsymbol{L^*a^*}, \boldsymbol{a^*b^*}, \boldsymbol{b^*L^*}$ are represented by three 1 x 288 vector $L_i^*, a_i^*, b_i^*, {L_i^*}^2, {a_i^*}^2, {b_i^*}^2, L_i^*a_i^*, a_i^*b_i^*, b_i^*L_i^*$ respectively, and $\boldsymbol{E}$ is an 1x288 unit vector. Then, based on the linear regression model, we have:

$$\boldsymbol{L_0} = \boldsymbol{BL_1} \tag{2.23}$$

where $\boldsymbol{L_0}$ is a matrix of color chart reference data with the same dimension of matrix $\boldsymbol{L}$ obtained in step 4, and $\boldsymbol{B}$ is a conversion matrix estimated by the method mentioned in step 3 for estimating $\boldsymbol{A}$. Thus, we obtain:

$$\boldsymbol{B} = \boldsymbol{L_0}{\boldsymbol{L_1}}^{\mathrm{T}}(\boldsymbol{L_1}{\boldsymbol{L_1}}^{\mathrm{T}})^{-1} \tag{2.24}$$

Using the estimated matrix $\boldsymbol{B}$, $\boldsymbol{L'}$ can be calculated by Eq. 2.25 as following:

$$\boldsymbol{L'} = \boldsymbol{BL_1} \tag{2.25}$$

The matrix $\boldsymbol{L'}$ and $\boldsymbol{L_0}$ are used to calculate color difference ΔE based on the formula[22] as following:

$$\Delta E = \frac{1}{228}\sum_{i=1}^{228}\sqrt{\left(L_i^{*\prime} - L_{0i}^*\right)^2 + \left(a_i^{*\prime} - a_{0i}^*\right)^2 + \left(b_i^{*\prime} - b_{0i}^*\right)^2} \tag{2.26}$$

where $L_i^{*\prime}, a_i^{*\prime}, b_i^{*\prime}$ is the ith component of the matrix $\boldsymbol{L'}$ and $L_{0i}^*, a_{0i}^*, b_{0i}^*$ is the ith component of the matrix $\boldsymbol{L_0}$.

After calculating the color difference, the corrected $L^*a^*b^*$ values need to be converted to RGB values so that the correction result can be visualized.

Firstly, $L^*a^*b^*$ values are converted into XYZ values as shown in Eq. 2.27.

$$\begin{aligned} X &= 0.9505\left(\frac{a^*}{500} + \frac{L^* + 16}{116}\right)^3 \\ Y &= \left(\frac{L^* + 16}{116}\right)^3 \\ Z &= 1.089\left(\frac{L^* + 16}{116} - \frac{b^*}{500}\right)^3 \end{aligned} \tag{2.27}$$

Then, the XYZ values are converted into RGB values in the sRGB color space[21]. (Eq. 2.28)

$$\begin{pmatrix} sR \\ sG \\ sB \end{pmatrix} = \begin{pmatrix} 3.2406 & -1.5372 & -0.4986 \\ -0.9689 & 1.8758 & 0.0415 \\ 0.0557 & -0.2040 & 1.0570 \end{pmatrix} \begin{pmatrix} X \\ Y \\ Z \end{pmatrix} \tag{2.28}$$

Lastly, device gamma correction is performed using the following formula Eq. 2.29. The corrected result is output as an 8-bit format image.

$$\begin{aligned} R_{8bit} &= floor\left[\left(1.055 \times sR^{1/\gamma} - 0.055\right) \times 255 + 0.5\right] \\ G_{8bit} &= floor\left[\left(1.055 \times sG^{1/\gamma} - 0.055\right) \times 255 + 0.5\right] \\ B_{8bit} &= floor\left[\left(1.055 \times sB^{1/\gamma} - 0.055\right) \times 255 + 0.5\right] \end{aligned} \tag{2.29}$$

where γ=2.4.

The color difference is calculated based on the CIE1976 color difference formula in the following equation:

$$\Delta E^*_{ab} = \sqrt{(\mathrm{L}^*_2 - \mathrm{L}^*_1)^2 + (a^*_2 - a^*_1)^2 + (\mathrm{b}^*_2 - \mathrm{b}^*_1)^2} \tag{2.30}$$

where the colors are represented in CIE $\mathrm{L}^*a^*\mathrm{b}^*$ color space; L^*_2, a^*_2 and b^*_2 are the actual values of the colors measured from each color patch and L^*_1, a^*_1 and b^*_1 are the reference values of the colors provided by the chart manufacture.

By using the method described above, the color difference of each scanning resolution settings were calculated and Table. 2.3 shows the results. This results indicates that the scanning resolution can affect the color difference. Scanning, especially for high-resolution scanning, it involves the process of spatial sampling objects at the microscopic level. There are two practical cases where a pixel in the resulting image correlates to the spatial sampling area on the color chart. 1) If the size of the sampling window is greater than the patch size, each pixel would contain mixed color information from neighboring color patches. As the sampling window size increases, the number of neighboring patches whose color information is mixed also increases. Then the calculated color difference becomes larger. 2) In the contrary, if the size of the sampling window is smaller than the patch size, some of the pixels represent color information merely from one complete patch and other pixels may contain mixed colors from different patches. As the sampling window size decreases, the percentage of the number of pixels whose color information comes from one complete patch increases. Then the calculated color difference becomes smaller. This means that the higher resolution setting contributes smaller color difference. Even for low resolution scanning, relatively higher resolution settings result in smaller color difference. Except for 200dpi setting, the others can achieve the color difference value within 2.0, which belongs to Grade A color tolerance[24]. The experimental results suggests that the proposed image acquisition system has enough capability in color reproduction even using low image resolution settings.

Table 2.3 Comparison of color difference in different resolution settings

Resolution	200DPI	279DPI	361DPI	493DPI
Color difference	2.02	1.99	1.84	1.64

Table 2.4. Sensitivities of human eyes to color difference[24)]

Color Tolerance	**Delta E (Color difference)**	**The extent of color difference**
Unmeasurable level	0～0.2	The extent that Human can't discriminate. It is impossible to measure the color differences using the special adjusted measuring instruments.
The limit of discrimination	0.2～0.4	It is possible to measure the color differences in the range of 0.2 ～ 0.4, using the special adjusted measuring instruments. The people who were trained can distinguish.
Grade AAA Color tolerance	0.4～0.8	This is the limit to set up the strict color difference standards with the decision of the human visual.
Grade AA Color tolerance	0.8～1.6	People can tell the color differences, if the samples are put side by side.
Grade A Color tolerance	1.6～3.2	In color comparison, this level is regarded as unrecognized and same color in general.
Grade B Color tolerance	3.2～6.5	Each colors of this range are regarded as the same colors. But the clients concerning paints and inks industry will make complaints about the color difference.
Grade C Color tolerance	6.5～13.0	This color tolerance corresponds to the color difference of JIS standard color chips.
Grade D Color tolerance	13.0～25.0	Each color over ΔE 13 is not same color anymore.

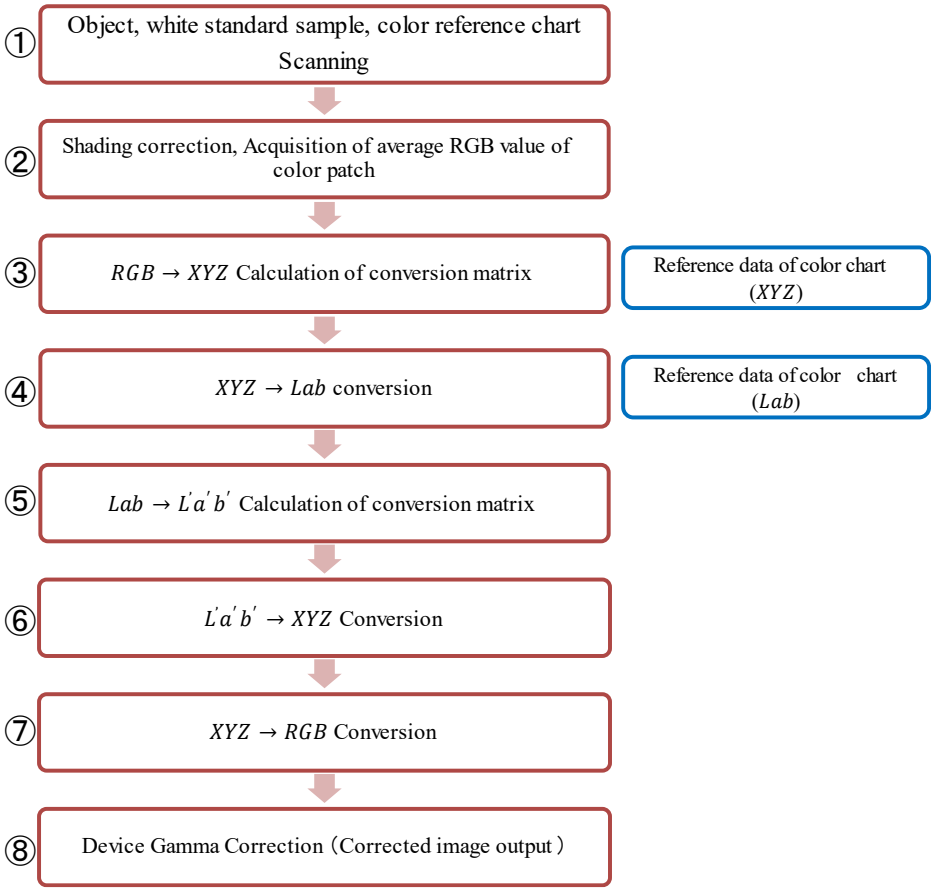

Fig. 2.8. The procedure of the color evaluation method developed by Ide Lab.

2.4 Conclusion

In this chapter, the line sensor-based high resolution imaging system used in this study is introduced and discussed. Some of the basic knowledge of image sensor are described at first, since they are related to the applications in the following chapters. The imaging mechanism of the system is explained in detail. The regular image processing and issues involved in image acquisition by the proposed system are addressed. An experiment for evaluating image quality in terms of image geometric distortion was conducted. The experimental results showed that the proposed image acquisition system is capable of producing high geometrically accurate images even at low resolution settings. As mentioned in previous, three applications would be presented in later chapters of this dissertation where they share a common basis that a line sensor-based high resolution imaging system is implemented at first, then the adjustments or modifications are conducted according to the application requirements.

2.5 References

1) P. D. Heermann and N. Khazenie: “Classification of Multispectral Remote Sensing Data using a Back-propagation Neural Network”, IEEE Transection on Geoscience and Remote Sensing, 30, 1, pp. 81-88 (1992)

2) K. M. Pohl, J. Fisher, J. J. Levitt, M. E. Shenton, R. Kikinis, W. Eric, L. Grimson, and W. M. Wells: “A Unifying Approach to Registration, Segmentation, and Intensity Correction”, Medical Image Computing and Computer-Assisted Intervention – MICCAI 2005. MICCAI 2005. Lecture Notes in Computer Science, 3749, pp. 310-318 (2005)

3) R. Bellucci, P. L. Carcagni, A. Della Patrib, R. Fontanc, C. Frosinini, M. C. Gambino, M. Greco, M. Mastroianni, M. Materazzi, E. Pampaloni, L. Pezzati, R. Piccolo and P. Poggi: “Integration of Image Data from 2D and 3D Optical Techniques for Painting Conservation Applications”, The Imaging Science Journal, 55, 2, pp. 80-89 (2013)

4) RED. COM, Inc.: “Color vs Monochrome Sensor”, http://www.red.com/learn/red-101/color - camera -sensors, accessed 20/09/2020

5) F. Blais: "A Review of 20 years of Range Sensors Development", Journal of Electronic Imaging, 13, pp.231-240 (2004)

6) H. C. Lee: "Introduction to Color Imaging Science", Cambridge University Press (2005)

7) M. Bigas, E. Cabruja, J. Forest, J. Salvi: "Review of CMOS Image Sensors", Microelectronics Journal, 37, 5, pp.433-451 (2006)

8) B. Bayer: "Color imaging array", Patent US3971065, 1976

9) W. Lu, and Y. P. Tan: “Color Filter Array Demosaicing: New Method and Performance Measures”, Image Processing, IEEE Transactions, 12, 10, pp. 1194-1210 (2003)

10) M. Lesser: "Charge coupled device (CCD) image sensors", High Performance Silicon Imaging – Fundamentals and Applications of CMOS and CCD sensors, pp.78-97 (2014)

11) A. Tanaka, K. Makino: "Linear Image Sensor with High Performance and Large Photosensitive Element", Sensors and Actuators A: Physical, 29, 3, pp.201-207 (1991)

12) IESNA RP-30-96, Museum and Art Gallery Lighting: A recommended Practice (Illuminating Engineering Society of North America, New York, 1996)

13) H. W. Ra, K. S. Song, C. W. Ok, Y. B. Hahn: Korean J. Chem Eng., 24, 2, pp. 197-203 (2007)

14) J. A. Toque: “Material Investigation through High-resolution Analytical Imaging and Spectrometry” (Doctoral Degree Thesis), Kyoto University, 2013

15) J. A. Toque, M. Komori, Y. Murayama, and A. Ide-Ektessabi: VISIGRAPP 2009, CCIS (Springer – Verlag Berlin Heidelberg), 68, pp. 19-132 (2010)

16) J. A. Toque, Y. Sakatoku, J. Anders, Y. Murayama, and A. Ide-Ektessabi: “MULTISPECTRAL IMAGING - The Influence of Lighting Condition on Spectral Reflectance Reconstruction and Image Stitching of Traditional Japanese Paintings”,

Proceedings of IMAGAPP 2009 – International Conference on Imaging Theory and Applications, pp. 13-20 (2009)

17) ISO 15739: "Photography – Electronics Still-picture Cameras – Noise Measurement, 1st Edition", 2003

18) A. Sharma: "Understanding color management", John Wiley & Sons, Hoboken (2018)

19) J.Y. Hardeberg: "Acquisition and reproduction of color images: colorimetric and multispectral approaches", Universal-Publishers, USA, pp.50-51 (2001)

20) L. Busin, N. Vandenbroucke and L. Macaire: "Color spaces and image segmentation", Advances in imaging and electron physics, 151, 1 (2008)

21) J. Schanda: "Colorimetry: understanding the CIE system", John Wiley & Sons, Hoboken, pp.61-62 (2007)

22) L. Mandic, S. Grgic and M. Grgic: "Comparison of Color Difference Equations", Proceedings ELMAR 2006, pp.107-110 (2006)

23) B. Zitova, and F. Jan: "Image registration methods: a survey", Image and vision computing, 21, 11, pp. 977-1000 (2003)

24) Nippon Denshoku Industries Co., LTD: "Example of the allowance by color", https://www.nippondenshoku.co.jp/web/english/colorstory/08_allowance_by_color.htm, accessed 02/12/2020

25) Y. Li, B. He: “Quantitative evaluation of image quality of CCD subpixel imaging using MTF”, Infrared and Laser Engineering, 42, 2, pp. 443-448 (2013)

26) Imaging Engineering USA, Inc.: “Units and conversions for resolution”, https://www.image-engineering.de/library/technotes/761-resolution-measurement-and-its-units, accessed 02/01/2022

27) Edmund Optics Inc.: “Application notes of knowledge center: Imaging Resolution”, https://www.edmundoptics.cn/knowledge-center/application-notes/imaging/resolution, accessed 02/02/2022

28) M. Born, E. Wolf: “Principle of Optics”, Cambridge University Press, Cambridge, pp. 140-150 (2013)

29) KenRockwell.com.: “Diffraction”, https://www.kenrockwell.com/tech/diffraction.htm, accessed 17/02/2022

30) Cambridge in Color: “Tutorials: Lens diffraction and photography”, https://www.cambridgeincolour.com/tutorials/diffraction-photography.htm, accessed 17/02/2022

Chapter 3

Spectral Reflectance Estimation based on Multispectral Imaging

3.1 Introduction

Imaging technology always plays a significant role in various fields. And increasing number of related applications have been developed and employed in such as medical imaging, remote sensing, heritage preservation in recent decades. Especially, in the field of digital archiving for cultural heritage preservation and historical research, there are various methods that can accurately record the information of heritage, akin to color, shape, spectral reflectance etc. For 2D cultural heritage, due to the precious nature of themselves, it was found necessary to develop an analysis method of cultural heritage and artworks like painting or scroll to support historical research as well as adequate restoration, by determining the materials used in the artwork. Conventionally, popular techniques that make use of high energy radiation such as X-ray Fluorescence or Accelerator Mass Spectrometry are employed in analyzing historical artworks and artifacts. Although XRF is categorized as a non-destructive analysis method, it requires radiation of high energy x-ray onto the object or even removal of material. Hence, we truly need a technique that is non-destructive and non-invasive. Analytical imaging is an important aspect of material analysis. It provides useful information about its various properties including mechanical, chemical, optical properties among others. Among these techniques multispectral imaging offers new frontiers for especially the analysis and investigation of materials[1,2]. Multispectral imaging refers to the acquisition of a series of digital images at a number of different optical wavelength. Nowadays it is widely applied to the field of restoration and conservation of art works. Multispectral images can be acquired either by using camera with specially designed spectral channels or by using a monochrome camera and placing one or a series of spectral filters in front of the imaging device. The latter one offers flexibility and variety of spectral channels that can be selected[3]. In other words, the light that entering camera sensor can be physically controlled. The most important feature of this imaging method is that the reflected light from object can be precisely divided by a set of filters, and the images acquired by this method contain more information than conventional RGB images. Once the multispectral images are obtained, it is easy to make use of them to acquire relative spectral reflectance data and then estimate the material used in the object or the elements that exists in pigments[1,2]. Spectral reflectance is a representation of the reflectivity of the object for light of certain wavelengths, and it is dependent on the chemical binding state of elements that are included in the object. Because spectral reflectance is a unique characteristic to object, many techniques or methods for analysis of materials using the spectral reflectance has been developed. The spectral reflectance data itself is also useful for restorations as the reference material. Compared with XRF and other high-energy analysis method, this filter based multispectral imaging method is more economical and practical[4]. Conventionally, the acquisition of a series of multispectral images needs several scans. Not only for longer scanning time, but it will also take more time to find the corresponding position. So, there is a need to

develop a system which can efficiently acquire multispectral images.

In this chapter, focus was given to multispectral imaging of 2D objects in visible region. The main purpose of this chapter is to develop a nondestructive and noninvasive multispectral image acquisition system, which is more efficient, practical, and useful for academic studies and restoration. To be specific, the multispectral image acquisition system can acquire a special multispectral image that contains several filters' states only by one scan. This technique can be realized via a specially designed rotating filter system. Through image separation and image interpolation, the special multispectral image is converted into normal multispectral images. The processed images can be used for estimation of spectral reflectance. The relevant techniques used for image processing and spectral reflectance estimation are addressed in detail.

3.2 Multispectral Imaging using Rotating Filter

3.2.1 Overview of Image Acquisition System

The whole scanning system mainly consists of a camera unit that includes a line sensor based-color camera with lens, a rotating multi-filter system, and light source as shown in Fig. 3.1. The camera used in this application is a line sensor-based color camera manufactured by Alex CO. LTD. The rotating multi-filter system consists of several selected filters and a motor for driving the system. The method used for selecting filters would be discussed in later subsection.

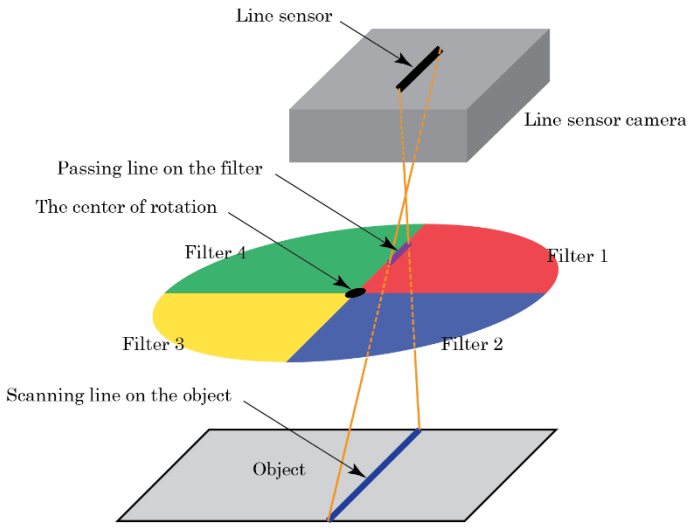

Fig. 3.1. Diagram of rotating multi-filter scanning system.

The scanning system is developed from the preliminary model introduced in Chapter 2 where they share a common basis of imaging mechanism. Since a RGB color camera is employed, the system is capable of acquiring both color images and multispectral images. There are several methods to acquire multispectral images or to design spectral-based digital image acquisition

system[14]. Among these methods, the method that using a monochrome camera and placing a series of spectral filters in front of the imaging device is widely used in many applications. This method is also known as narrow band capture, which offers better flexibility and variety of spectral channels that can be selected. However, it is generally time consuming for multiple scans, and may occur the issue related to image registration. Considering the practicality and efficiency of the system, and the basic task of digital archiving, a combination of RGB color camera and absorption filters is employed in this study. Multispectral imaging in this way greatly shortens the time for image acquisition. However, yet any improvement comes at a cost. Although the RGB color camera comes with three color filters initially, it is also constrained by the spectral sensitivity of corresponding channel according to the color of sensor. For a practical application, the choice of which technique and method to use will highly depend on the balance between the intended purpose, budget, and accuracy.

Due to the relationship between motor rotation speed and exposure time of camera sensor, the rotational motor should supply a tunable-speed mode, so that proper image could be acquired. In this study, white light-emitting diode (LED) was selected as light source for illumination. In numerous types of light source, LED has lower energy dissipation, lighter weight, more controllable spectrum, and longer lifetime. Especially, it is safer to any valuable object such as artworks because of its lower energy dissipation.

3.2.2 Mechanism of Image Acquisition using Rotating Filter

Compare with the technique that setting a series of filters in front of the imaging device, the filters used in the rotating multi-filter system are different from conventional ones, they were modified to a special designed combination as shown in Fig. 3.1. When the scanner scans from one side to another side of an object, the rotating multi-filter system keeps rotating during that period, and the camera will record all that periodically repeated corresponding states of the filters. Finally, only one image is generated that contains all filters information instead of a number of images, which generally generated by using conventional multispectral imaging system. The proposal method is obviously more efficient than conventional method which needs multi-time scan.

For acquiring the image that contains all filters information, the relationship between several parameters needs to be clear firstly. The rotation speed of the motor can be described by:

$$v\ [\mathrm{rpm}] = \frac{v}{60} \cdot 360\ [\mathrm{deg/sec}] = 6v\ [\mathrm{deg/sec}] \tag{3.1}$$

So, the time required for one rotation T_0 can be expressed as:

$$T_0 = \frac{360}{6v}\ [\mathrm{sec}] = \frac{60}{v}\ [\mathrm{sec}] \tag{3.2}$$

However, depending on the type of filter, the same state of the filter may be repeated multiple times during one rotation. Let m be the number of filters used in the rotating multi-filter system and assume that the filter state returns to its original state by $\frac{1}{\mathrm{m}}$ rotation, then the time until the filter state returns to its original state T_{f} (cycle of filter state) can be expressed as following equation.

$$T_{\mathrm{f}} = \frac{60}{v} \cdot \frac{1}{\mathrm{m}} \ [\mathrm{sec}] = \frac{60}{\mathrm{m}v} \ [\mathrm{sec}] \tag{3.3}$$

One the other hand, the exposure time of camera is $T_{\mathrm{ex}}\ [\mu\mathrm{sec}] = T_{\mathrm{ex}} \cdot 10^{-6}[\mathrm{sec}]$, and the state of the filter is Θ_k $(k = 1, \dots, N)$. If the acquired image contains N states of filters, which is repeated periodically, the relationship between the exposure time of camera T_{ex} and the filter state cycle can be described as:

$$NT_{\mathrm{ex}} \cdot 10^{-6} = T_{\mathrm{f}} = \frac{60}{\mathrm{m}v} \ [\mathrm{sec}] \tag{3.4}$$

The equation (3.4) can be integrated as:

$$vNT_{\mathrm{ex}} = \frac{60 \cdot 10^{6}}{\mathrm{m}} \tag{3.5}$$

Hence, If the above relationship can be satisfied, the image which contains periodically repeated N states of filters can be acquired. Fig. 3.2 shows a case of image with four states of filters.

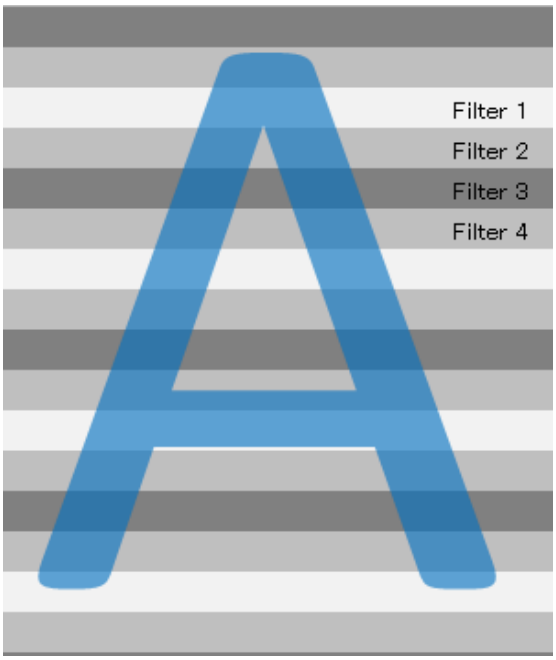

Fig. 3.2 Diagram of scanned multispectral image by the proposed image acquisition system.

3.2.3 Image Processing

Conventionally, multispectral images can be acquired by using a monochrome camera and a series of filters in front of the imaging device. Then a number of monochromatic images can be acquired with corresponding spectral channels. But based on the method for multispectral image acquisition in this dissertation, the filters were modified and applied to a specially designed rotating multi-filter system, and only one image is generated from imaging. The acquired image contains all filters information instead of a number of monochromatic images. So, the original image that acquired by rotating multi-filter system needs to be separated into several images corresponding to the filter states. After separation processing, since there is no information in some area of the separated images, the images need to be interpolated and corresponding multispectral image can be obtained[5].

Through the image process mentioned above, the interpolated images are converted into normal multispectral images that can be employed in subsequent image processing and application. As the image shown in Fig. 3.2, the acquired image contains several filter states, which is repeated periodically from the top to bottom of image. For next step image interpolation, the original image needs to be segmented in accordance with the filter state firstly.

Generally, the brightness $I_{\mathrm{sep}}^{(k)}(x,y)$ of corresponding position (x,y) on separated image k $(k = 1, \dots, N)$ can be described by the following equation:

$$I_{\mathrm{sep}}^{(k)}(x,y) = \begin{cases} I_{\mathrm{raw}}(x,y) & (y = iN + k) \\ 0 & (y \neq iN + k) \end{cases} \qquad i = 0,1, \dots, \frac{Y}{N} - 1 \tag{3.6}$$

And the image can be segmented by the brightness $I_{\mathrm{sep}}^{(k)}(x,y)$ into N separated images. These N separated images have same size X × Y as the original image, and $I_{\mathrm{raw}}(x,y)$ represents the brightness of pixel on original image. After segmentation, there is certain pixel information on the position $y = iN + k$ of separated images, but the rest positions have no pixel value, which means the separated images are not available for normal use. So, the next step is image interpolation.

For image interpolation, based on the separated image k $(k = 1, \dots, N)$, the missing pixel value or image information need to be linearly interpolated to the corresponding position in y-axis direction. And the brightness ${I_{Int}}^{(k)}(x,y)$ of corresponding position (x,y) on interpolated image can be described by Eq 3.7:

$$I_{Int}{}^{(k)}(x, iN+k+j) = I_{\text{sep}}^{(k)}(x, iN+k)\cdot\frac{N-j}{N} + I_{\text{sep}}^{(k)}(x, (i+1)N+k)\cdot\frac{j}{N}$$
$$\begin{cases} i = 0,1,\ldots,\dfrac{Y}{N}-1 \\ j = 0,1,\ldots,N-1 \end{cases} \tag{3.7}$$

The interpolation processing is based on this expression of brightness, and N interpolated images would be acquired after the processing.

3.2.4 Evaluation of Spatial Resolving Power of the System

Since the image interpolation is involved in the image processing as mentioned above, it is necessary to evaluate if the interpolated results are adequate or not. In the interpolation process, linear interpolation is used in the sub-scanning direction at this stage, but it can be expected that the resolving power in the sub-scanning direction will decrease in this process. However, it is difficult to conduct an evaluation experiment using actual filters and control the timing of exposure start point. So, a simulation to test the decrease in resolution in the sub-scanning direction was conducted. Notably, the resolving power used here denotes the resolving power in the sub-direction of scanning.

In this simulation, sharpness as a characteristic representing the reproducibility of image contours and microstructures is used as the resolution, and the modulation transfer function (*MTF*) is used as a typical physical evaluation scale for sharpness[6,7]. The *MTF* inputs a sinusoidal image of spatial frequency u into the image system, then measures the ratio of the output modulation $M_{\text{out}}(u)$ to the input modulation $M_{\text{in}}(u)$ for each spatial frequency. So, we have:

$$M_{\text{in}}(u) = \frac{Max_{\text{in}}(u) - Mini_{\text{in}}(u)}{Max_{\text{in}}(u) + Mini_{\text{in}}(u)} \tag{3.8}$$

$$M_{\text{out}}(u) = \frac{Max_{\text{out}}(u) - Mini_{\text{out}}(u)}{Max_{\text{out}}(u) + Mini_{\text{out}}(u)} \tag{3.9}$$

where, $Max_{\text{in}}(u)$, $Mini_{\text{in}}(u)$ denote the maximum and minimum of the input waveform; $Max_{\text{out}}(u)$, $Mini_{\text{out}}(u)$ denote the maximum and minimum of the output waveform. *MTF* can be expressed as following:

$$MTF(u) = \frac{M_{\text{out}}(u)}{M_{\text{in}}(u)} \tag{3.10}$$

In general, the higher the *MTF* value, the sharper the image.

In this simulation, assume a target image is 8-bit, and the sine wave described as shown in the

following equation is used as the input to the pixel position (x, y). The acquired image is used as a virtually captured image.

$$input(y) = \frac{255}{2} + \frac{255}{2}\sin\left(2\pi u(y + y_0)\right) \tag{3.11}$$

Where, y_0 is the initial position.

Since the input waveform is shown as the above equation, the input modulation is $M_{\text{in}}(u) = 1$, and from Eq.3.10, $MTF(u) = M_{\text{out}}(u)$. To verify the proposed method, the virtually captured image is decomposed into N images, then N images need to be interpolated correspondingly. Lastly, the interpolated N images are used to readout the output waveform respectively. The case of $N = 2, 3, 4, 5$ were verified in the simulation. A virtual image captured immediately after the sine wave input is used as a reference for comparison. This image is not processed with image separation and image interpolation. For the spatial frequency to be verified, $u = 0.5$ [cycles/pixel] is used as the maximum of the spatial frequency, where resolving is possible in the ideal state and the pixel size matches half wavelength; while $u = 0.05$ [cycles/pixel] is used as the minimum of the spatial frequency, where resolving is much sufficient. 10 sine waves of spatial frequency are used for input in the simulation. In general, [cycles/mm] is the unit applied to describe spatial frequency. The cycle refers to the bright to dark to bright transitions. However, for simplicity, in this simulation, the unit is changed in order to perform evaluation that does not depend on the resolution at the time of image acquisition. For the setting of the initial position, 10 points of $y_0 = 0, 0.1, \ldots, 0.9$ at the input of each spatial frequency were applied. The minimum of output $M_{\text{out}}(u, y_0)$ is used as modulation $\widehat{M}_{\text{out}}(u)$ at that spatial frequency. Fig. 3.3 shows the procedure of the simulation explained above.

The results of the simulation are shown as Fig. 3.4. Some of the spatial frequency u and their corresponding *MTF* are not plotted, since that the wavelength of the output waveform is completely different from the input and cannot be resolved at all. It can be observed that the higher the spatial frequency, the smaller the *MTF* value, which is consistent with the phenomenon where thinner lines are difficult to resolve. Moreover, with the smaller spatial frequency, when the image is divided into a larger number of pieces (larger number of N), the more space needs to be interpolated for each separated image and the more difficult to resolve image detail. This big gap between two lines of the pixel leads to low resolution from the beginning. As for comparison target, since there is no separation and interpolation involved, when $u = 0.5$, $y_0 = 0$, the output image becomes a uniformly gray image and the *MTF* becomes 0. $MTF(u) = 0.5$ is commonly used as a decent indicator of perceived sharpness. It is used to know at what spatial frequency the imaging system is able to transfer half of the possible captured contrast to the raw data[17]. In this study, the spatial frequency u at which $MTF(u) = 0.5$ is treated as a resolvable value and used as an index of resolving power. For the case of $N = 2, 3, 4, 5$, when $MTF(u) = 0.5$ the corresponding spatial frequency $u = 0.07, 0.09, 0.12, 0.19$ [cycles/pixel], respectively.

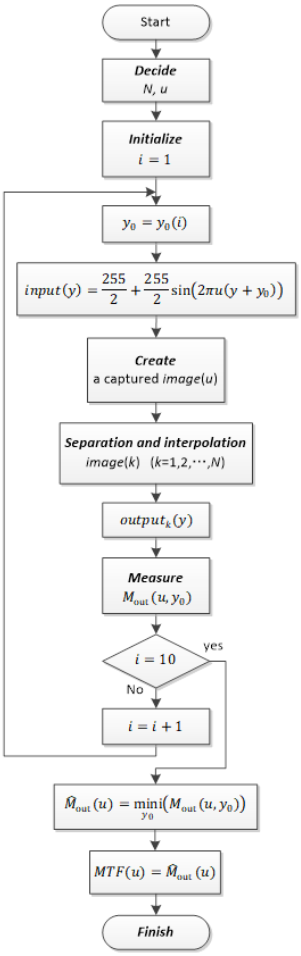

Fig. 3.3 Procedure of the simulation for evaluating resolving power of the proposed system.

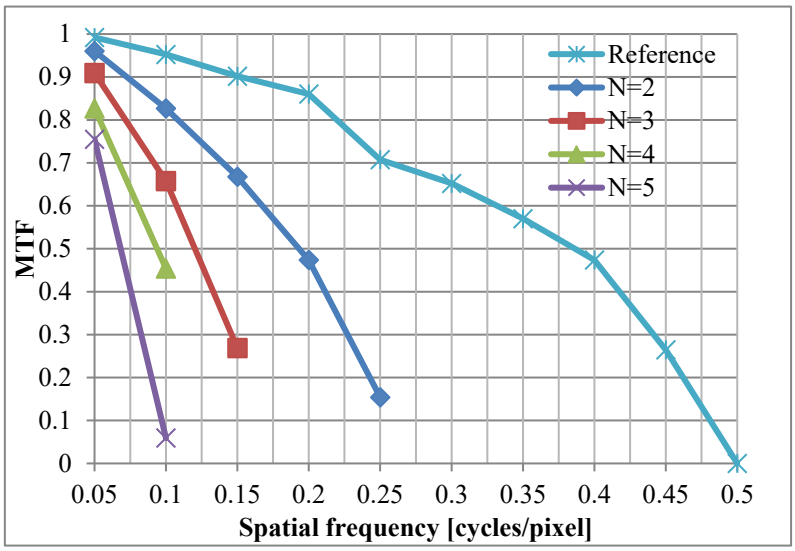

Fig. 3.4. The results of the simulation for evaluating resolving power of the proposed system.

3.3 Spectral Reflectance Estimation

3.3.1 Estimation of Spectral Reflectance based on Indirect Method

A color in the RGB color model can be described by indicating how much of each component of the R(red), G(green) and B(blue) is included. With such color model, a RGB color image can be expressed as:

$$\boldsymbol{v} = [R, G, B]^{\mathrm{t}} \tag{3.12}$$

For an image with a different color model that has more components or channels, the image can be described as:

$$\mathbf{v} = [v_1,\ v_2, \dots, v_T]^{\mathrm{t}} \tag{3.13}$$

In Eq. 3.13, if $T = 3$ and $v_1 = R,\ \ v_2 = G,\ \ v_3 = B$, then this image is in RGB color model.

It is a fact that the camera sensor response is a function of the spectral reflectance. In general, the camera sensor response can be influenced by two factors: the spectral sensitivity of camera sensor and the spectral radiance of the illumination. The relationship can be described by following equation:

$$I(x, y, \lambda) = E(x, y, \lambda) r(\lambda) \tag{3.14}$$

where $I(x, y, \lambda)$ denotes the energy distribution of the camera sensor at pixel (x, y), $E(x, y, \lambda)$ denotes the energy distribution of the illumination at pixel (x, y), and $r(\lambda)$ denotes the spectral reflectance of the object.

For an image obtained by an imaging system, we have:

$$\begin{aligned} v_t(x, y) &= \int_{\Omega} F_t(\lambda) S(\lambda) I(x, y, \lambda) d\lambda + n_t(x, y) \\ &= \int_{\Omega} F_t(\lambda) S(\lambda) E(x, y, \lambda) r(\lambda) d\lambda + n_t(x, y) \end{aligned} \tag{3.15}$$

where t $(t = 1,2, \dots, T)$ denotes the number of channels used to the imaging system, $\boldsymbol{v}_t$ is the pixel value at the position (x, y). And $F_t(\lambda)$ denotes the spectral transmittance of the t th filter, $S(\lambda)$ is the spectral sensitivity of the camera module, Ω is the wavelength range applied in the experiment. In addition, $n_t(x, y)$ is used for describing image noise. Here, each spectral characteristic is represented by a discrete value and represented by a matrix. Let L be the

number of discrete values in the wavelength range Ω, we can obtain:

$$\mathbf{v} = \mathbf{FSEr} + \mathbf{n} \tag{3.16}$$

For simplicity, the pixel position is omitted, then the spectral characteristic can be expressed as following equations.

$$F(\lambda): \quad \mathbf{F} = [\mathbf{f}_1, \mathbf{f}_2, \dots, \mathbf{f}_t, \dots, \mathbf{f}_T]^{\mathrm{t}}$$
$$\text{Where,} \quad \mathbf{f}_t = [F_t(\lambda_1), F_t(\lambda_2), \dots, F_t(\lambda_L)] \tag{3.17}$$

$$S(\lambda): \quad \mathbf{S} = \begin{bmatrix} S(\lambda_1) & & \mathbf{0} \\ & S(\lambda_2) & \\ \mathbf{0} & & \ddots \\ & & S(\lambda_L) \end{bmatrix} \tag{3.18}$$

$$E(\lambda): \quad \mathbf{E} = \begin{bmatrix} E(\lambda_1) & & \mathbf{0} \\ & E(\lambda_2) & \\ \mathbf{0} & & \ddots \\ & & E(\lambda_L) \end{bmatrix} \tag{3.19}$$

$$r(\lambda): \quad \mathbf{r} = [r(\lambda_1), r(\lambda_2), \dots, r(\lambda_L)]^{\mathrm{t}} \tag{3.20}$$

For simplicity in the experiment, the image noise is omitted as well, then Eq. 3.16 can be expressed as:

$$\mathbf{v} = \mathbf{Xr} \tag{3.21}$$

where, the matrix $\mathbf{X}$ is a $T \times L$ matrix that satisfies $\mathbf{X} = \mathbf{FSE}$. It means that the L dimensional vector $\mathbf{r}$ is linearly mapped to the T dimensional camera sensor response vector $\mathbf{v}$ according to the matrix $\mathbf{X}$.

The estimation of spectral reflectance can be accomplished by calculating vector $\mathbf{r}$. However, the calculation can only be solved properly when $T = L$. So, a proper method is needed to solve above issue.

The reflectance reconstruction techniques can be classified into three categories: direct reconstruction, reconstruction by interpolation, and indirect reconstruction or learning (sample)-based reconstruction[8,9]. First, direct reconstruction is based on the inverse of the overall spectral sensitivity of a camera system, which is a matrix multiplication of the spectral distribution of the light source, the spectral transmittances of the spectral filters and the spectral response of the camera sensor. Second, the camera responses can be interpolated to find an

approximation of the corresponding spectral reflectance factor, and therefore the method is called reconstruction by interpolation. Finally, indirect reconstruction is also called learning (sample)-based reconstruction. It means that a calibration target is first used to build the transform between camera signals and spectral reflectance factor, and after that, camera signals of other targets can be transferred into spectral reflectance factor.

Compared with direct reconstruction, learning (sample) based reconstruction is a better choice. It is more device independent. The camera sensor and light source spectral characteristics can be approximated by a conversion matrix which is estimated by a learning sample.

In mathematics, and in particular linear algebra, a pseudoinverse $\boldsymbol{A}^{+}$ of a matrix $\boldsymbol{A}$ is a generalization of the inverse matrix. The most widely known type of matrix pseudoinverse is the Moore–Penrose pseudoinverse[10]. A common use of the pseudoinverse is to compute a 'best fit' (least squares) solution to a system of linear equations that lacks a unique solution. In this study, the pseudoinverse model was employed, which is a modification of the Wiener estimation by regression analysis[11,12]. The inverse transfer function was calculated based on the pseudoinverse method using the camera sensor responses from the selected spectral channel and the measured spectral reflectance of a learning sample. The learning sample is a specially designed pigments chart with 252 patches including selected Japanese organic and inorganic mineral pigments. More details of the learning sample would be presented in section 3.3.3.

In this model, a matrix $\mathbf{G}$ is derived by minimizing $\|\mathbf{R}-\mathbf{GV}\|$ from a known spectral reflectance of a learning sample $\mathbf{R}$ matrix. $\mathbf{V}$ stands for the corresponding pixel value. So, the matrix $\mathbf{G}$ can be expressed as following:

$$\mathbf{G} = \mathbf{R}\mathbf{V}^{+} = \mathbf{R}\mathbf{V}^{\mathrm{t}}(\mathbf{V}\mathbf{V}^{\mathrm{t}})^{-1} \tag{3.22}$$

By multiplying the derived matrix $\mathbf{G}$ to $\mathbf{v}$ which stands for the pixel value of the target image in Eq. 3.16, the desirable spectral reflectance $\widehat{\mathbf{R}}$ can be estimated by using:

$$\widehat{\mathbf{R}} = \mathbf{G}\mathbf{v} \tag{3.23}$$

3.3.2 Spectral Reflectance Estimation based on Image Acquisition using Rotating Filter

In general, a monochrome camera used in multispectral imaging can capture a single channel image by one scan. For a color camera, it can obtain three times as many bands as a monochrome camera that acquired. Unlike monochrome cameras, which have only one sensor and a wide range of sensor spectral sensitivity distribution, color cameras have a relatively narrow range of spectral sensitivity per sensor. But the accuracy of spectral reflectance estimation can be improved by optimizing the filter selection. Since an RGB color camera has three channels, when the number of acquired images is N, the number of channels in the generated multispectral image is $T = 3N$.

From image acquisition to spectral reflectance estimation, three processes are needed including

image separation, image interpolation and spectral reflectance estimation. The former two steps are as shown in section 3.2.3. The last one step is discussed in last section 3.3.1. In this section, the images processed with separation and interpolation are regarded as multispectral observation images.

Since a combination of several filters are used in the proposed imaging system, the acquired image changes depending on the filters used in the rotating filters, the number of acquired images, and the initial position of the rotating filter in image acquisition. Let M be the number of filters used in the rotating filters, $F_m(\lambda)$ be the spectral transmittance of the m $(m = 1, \dots, M)$ th filter, $F^{(\theta)}(\lambda)$ is the filter at position θ, N be the number of acquired images, and the initial position for image acquisition is α, then the spectral transmittance $\tilde{F}_n(\lambda)$ of the filter corresponding to n $(n = 1,2, \dots, N)$ th image can be expressed as following equation.

$$\tilde{F}_n(\lambda) = \int_{\alpha+(n-1)\cdot\frac{2\pi}{N}}^{\alpha+n\cdot\frac{2\pi}{N}} F^{(\theta)}(\lambda)d\theta \tag{3.24}$$

Where $F^{(\theta)}(\lambda)$ is the filter at position θ, so we have:

$$F^{(\theta)}(\lambda) = \begin{cases} F_1(\lambda) & : \quad 0 \le \theta < \dfrac{2\pi}{M} \\ F_2(\lambda) & : \quad \dfrac{2\pi}{M} \le \theta < 2 \cdot \dfrac{2\pi}{M} \\ & \vdots \\ F_M(\lambda) & : \quad (M-1) \cdot \dfrac{2\pi}{M} \le \theta < 2\pi \end{cases} \tag{3.25}$$

Since a RGB color camera has three channels, considering the spectral characteristics of lens and other imaging components, the pixel value $\tilde{v}_{i,j}(x, y)$ at position (x, y) of the acquired image can be described as following equation.

$$\tilde{v}_{n,j}(x, y) = \int_{\Omega} \hat{F}_n(\lambda)\hat{S}_j(\lambda)E(x, y, \lambda)r(\lambda)d\lambda + n(x, y) \tag{3.26}$$

Where j $(j = 1,2,3)$ denotes the number of channels and $\tilde{S}_j(\lambda)$ is the spectral sensitivity distribution of three channels related to the spectral characteristics of lens and other imaging components. $n(x, y)$ is the image noise.

The above equation can be simplified as following:

$$\tilde{\mathbf{v}} = \mathbf{AEr} + \mathbf{n} \tag{3.27}$$

The pixel vector $\tilde{\mathbf{v}}$, filters and camera sensor information can be expressed as:

$$\tilde{\mathbf{v}} = \left[v_{1,1}, v_{2,1}, \dots, v_{N,1}, v_{1,2}, v_{2,2}, \dots, v_{N,2}, v_{1,3}, v_{2,3}, \dots, v_{N,3}\right]^{\mathrm{t}} \tag{3.28}$$

$$\mathbf{A} = \left[\mathbf{a}_{1,1}, \mathbf{a}_{2,1}, \dots, \mathbf{a}_{N,1}, \mathbf{a}_{1,2}, \mathbf{a}_{2,2}, \dots, \mathbf{a}_{N,2}, \mathbf{a}_{1,3}, \mathbf{a}_{2,3}, \dots, \mathbf{a}_{N,3}\right]^{\mathrm{t}}$$

$$\mathbf{a}_{n,j} = \left[\tilde{F}_n(\lambda_1)\tilde{S}_j(\lambda_1), \tilde{F}_n(\lambda_2)\tilde{S}_j(\lambda_2), \dots, \tilde{F}_n(\lambda_L)\tilde{S}_j(\lambda_L)\right] \tag{3.29}$$

where $n = 1, 2, \dots, N$, $j = 1, 2, 3$.

For simplicity, image noise is omitted, then the representation of pixel value can be simplified as:

$$\tilde{\mathbf{v}} = \tilde{\mathbf{X}}\mathbf{r} \tag{3.30}$$

Notably, $\tilde{\mathbf{X}}$ is a $3N \times L$ matrix that satisfies $\tilde{\mathbf{X}} = \mathbf{AE}$. This equation is used for describing the pixel vector of the multispectral image acquired by the proposed rotating filter scanning system. Using this multispectral image, the spectral reflectance is estimated by the method explained in section 3.3.1.

3.3.3 Learning Sample

As discussed in the previous section, an indirect method which is also known as learning sample based-method is employed in spectral reflectance estimation. Since the learning sample is used to approximate the spectral characteristics of the imaging components including the camera and light source in estimating spectral reflectance, it is one of the crucial parts of the proposed method. To solve the linear relationship between the recorded camera sensor response with the interaction of the light source and the object's material, using a learning sample is a much easier way to accomplish so. Compared with direct method, it does not need to know prior knowledge of the camera spectral sensitivity and light source spectral radiance. In other words, the learning sample based method is device independent, which is not affected by any systemic change[13]. Conventionally, many standards or reference color chart, for instances, the IT8 series chart, the Gretag-Macbeth color chart, and the Kodak series color chart, are used as learning sample[15]. These charts are good and easy to be used as samples for colorimetry, but the color patches on these charts do not contain natural colors that comes from natural materials. Considering the practical usage of the proposed method in this study, if the intended application is related to digital archiving for cultural heritage like traditional Japanese painting, these charts are not suitable for it.

Therefore, a specially designed learning sample with Japanese pigments is employed in this study. The learning sample consists of 252 commonly used Japanese pigments including natural and artificial pigments; ancient and modern; and organic and inorganic. As mentioned above, the reason for selecting Japanese pigments as learning sample is that the method is focusing on the usage of digital archiving for cultural heritage. These pigments include copper-based pigments, mercury-based pigments, iron-based pigments, organic pigments, old artificial pigments, natural pigments introduced more recently, and some metallic pigments. Notably,

metallic pigments such as silver and gold are commonly used pigments in some traditional Japanese artworks. The historical time span corresponding to these pigments across from pre-Edo era, Edo era, and beyond. Both in terms of age span and coverage of pigment types, this learning sample is well suited to be applied to spectral reflectance estimation for traditional Japanese artworks. Fig. 3.5 (a) shows the actual learning sample used in the experiment, while Fig. 3.5 (b) shows the measured spectral reflectance corresponding to each pigments sample. It also indicates that the sample has well coverage of spectrum from 380-850nm. Notably, the focus is given to the visible light range from 400-700nm in this study.

The method for spectral reflectance estimation have been discussed in previous section. The learning sample is used to approximate the spectral characteristics of imaging components, which is a calculation for further estimating the conversion matrix for spectral reflectance estimation. Since the linear relationship between the sensor response and spectral reflectance of the object, the solution for spectral reflectance can be calculated by using the conversion matrix. Considering the case in this study where the image acquisition system is equipped with rotating filter and color camera, according to the Eq. 3.30, we have:

$$\widetilde{\mathbf{G}} = \mathbf{R}\widetilde{\mathbf{V}}^{+} = \mathbf{R}\widetilde{\mathbf{V}}^{\mathrm{t}}\left(\widetilde{\mathbf{V}}\widetilde{\mathbf{V}}^{\mathrm{t}}\right)^{-1} \tag{3.31}$$

Based on pseudoinverse method mentioned in previous, the conversion matrix $\widetilde{\mathbf{G}}$ is derived by minimizing $\left\|\mathbf{R} - \widetilde{\mathbf{G}}\widetilde{\mathbf{V}}\right\|$ from the known spectral reflectance of the learning sample $\mathbf{R}$ matrix. $\widetilde{\mathbf{V}}$ stands for the corresponding pixel value on the learning sample.

By multiplying the derived matrix $\widetilde{\mathbf{G}}$ to $\tilde{\mathbf{v}}$ which stands for the pixel value of the target image in Eq. 3.30, the desirable spectral reflectance $\hat{\boldsymbol{r}}$ can be estimated by using:

$$\hat{\boldsymbol{r}} = \widetilde{\mathbf{G}}\tilde{\mathbf{v}} \tag{3.32}$$

Furthermore, there is a discussion for the relationship between the spectral properties and the amount of sample which is based on the previous research in the laboratory[13]. This relationship is way more complicated to draw a conclusion that determining either of the spectral properties or the amount of sample is the most influential factor in spectral reflectance estimation. To obtain the most accurate estimation results, it should be considered that the appropriate combination of the amount of sample and its spectral properties, and the intended application. This is also a criterion for those who wants to build up an identical system for their working environment. The components of the image acquisition system are nothing very special when listed individually. But the design of the learning sample, especially the selection of each sample will greatly influence the final accuracy of the estimation. For an instance, in the case of this study, various Japanese pigments are selected and used in the application. It can be regarded as an optimized selection for the traditional Japanese artworks. Even so, the estimated results for some types of pigments were not good enough as expected such as the pigments with shiny surface or very dark. Hence, if the proposed method especially the learning sample is employed in a western country, then the pigments or colorants may differ from Japan, which means that the selection of samples are not suitable for their artworks. To solve the above issues, constructing database in terms of different art culture, and designing particular learning sample

for different countries would be a better choice.

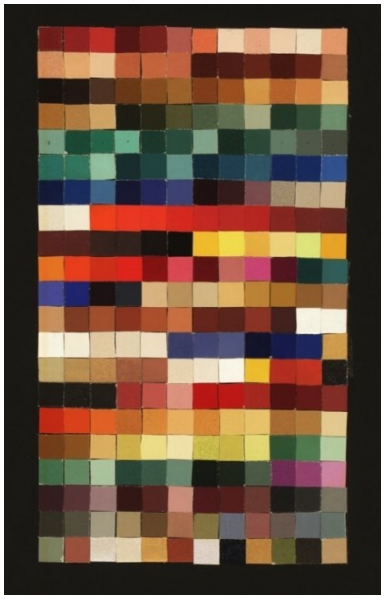

(a)

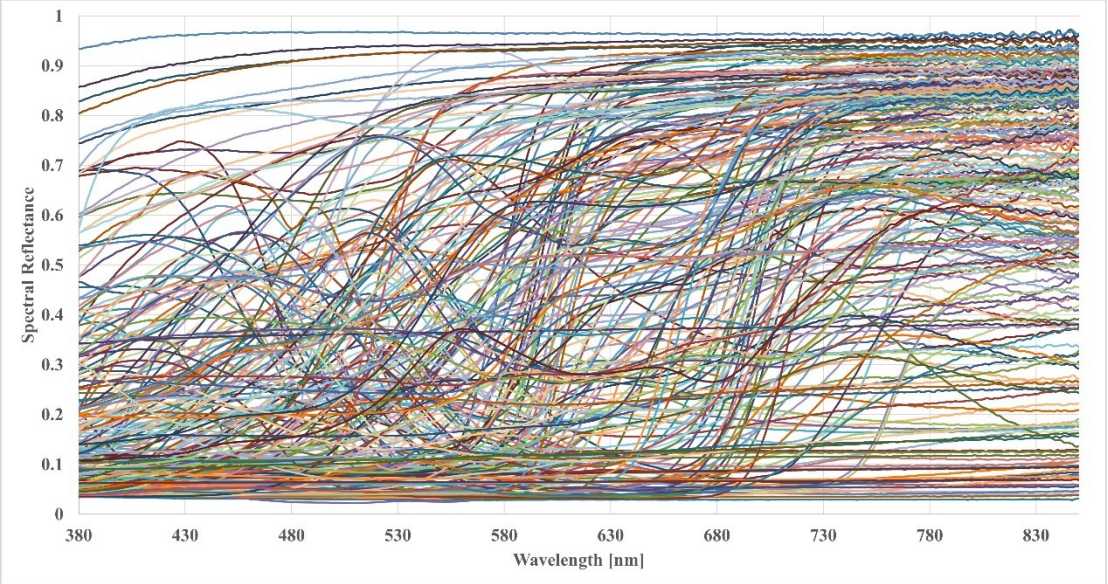

(b)

Fig. 3.5 The learning sample designed based on Japanese pigments and measured spectral reflectance data. (a) Specially designed learning sample for calculating the transformation matrix for spectral reflectance estimation; (b) Measured spectral reflectance of the 252 Japanese pigments samples, which shows well coverage of spectrum.

3.3.4 Filter Selection

Filter selection is one of the important procedures in this application. The acquired multispectral images can be affected by several factors including the filters used in the rotating filter combination, the number of the acquired images, and the initial position of the rotating filter. These factors can also affect the accuracy of spectral reflectance estimation. However, since the proposed method does not have a mechanism to control the initial position of the rotating filter for image acquisition, a simulation method is proposed for optimizing the filter selection and the number of acquired images, so that the accuracy of reflectance estimation can be maximized as much as possible. There are several proposed methods for optimal filter design in multispectral imaging technology, and based on these methods, an optimization method is developed for rotating filter. And the basis of estimation of optimal filter combination is the Wiener estimation method[14,16].

The procedure of the proposed simulation method is as shown in Fig. 3.6. Before the simulation, a learning sample[13] with known spectral reflectance data is needed, which is discussed in last subsection. The learning sample is used to calculate the conversion matrix for reconstruct spectral reflectance later, which was discussed in previous. The spectral sensitivity related data of imaging components including light source, camera module is needed for the basic imaging model of the simulation. The first step is to decide which filters to use and how many images are acquired after image processing. Then, decide the initial position of the rotating filter. Calculate the camera response corresponding to the spectral transmittance sample in the assumed situation by Eq. 3.30. Next, the regression coefficient matrix (transformation matrix or conversion matrix) is calculated by Eq. 3.22 using the spectral reflectance data matrix of the learning sample and the camera response matrix. The estimated spectral reflectance data of the learning sample is calculated by the pseudoinverse method shown in subsection 3.3.2. The error between this estimated data and the reference data is calculated by the mean absolute error as shown in following equation.

$$MAE = \frac{1}{K}\sum_{k=1}^{K}\left|\hat{\mathbf{R}} - \mathbf{R}\right| \tag{3.33}$$

The procedure of the simulation after the initial position setting are repeated. When the simulation is accomplished at all the initial positions with the combination of the filter configuration and the number of acquired images, the average, maximum and minimum values of the estimation error are evaluated as the estimation accuracy of this combination of filters. Lastly, the error at the initial position α is recorded as MAE_α, and Eq. 3.34 is used as an evaluation index.

$$\begin{matrix} \underset{\alpha}{\text{mean}}(MAE_\alpha) \\ \underset{\alpha}{\max}(MAE_\alpha) \\ \underset{\alpha}{\text{mini}}(MAE_\alpha) \end{matrix} \tag{3.34}$$

The above is all related to the simulation for optimizing the filter selection and the number of acquired images.

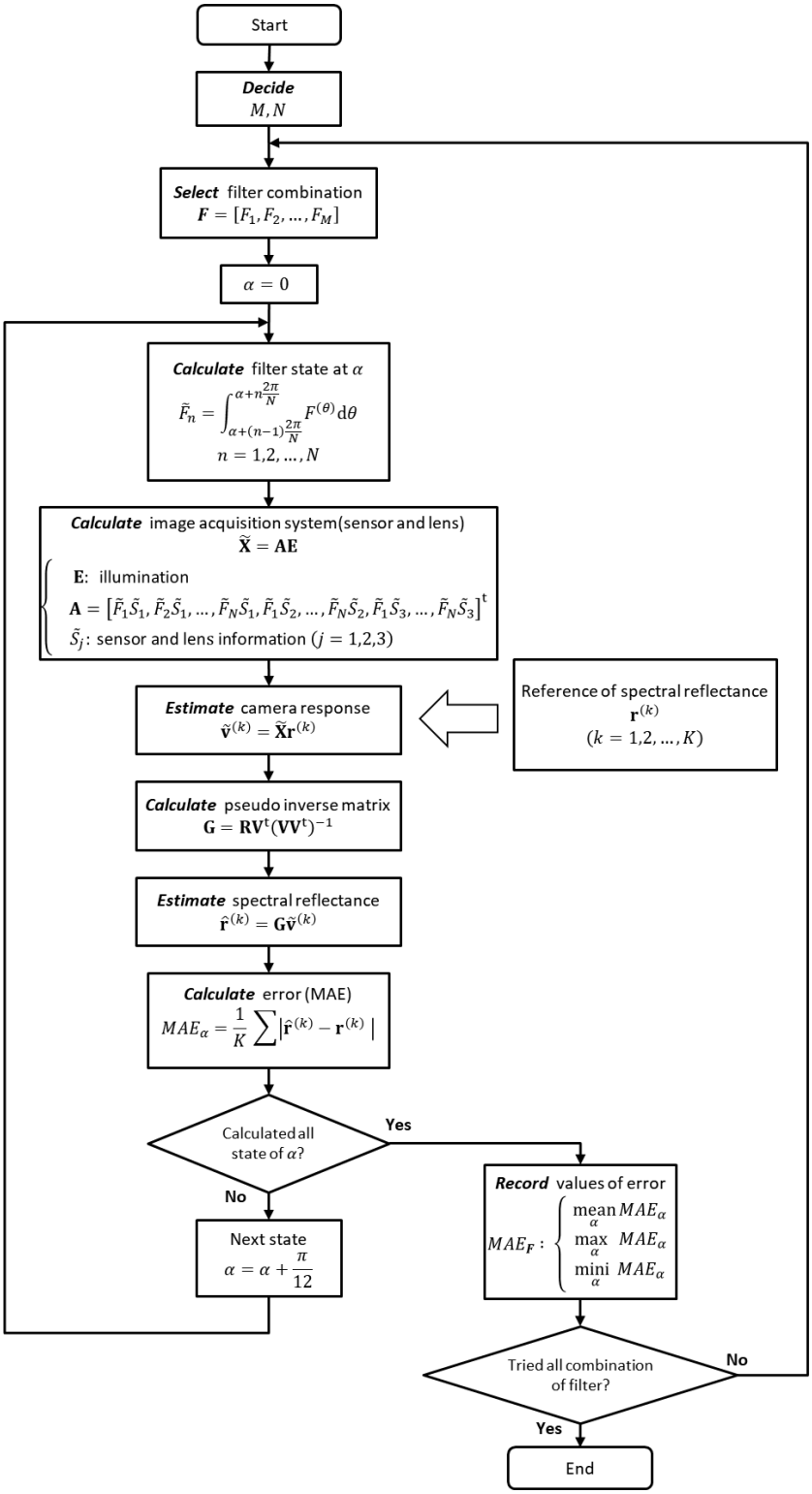

Fig. 3.6 Procedure of the simulation for filter selection

As shown in Fig. 3.7, this is the actual learning sample used in the experiment[13]. As mentioned in previous, it contains palette of Japanese organic and inorganic mineral pigments. Totally, the learning sample consists of 252 different pigments, which represent a wide variety of pigments including natural pigments and artificial pigments. Fig.3.8 shows that the reference spectral reflectance of the learning sample, which shows a broad spectrum of colors. In this study, all 29 filters from Fuji Film Corporation were investigated. Fig. 3.9 shows the spectral characteristics of the filters investigated prior to selecting the best combination for accurately reconstructing spectral reflectance. D65 illumination standard is used in the simulation and Fig. 3.10 shows its spectral distribution. The spectral transmittance data of the lens filter (Baader UV/IR-Cut/L Filter 2'' #2459210A) is shown in Fig. 3.11. Fig.3.12 gives the spectral sensitivity distribution of the color camera DS 6700 used in the simulation. The number of filters used to build the rotating filter is $M = 3, 4$, and the number of the acquired images is $N = 3, 4$. The wavelength range selected in this simulation is 400~700 nm (visible light range) with an interval 20 nm and the number of wavelength factorizations is $L = 16$. The initial position of the rotating filter α is tested with an interval $\pi/12$, and the simulation is conducted repeatedly from $\alpha = 0$ to the value that is the same as the first combination. Moreover, as a comparison with the proposed method, we also simulated the spectral reflectance estimation where three images were acquired separately with the conventional method using normal filters that does not rotate. The whole procedure of the simulation on computer were set to mimic the process in actual experimnt including the multispectral image acquisition using rotating filter, and the spectral reflectance estimation from the acquired multispectral images. The error of the estimtion was used as evaluation criteria for filter selection.

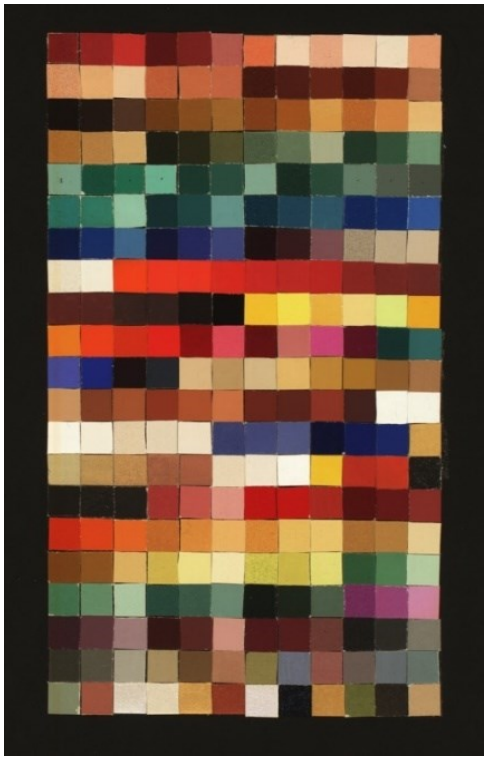

Fig. 3.7 The learning sample with specially selected Japanese pigments used for spectral estimation.

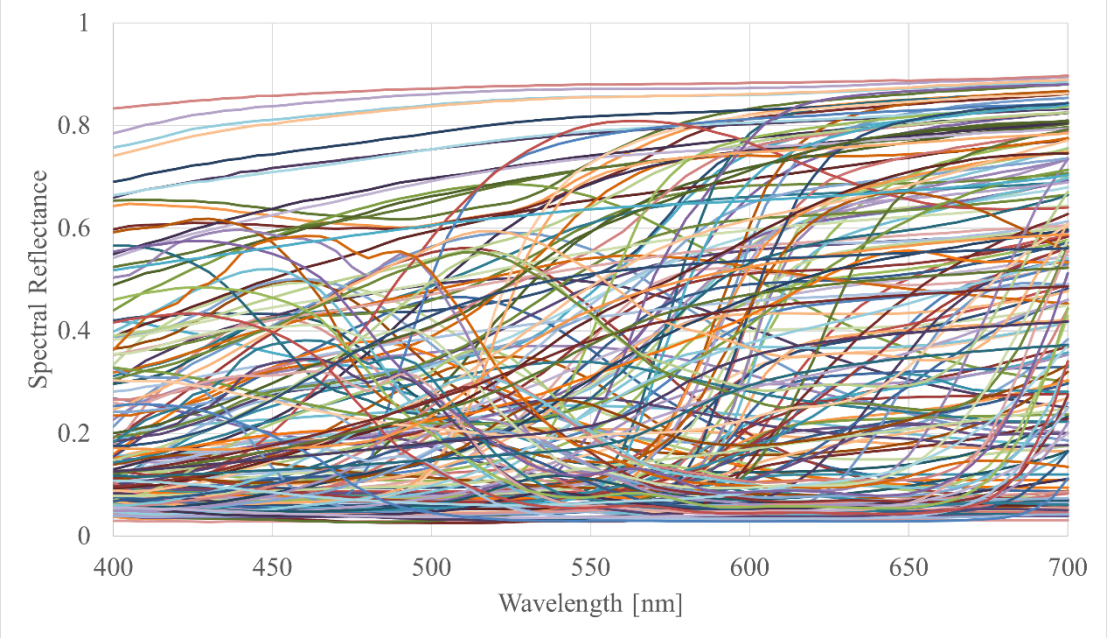

Fig. 3.8 Measured spectral reflectance of the learning sample.

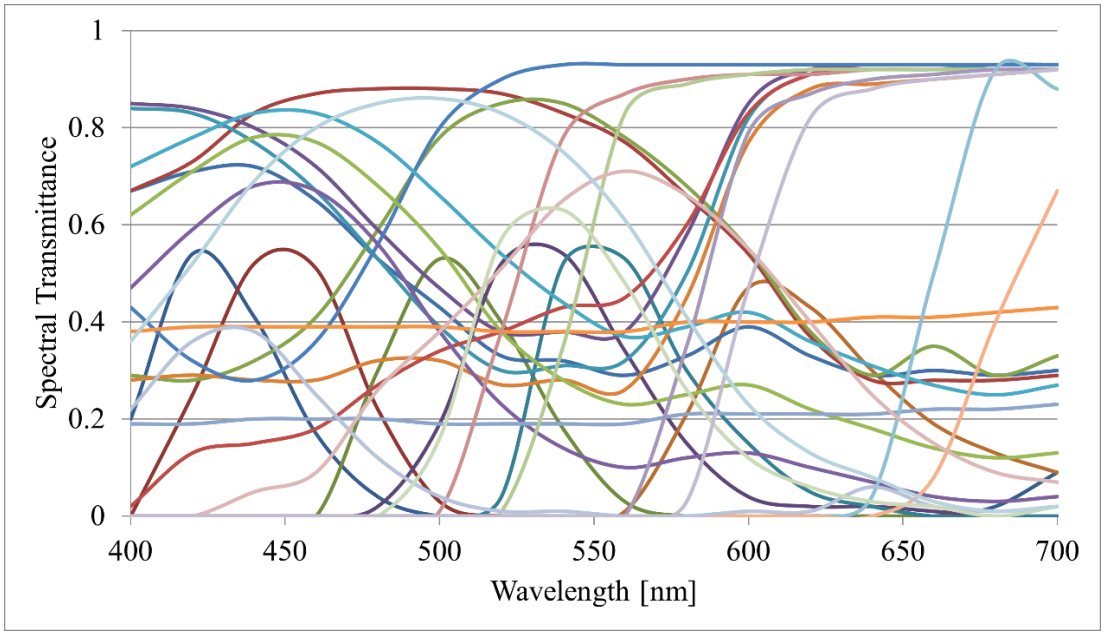

Fig. 3.9 Spectral transmittance of 29 absorption color filters used in the simulation.

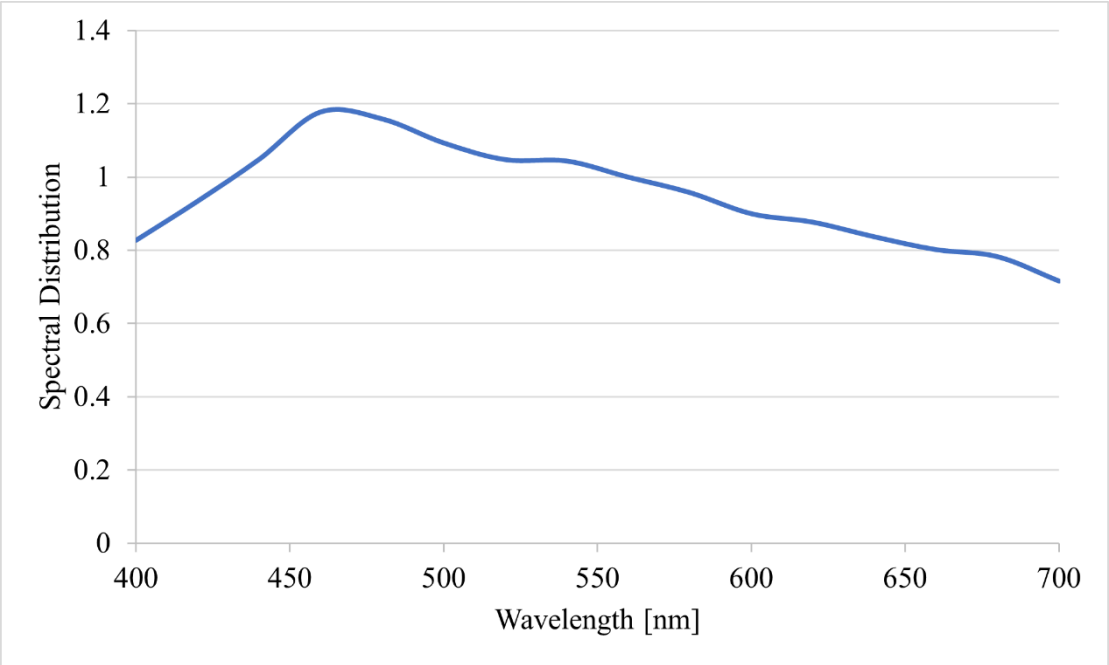

Fig. 3.10 Spectral distribution of D65 standard light source. The data values are normalized by the data in the range of 560nm.

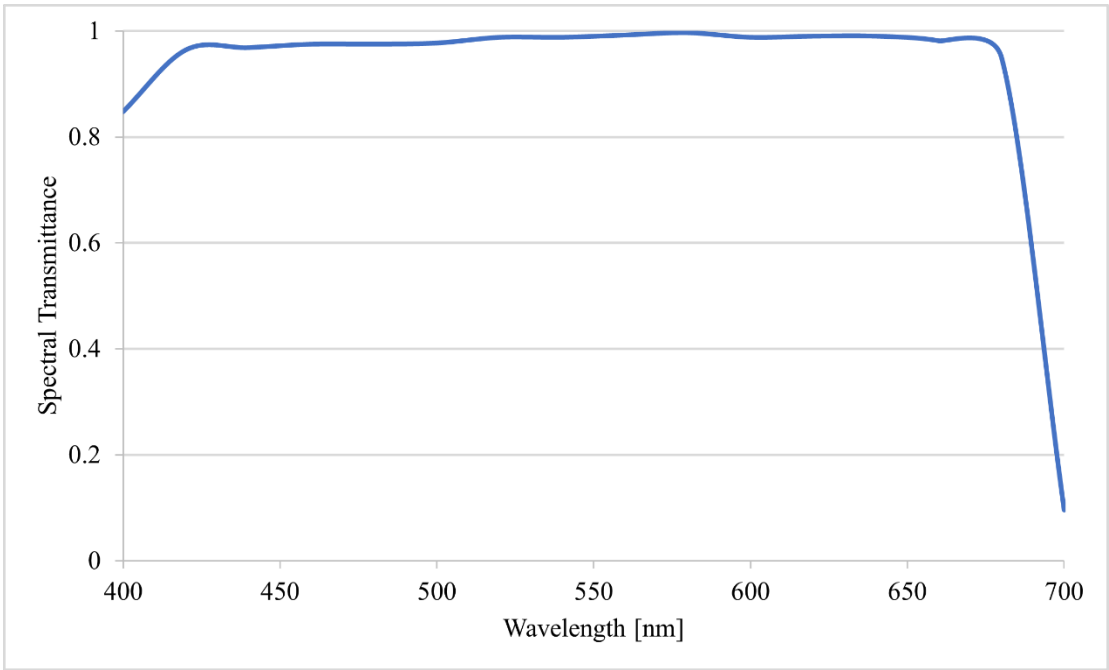

Fig. 3.11 Spectral transmittance of the UV/IR cut filter used in the experiment.

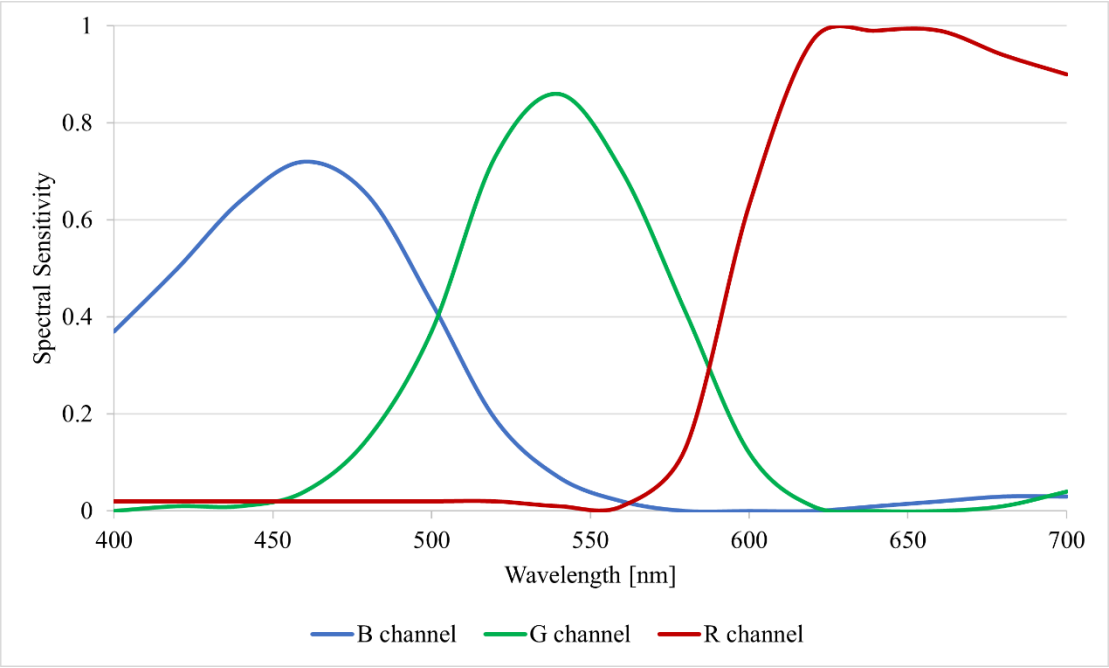

Fig. 3.12 Spectral sensitivity of Alex color camera (DS6700) used in the experiment.

Table 3.1 and Table 3.2 shows the simulation results by the proposed method and conventional method. The table of the proposed method is divided for each combination of the number of acquired images N and the number of filters used to build the rotating filter K, and each table shows the average value, maximum value, and minimum value of the error MAE_α. The filter combination of each group that has smallest average error is selected and ranked from 1st to 3rd.

In Table 3.1, the best results are obtained for the group with $M = 4, N = 4$. It can be found that this is the combination with the largest difference between the maximum value and the minimum value. Since the proposed method takes advantage of 'one scan' to make the image acquisition efficiently, the maximum value of MAE_α also needs to be taken into consideration as the optimum filter condition. The sub-accurate result is the combination with $M = 4, N = 3$. Except for the maximum value of ΔE_α of the combination with $M = 4, N = 4$, the other values are the smallest of all, correspondingly. From the result above, it can be summarized that the optimum filter combination of the proposed method is the combination of BPB42, CCM50, BPB60, and LBB20 at $M = 4, N = 3$ when the initial position α is unknown. However, if the initial position α is known to some extent, the optimum filter combination of the proposed method is the combination of BPB42, LBB20, BPB55, and ND0.7 at $M = 4, N = 4$. On the other hand, compared with the conventional method that not to use rotating filter, the filter combination with $M = 4, N = 3$ has more accurate result, while the scanning time is shorten to one-third that of the conventional method.

The experiment with actual filters is discussed in the next section. As the selected combination of the filters used to build the rotating filter, all the combinations with $M = 4, N = 3$, the most

accurate one in the combinations with $M = 4, N = 4$ are used in the experiment. As a comparison with the proposed method, two combinations of the conventional method are used in the experiment. These selected combinations of filters are named as combination A1, A2, A3, B1, C1, C2.

Table 3.1 The results of simulation for filter selection using the proposed system.

(a) $M = 3, N = 3$

	MAE ($\times 10^{-3}$)			Composed filter			
Rank	mean(MAE_α)	max(MAE_α)	mini(MAE_α)	1	2	3	4
1	4.127	4.127	4.127	BPB42	CCR50	SP5	
2	4.130	4.131	4.130	BPB42	CCG50	SP5	
3	4.152	4.152	4.152	BPB42	BPB53	BPB55	

(b) $M = 4, N = 3$

	MAE ($\times 10^{-3}$)			Composed filter			
Rank	mean(MAE_α)	max(MAE_α)	mini(MAE_α)	1	2	3	4
1	3.233	3.272	3.205	BPB42	CCM50	BPB60	LBB20
2	3.248	3.288	3.222	BPB42	CCM40	BPB60	LBB20
3	3.266	3.341	3.223	BPB42	CCB50	BPB60	LBB20

(c) $M = 3, N = 4$

	MAE ($\times 10^{-3}$)			Composed filter			
Rank	mean(MAE_α)	max(MAE_α)	mini(MAE_α)	1	2	3	4
1	4.127	4.129	4.125	BPB42	CCR50	SP5	
2	4.130	4.132	4.129	BPB42	CCG50	SP5	
3	4.200	4.201	4.199	BPB42	CCR50	LBB8	

(d) $M = 4, N = 4$

	MAE ($\times 10^{-3}$)			Composed filter			
Rank	mean(MAE_α)	max(MAE_α)	mini(MAE_α)	1	2	3	4
1	2.320	4.280	1.922	BPB42	LBB20	BPB55	ND 0.7
2	2.795	3.625	2.618	BPB42	LBB8	SP2	SP5
3	2.807	3.547	2.636	BPB42	CCR50	BPB53	SP5

Table 3.2 The results of simulation for filter selection using the conventional method.
(Three filters and RGB camera)

	MAE ($\times 10^{-3}$)	Filter combination		
Rank		1	2	3
1	4.017	BPB53	CCC50	ND 0.4
2	4.127	BPB42	CCR50	SP5
3	4.131	BPB42	CCG50	SP5

3.3.5 Experiment and Discussion

In this section, an experiment based on the simulation results and discussion shown in last section was conducted. The selected four combinations of filters, A1, A2, A3, B1, were used to build the rotating filter and applied in the image acquisition. For a comparison, two combinations of the filters, C1 and C2, were used as normal filters in the image acquisition. (Fig. 3.15) The scanning object was the same color chart with known spectral reflectance data introduced in the simulation.

The image acquisition system used in the experiment is as shown in Fig. 3.13 and the imaging mechanism is the same as mentioned in previous. The main components of the imaging system include a color camera with linear sensor manufactured by Alex (DS 6700), a lens from Nikon (MicroNikkor24mm) with a UV/IR cut filter (Baader UV/IR-Cut/L Filter 2'' #2459210A), and a group of white LED light source from CCS. The related spectral characteristic data of above components are shown in Fig. 3.12, Fig. 3.11, Fig.3.14, respectively. A motor from Oriental Motor (BXM230M-GFS) is used to drive the rotating filter.

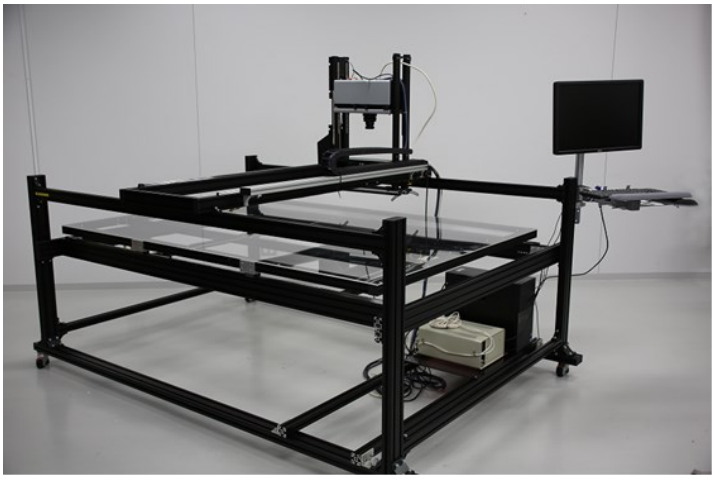

Fig. 3.13 The actual image acquisition system used in the experiment. It is a three axis high resolution scanner developed in the laboratory.

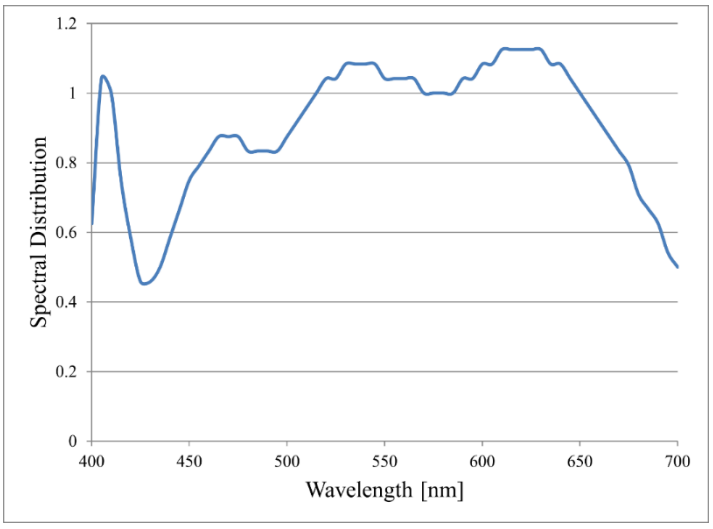

Fig. 3.14 Spectral distribution of the LED light source used in the experiment. The data values are normalized by the data in the range of 540nm.

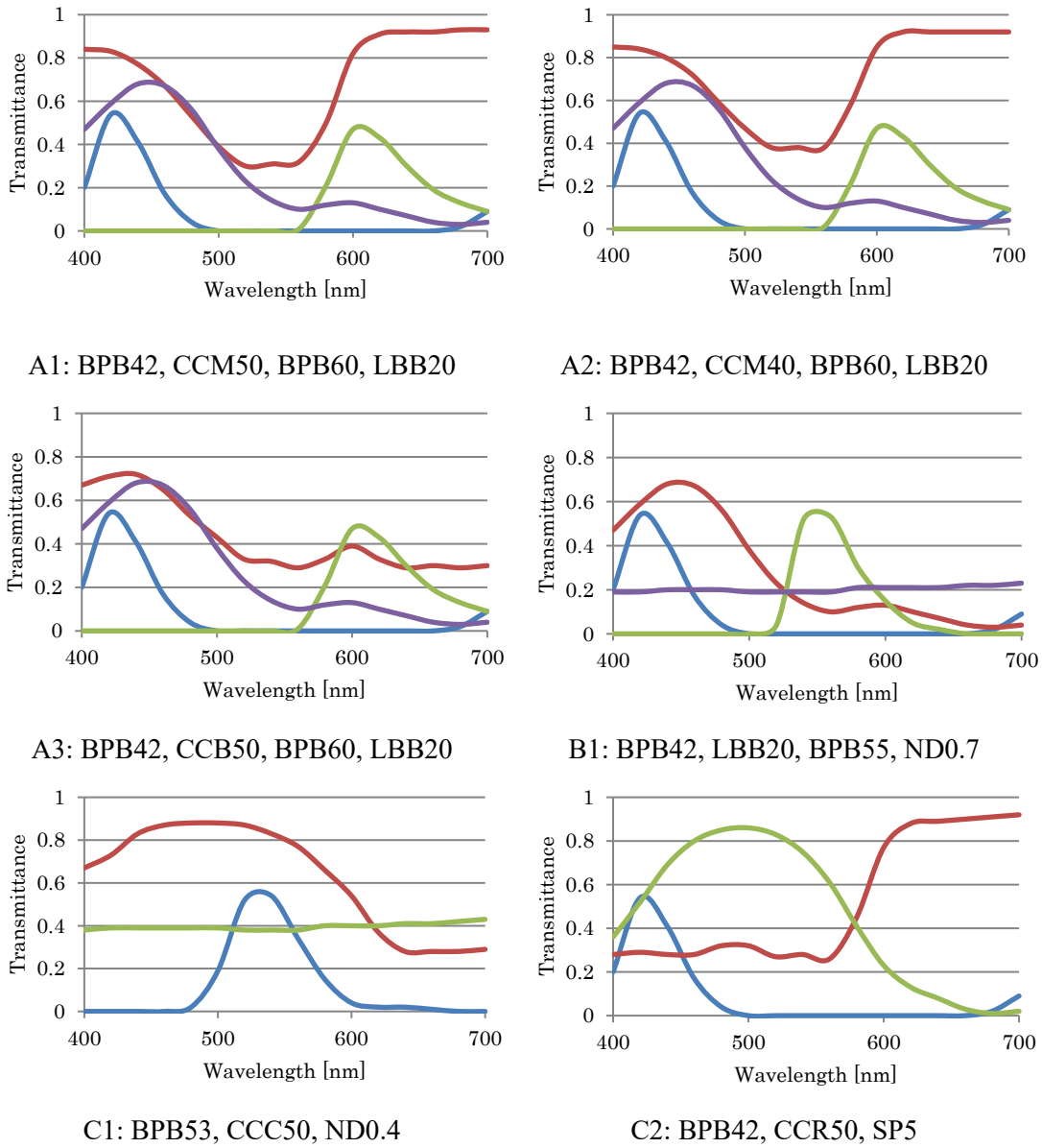

Fig. 3.15 The filter combinations used in the experiment. A1, A2, A3 and B1 were selected by the simulation for filter selection with the best performance under the proposed system; C1 and C2 were selected by the simulation with the best performance under conventional method.

For the consistency of the experiment condition, the sensitivity of the three channel R, G, B of color camera was adjusted to a same level without any filter at first. Then, the rotating filter was set in front of the camera lens and choose one that has maximum sensitivity response at the time. The white standard was set as 230. The scanning resolution was adjusted as 329 dpi, and the exposure time was 4000 μsec. Since the rotational motor has a max speed mode of 3000 rpm, to ensure the number of the acquired images is 3, 4 $(N = 3,4)$, the motor speed was set as 2500 rpm and 1875 rpm, respectively. The resolution of scanning direction was set as 329 ×2. The image acquired after one scan was stretched twice in the scanning direction, but it was taken as an acquired image by averaging two pixels adjacent to the scanning direction to make

one pixel. The wavelength range is visible light region of 400~700 nm. Since the initial position cannot be controlled when using the rotating filter, to be more rigorous, 10 scans were conducted for each filter combination. The mean absolute error (*MAE*) between the estimated spectral reflectance and the reference data of the learning sample was calculated for each scan, and the average value, maximum value, and minimum value of the *MAE* of 10-time scans were calculated. Since the conventional method (non-rotating) does not need to consider the initial position, the image acquisition with each filter was conducted once. Then, the *MAE* of the estimation was calculated.

Table 3.3 shows the mean absolute error (*MAE*) between the estimated spectral reflectance and the reference ones of the learning sample, which indicates the accuracy of the estimation results. Fig. 3.16-3.21 shows the comparison of the selected patches on the learning sample that includes moderate two, the best one and worst one of all estimated results, respectively.

Compared with the estimation results presented previously, the error in the actual experiment is approximately 5 to 6 times that of the simulation. Meanwhile, B1, which was ranked fourth by the accuracy of the estimation in the simulation, shows the best result of all. For the group $M = 4, N = 3$ including the combinations named as A1, A2, A3, the accuracy of the estimated results in the actual experiment are ranked as A3, A1, A2. The reason for these differences between the simulation and actual experiment is that the image noise factor was ignored in the simulation for calculation simplicity, which may affect the estimated results to change. Compared with the comparison of the proposed method and the conventional method, in the actual experiment, the accuracy of the estimation by the proposed method becomes worse. This may be caused by the precision of making the rotating filter.

On the other hand, when we observe the figures of the selected patch data, especially for the best results of estimated spectral reflectance, it is hardly to find the deviation between the estimated one and the reference one. In fact, the mean absolute error for these best results is $MAE = 3.356, 3.908, 4.325, 2.644\ (\times 10^{-3})$ in each case of combination A1, A2, A3, and B1. In the figure of showing the moderate estimation results, which have approximately the same error as the average error of 10-time experiment, the inflection points and outlines are very similar. It means that the estimated spectral data can be used to distinguish the reflection characteristics of the pigments on the corresponding patches. For the worst results of the estimation, the selected patches all have an almost constant spectral reflectance without volatility. To be specific, as shown in Fig. 3.22, the selected patch on the left is slightly bluish dark color with gloss, the one on the right is bright white color with gloss. In the case when encounter such kind of patches, the rough shape of the estimated spectral reflectance curve is similar with the reference data, but the value of the spectral reflectance data is lower than the reference data and the accuracy of estimation is relatively lower. In addition, the combination B1, which obtained the best result in the experiment, contains a filter 'ND 0.7'(Neutral density 0.7). Suffix number 0.7 denotes the density of the filter. The higher the number, the darker the filter. Neutral density filters are designed to reduce transmission evenly across a portion of a specific spectrum. In brief, ND filters are used to reduce the amount of light entering to the camera without affecting the color. So, the change of light amount by using this filter contributed to the accuracy of spectral reflectance reconstruction.

Table 3.3 MAE between reference and estimated value.

	MAE $(\times 10^{-2})$		
	mean	Max	mini
A1	1.793	1.982	1.704
A2	1.865	2.029	1.736
A3	1.781	1.846	1.666
B1	1.612	1.731	1.500
C1	1.731		
C2	1.621		

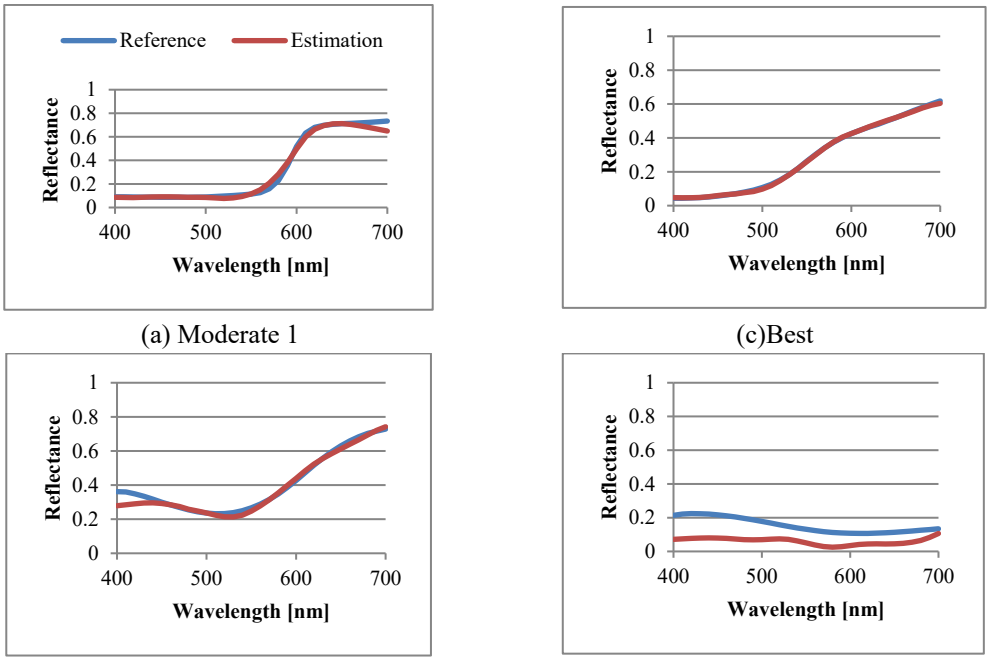

(a) Moderate 1 (c)Best

(b) Moderate 2 (d)Worst

Fig. 3.16 Typical examples of estimated spectral reflectance using filters of A1 in rotating mode. (a) and (b) show two results of the estimation with moderate error; (c) shows the best result of the estimation with minimum error; (d) shows the worst result of the estimation with maximum error, respectively.

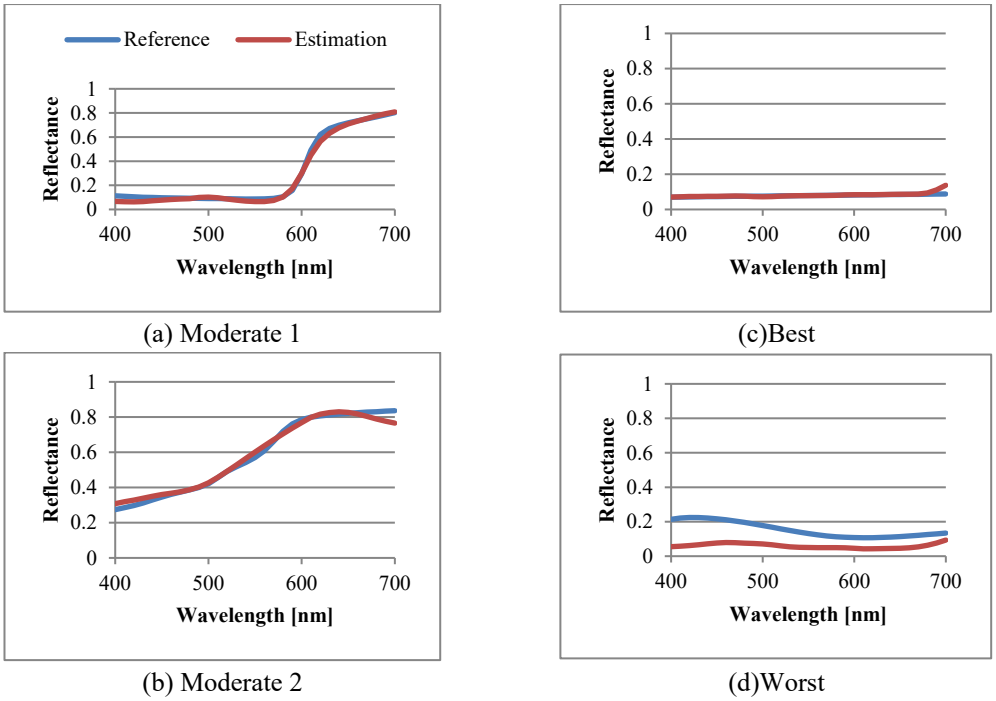

Fig. 3.17 Typical examples of estimated spectral reflectance using filters of A2 in rotating mode. (a) and (b) show two results of the estimation with moderate error; (c) shows the best result of the estimation with minimum error; (d) shows the worst result of the estimation with maximum error, respectively.

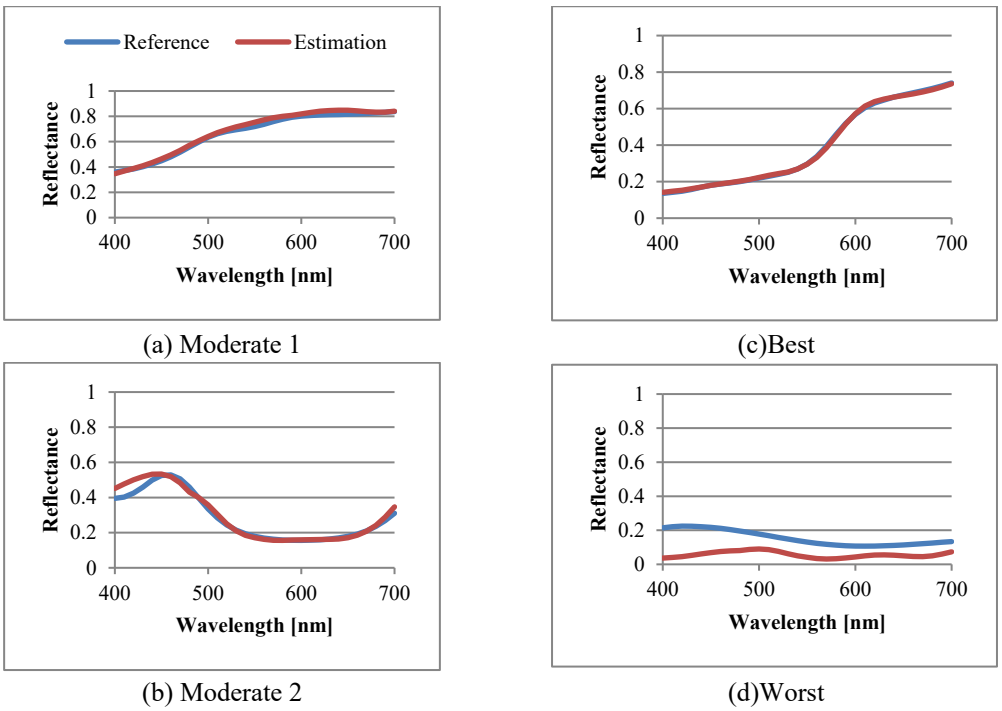

Fig. 3.18 Typical examples of estimated spectral reflectance using filters of A3 in rotating mode. (a) and (b) show two results of the estimation with moderate error; (c) shows the best result of the estimation with minimum error; (d) shows the worst result of the estimation with maximum error, respectively.

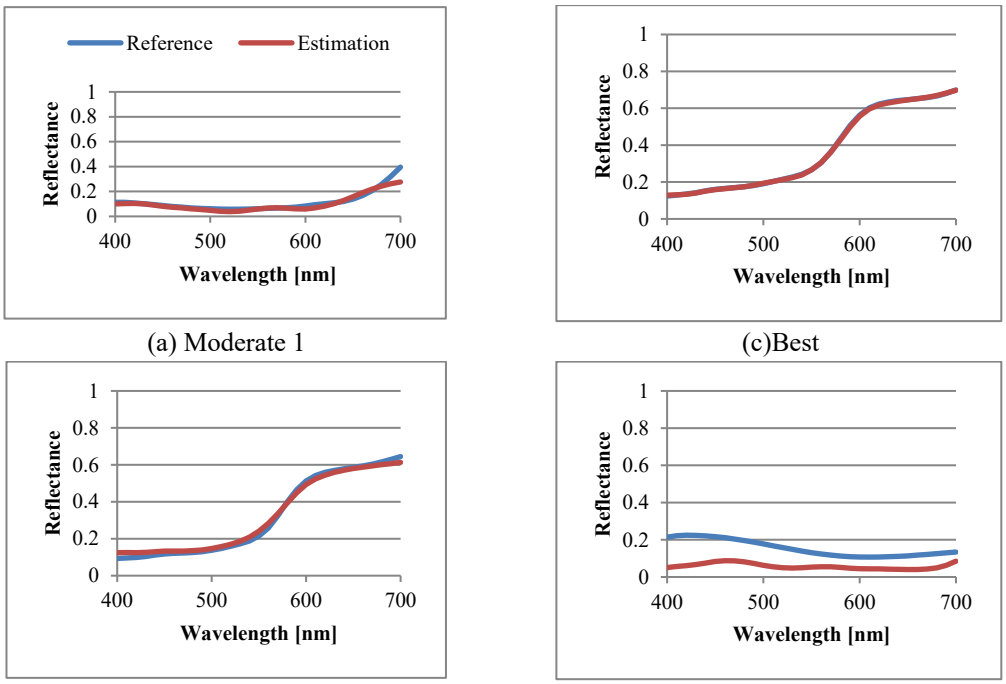

Fig. 3.19 Typical examples of estimated spectral reflectance using filters of B1 in rotating mode. (a) and (b) show two results of the estimation with moderate error; (c) shows the best result of the estimation with minimum error; (d) shows the worst result of the estimation with maximum error, respectively.

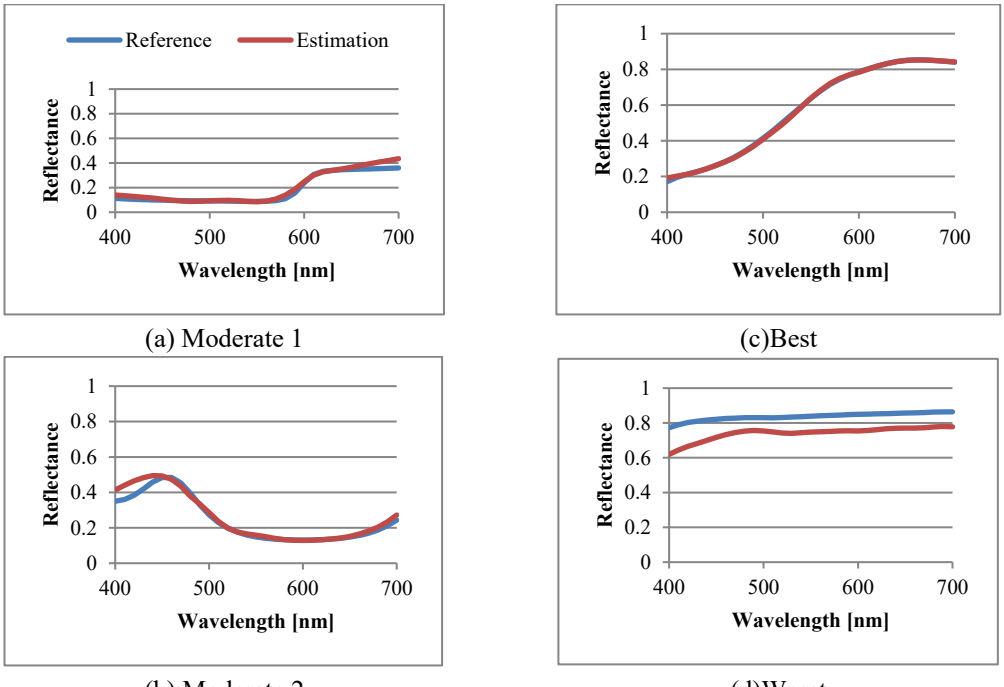

Fig. 3.20 Typical examples of estimated spectral reflectance using filters of C1 in non-rotating mode. (a) and (b) show two results of the estimation with moderate error; (c) shows the best result of the estimation with minimum error; (d) shows the worst result of the estimation with maximum error, respectively.

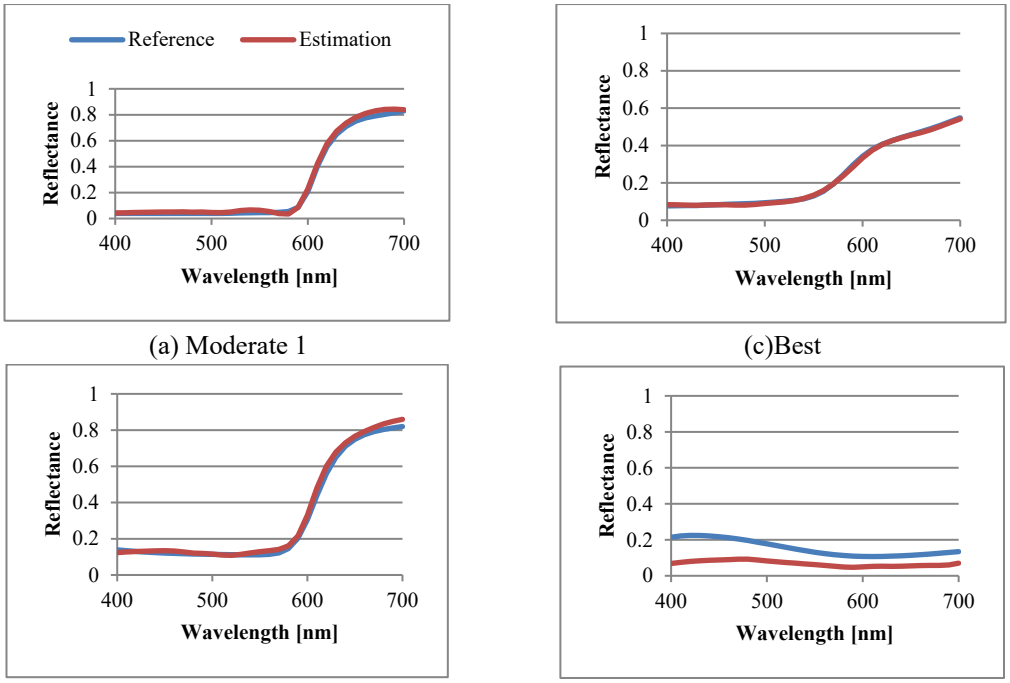

Fig. 3.21 Typical examples of estimated spectral reflectance using filters of C2 in non-rotating mode. (a) and (b) show two results of the estimation with moderate error; (c) shows the best result of the estimation with minimum error; (d) shows the worst result of the estimation with maximum error, respectively.

Fig. 3.22 Pigments which indicate worst results of estimated spectral reflectance (a) shows the pigment that corresponds to the worst results of estimation in A1,A2,A3,B1,C2. (b) shows the pigment that corresponds to the worst result of estimation in C1. These two pigments have some specular reflections.

3.4 Conclusion

A spectral reflectance estimation method based on multispectral imaging using a rotating filter scanning system is proposed. Compared to the conventional method that needs several scans to acquire relevant multispectral images, the proposed method can acquire the multispectral images with only one scan. Through a series of image processing, including image separation and interpolation processing, the processed images are used in the estimation of spectral reflectance. The concept of the proposed image acquisition system and its imaging mechanism are explained at first. The related image processing procedure for the image obtained by the

proposed system is described in detail. An evaluation of spatial resolving power of the system is also presented to show the system is capable of such application.

After that, the issue related to the estimation of spectral reflectance is discussed. The method using a learning sample is employed in this study. It means that a calibration target is first used to build the transform between camera signals and spectral reflectance factor, and after that, camera signals of other targets can be transferred into spectral reflectance factor. Followed by a mathematical model of applying the proposed image acquisition system is described. A simulation is conducted to optimize the filter selection, so that the accuracy of reflectance estimation can be maximized as much as possible.

Lastly, an actual experiment is conducted on the learning sample using the proposed rotating filter selected in the simulation. However, there is some contradiction between the actual experimental result and the simulation result. The reason is probably the result of image noise and the precision of self-made rotating filter. So, this is also a future work to implement the simulation that takes into account the effects of image noise and to design a more physically ideal rotating filter. The accuracy of the estimated spectral reflectance is comparable to the results acquired by the conventional method, especially when efficiency issue is considered. On the other hand, since the learning sample used in the experiment consists of the square with a side length of 10 mm, it can be observed that the decrease of resolution caused by the image separation and interpolation did not affect the accuracy of the estimation. But a more robust method to make sure that the same accuracy can be achieved when encounter more precise or complex object is still a future task.

3.5 References

1) J. A. Toque: "Multispectral Imaging: the influence of lighting condition on spectral reflectance reconstruction and image stitching of traditional Japanese paintings", International Joint Conference on Computer Vision (Imaging and Computer Graphics Theory and Applications (VISIGRAPP)), pp.13-20 (Feb. 2009)

2) J. A. Toque, Y. Sakatoku and A. Ide-Ektessabi: "Analytical imaging of cultural heritage paintings using digitally archived images", Computer Vision and Image Analysis of Art, 7531, pp.75310N (Feb. 2010)

3) J. Y. Hardeberg: "Acquisition and reproduction of color images: colorimetric and multispectral approaches", Universal-Publishers, USA, pp.50-51 (2001)

4) J. R. Mansfield, M. Attas, C. Majzels, E. Cloutis, C. Collins and H.H. Mantsch: "Near infrared spectroscopic reflectance imaging: A new tool in art conservation", Vibrational Spectroscopy, 28, pp.59-66 (2002)

5) R. Ogino, J. A. Toque, P. Zhang, and A. Ide-Ektessabi: “A High Speed Dynamic System for Scanning Reflective Surface with Rotating Polarized Filters”, Digital Heritage. Progress in Cultural Heritage: Documentation, Preservation, and Protection. Euro Med 2014. Lecture Notes in Computer Science, 8740, pp. 59-69 (2014)

6) R. H. Wade: "A brief book at imaging and contrast transfer", ultramicroscopy, 46, pp.145-

156 (1992)

7) G. D. Boreman: “Modulation Transfer Function in Optical and Electro-Optical Systems”, SPIE Press, Bellingham, WA (2001)

8) Y. Zhao and R. S. Berns: “Image-based Spectral Reflectance Reconstruction using the Matrix R Method”, Color Research & Application, 32, 5, pp. 343-351 (2007)

9) M. Yamaguchi, H. Haneishi, and N. Ohyama: “Beyond red–green–blue (rgb): Spectrum-based color imaging technology”, Journal of Imaging Science and Technology, 52, 1, pp. 10201-1 (2008)

10) J. Barata and M. Hussein: “The Moore-Penrose Pseudoinverse: A Tutorial Review of the Theory”, Brazilian Journal of Physics, 42, 1-2, pp. 146-165 (2012)

11) V. Cheung, S. Westland, C. Li, J. Hardeberge, and D. Connah: J. Opt. Soc. Am. A 22, pp. 1231-1240 (2005)

12) N. Shimano, IEEE Trans. Image Process, 15, 1848-1856 (2006)

13) J. A. Toque: “Material Investigation through High-resolution Analytical Imaging and Spectrometry” (Doctoral Degree Thesis), Kyoto University, 2013

14) D. C. Day: “Filter Selection for Spectral Estimation Using a Trichrmatic Camera” (Master Degree Thesis), R.I.T, 2001

15) Y. Murakami, K. Fukura, M. Yamaguchi, N. Ohyama, Optics Express, 16, 6, 4106-4120 (2008)

16) H. Haneishi: “Filter Optimization for Accurately Estimation Spectral Reflectance”, Journal of the Society of Photography and Imaging of Japan, 65, pp. 245-250 (2002) [in Japanese].

17) Y. Miyake: “Analysis and evaluation of digital color images (Second edition)”, University of Tokyo Press, Tokyo, pp. 95-111 (2000)

Chapter 4

Color Reproduction of Ultrahigh-Resolution Transmissive Scanned Images of Glass Plate Negatives

4.1 Introduction

Cultural heritage objects are threatened with the destruction caused by decay or damage due to aging, unpredictable natural and man-made disaster such as fire, earthquake, and war. Deterioration or disappearance of any cultural or natural heritage constitutes a great loss to all nations of the world. Due to the precious nature of cultural heritage, it is necessary to choose a proper solution for their preservation and conservation. There are various methods nowadays that can record different information of cultural heritage, such as color, shape, spectral reflectance, etc. Such recording methods also refer to digital archiving which has been gathering increasing interests of researchers in the past few years[1,2]. The motivation is to ensure that future generations could inherit and admire these amazing works.

A variety of technologies have been applied to the preservation of cultural heritage. Photography is one of the leading techniques which provides a new frontier to the field of archiving. However, due to the limitation of the technique development in the old days, some of the archiving results cannot satisfy all the demands, especially in some exceptional scenarios. For an instance, Horyuji Kondo wall painting, which belongs to UNESCO World Heritage Site under the name Buddhist Monuments in the Horyuji Area, was photographed onto a one-to-one scale glass dry plate with multiband filters (Appearance color: Yellow, Red, Green, Blue) 85 years ago (1935) [3]. These glass-based dry plates are the only documentation material that recorded the original appearance of the wall painting during that time, but the coating layer is now fragile and sensitive to storage conditions[4]. A calamitous fire that broke out later in 1949 which resulted in the severe damage to the wall paintings[5]. Fortunately, the color image of the wall painting can be reproduced using the glass dry plates by a traditional technique with the negative-positive process. However, this reproducing process that is known as collotype printing[6], reproduces the color by a trained craftsman using the glass dry plates manually. The only evaluation criteria for the reproduction is the experience of the craftsman. This is very subjective.

Area sensor-based imaging system is widely used in the digital archiving nowadays. This technique can accomplish the image acquisition work easily and efficiently. Such imaging system offers fairly uniform light distribution, relatively high resolution and relatively accurate color rendering[7]. However, if an area sensor-based imaging system and a linear sensor-based imaging system are compared under an identical imaging setup condition including the same theoretical imaging resolution, the light source, etc., it has some demerits that commonly manifested as geometric image distortion and insufficient resolution. In terms of the imaging mechanism and structure feature, a line sensor-based imaging system has higher detail expressiveness and higher spatial resolving capability than an area sensor-based ones, which makes it more suitable for resolving fine details of cultural heritage. In addition, a line sensor-

based camera is a better choice for recording color of cultural heritage with higher color fidelity. The most crucial point is that the line sensor based-camera has less geometrical optic problem for imaging and no issue of pixel interpolation[8,9]. Since the object employed in this study is a transmissive glass dry plate, which require high resolution, a transmission-type imaging system with a linear sensor is well suited for such objects. It can also cover a bigger area which reduces the acquisition and postprocessing time.

Using high-resolution scanning technology, high-quality image acquisition of the glass dry plate is guaranteed. For high-precision color reproduction, a method for producing one color image by incorporating the color information of each filter into the multiband images is proposed. The color information of the multiband filters is based on the mathematical relationship between the spectral characteristics and different standard color spaces. The RGB information of each filter is used to calculate a parameter named as filter coefficient, which is used in color reproduction together with acquired multiband images. Additionally, a standard IT8.7/2 color chart is captured as a target object to evaluate the accuracy of color reproduction result[10,11]. The influence of light intensity per filter on color reproduction is also investigated.

Therefore, in this study, a specially designed scanner was developed for the image acquisition of the glass dry plate in high resolution. On the other hand, to ensure that the true color of the wall painting was reproduced systematically and faithfully, much attention was also paid to develop a color reproduction method utilizing the information of multiband filters, which is a solution to maximize the use of the remaining documentation materials.

4.2 Image Acquisition of Glass Dry Plate of Horyuji Wall Painting

4.2.1 Mechanism of Imaging System

Scanning technology used in digitally archiving cultural heritage has been developing for many years. Compared with conventional photographic technique, it can offer better uniform light distribution, higher resolution, and more accurate color. However, most conventional scanners are strict with object dimension and some of them need contact to flatten the object surface, which is a severe issue for archiving cultural heritage. Additionally, with development of display and other output technology such as high-quality printing, increasing demands for high-resolution image and high-fidelity color reproduction have been growing rapidly. For this reason, in this study, a high-resolution flatbed scanner for digitizing large format transmissive object is designed. The scanner provides wide scanning resolution that ranges from 600-3000 dpi, and it is also capable of high-fidelity color reproduction.

All the high-resolution images were acquired by the scanning system as shown in Fig. 4.1. The scanning system mainly includes a line-sensor based camera module, a stepping motor for driving the object stage, an LED light source group which is well designed for high color fidelity and minimum light irradiation, and a scanner frame structure. The line-sensor based camera module consists of a monochrome CMOS camera TLC-8000CL manufactured by Takenaka which has 8000 pixels for the single channel, and an ApoRodagon-N 105mm lens with a UV-IR cut filter. The LED light source is a linear light source in which point light sources

are arranged in a line. In the transmissive imaging mechanism, transmitted light with a very high directivity of the light source is acquired by the camera because the light source is installed just facing the camera. As a result, the image shows a clear array of point light sources. In order to obtain uniform transmitted light with the camera, an appropriate distance was taken between the light source and the object and installed an acrylic resin panel in front of the LEDs. The panel made of acrylic resin plays a role as a diffuser, and the light from the point light source is diffusely reflected between particles in the acrylic resin, so that the light emitted from the panel becomes diffuse light.

In this study, the scanner was used to digitize the object at 2400 dpi. At this high-resolution setting, the image of the whole object cannot be acquired within only one scan but multi-scans. The object needs to be moved with fixed interval along the sub-scanning direction for several scans. Finally, all acquired images can be stitched to form the complete image of the object. Since the width of glass dry plates of Horyuji Kondo wall painting is 45 cm, in terms of the scanning setting, one glass dry plate needs nine scans with a 5 cm moving interval along the sub-scanning direction for each scan.

Before a scanning work, adjusting the light intensity is a necessary process. This is also required for calibrating the uneven distribution of light in image processing. In the case of utilizing a transmissive imaging device, the white point is defined as light with 100% transmittance in which nothing is placed on the object stage. Additionally, the maximum pixel value of the gradation should be adjusted to around 220. The reason for this setting is to avoid causing too much image noise.

4.2.2 Digital Archiving of Horyuji Kondo Wall Painting

A fire broke out in the Kondo (Main Hall) of Horyuji in Nara Prefecture, Japan, on January 26th, 1949. As a result, severe burnt damage destroyed the precious wall painting located in Kondo, which is a disaster to the entire art world and to Buddhism in general. In terms of the related historical material, it is agreed that the wall paintings were made around A.D. 700 which means the artworks are already 1300 years old. Theoretically, it may represent the early iconic east Asian painting skill and is the prototype for the relevant artwork appeared from then on.

Many preservations and restoration works had been done before the fire, including repairing the building structure, making copies of the wall painting, etc. Among these works for the preservation, fortunately, a photographic archiving project let the image of the wall painting survived. The wall painting was photographed onto a glass based dry plate which is an improved photographic plate invented by Richard Leach Maddox in 1871. Compare with the old plastic film, the glass based dry plate is more stable, less prone to deterioration and could be stored for longer time. However, the fact is that the coating layer is still fragile to protect and sensitive to the storage conditions. So, the high-resolution imaging system introduced in the last section was used to digitally archive these precious artworks.

The images of the glass dry plates of Horyuji wall painting acquired by the proposed imaging system are as shown in Fig. 4.2. These images are copies of the original negatives taken through four filters with different extraction wavelength ranges. In this study, the glass dry plates

imaged through yellow, red, green and blue filters are defined as glass dry plate black(K), cyan(C), magenta(M) and yellow(Y), respectively. The filters used in the experiment of this study are addressed in detail in the next section.

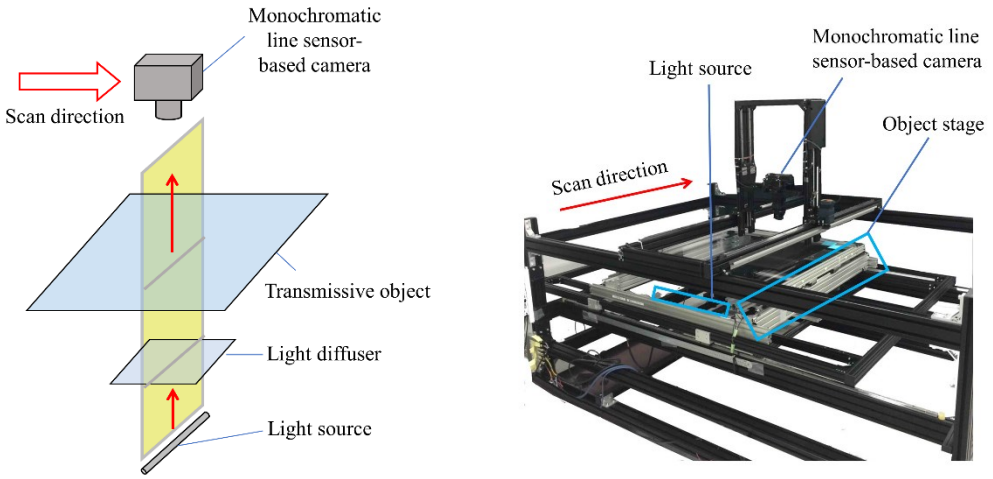

(a) (b)

Fig. 4.1. Schematic representation of the high-resolution scanner used in this study. (a) shows a schematic diagram of the transmission type scanner; (b) shows a photograph of the transmission type scanner used in the experiment.

C M Y K

Fig. 4.2. The images of the glass dry plates of Horyuji wall painting acquired by the proposed imaging system. Four pieces of glass dry plates imaged through red, green, blue, and yellow filters are defined as the images of glass dry plate cyan(C), magenta(M), yellow(Y) and black(K), respectively.

4.3 Empirical Color Reproduction Derived from the Original Archiving Filters

The process of photographic project conducted 85 years ago can be regarded as a type of multi-band imaging process for recording the appearance of the wall painting. If the acquired four images are used to reproduce the color of the wall painting, from the definition of the CIE 1931XYZ color space[13], it is necessary to know the spectral reflectance information of the actual object, which in this case is the spectral reflectance information of the wall painting itself. However, the wall painting no longer exists, it is impossible to obtain this information. So, the spectral information of four color filters were used to calculate the filter coefficient which stands for the ratio of RGB components in each filter. Then the filter coefficients are used to calculate with the pixel values of the acquired multiband monochromatic images to obtain the corresponding RGB channel values of the wall painting. As stated in the introduction of this chapter, reproducing the color of the wall painting by filter coefficient is a solution to maximize the use of the remaining documentation materials.

The multiband filters used in this study are shown in Fig. 4.3. These filters were the same ones used to photograph the wall painting onto the glass dry plates about 85 years ago. For convenience, the filters are named as filter 1, 2, 3 and 4, where the corresponding glass dry plates are named as glass dry plate black(K), cyan(C), magenta(M) and yellow(Y), respectively. The CMYK color is a subtractive color model commonly used in color printing. It is also known as process color or four color. The ink reduces the light that would otherwise be reflected. Such a model is called subtractive because inks subtract the colors red, green, blue from white light. White light minus red leaves cyan, white light minus green leaves magenta, and white light minus blue leaves yellow. This is also how the four color filters were used to separate color of the wall painting into cyan, magenta, and yellow to produce four glass dry plates. The yellow filter is used to produce black glass dry plate. In printing engineering, to produce deeper black tones, unsaturated and dark colors are produced by using black plate instead of the combination of cyan, magenta, and yellow.

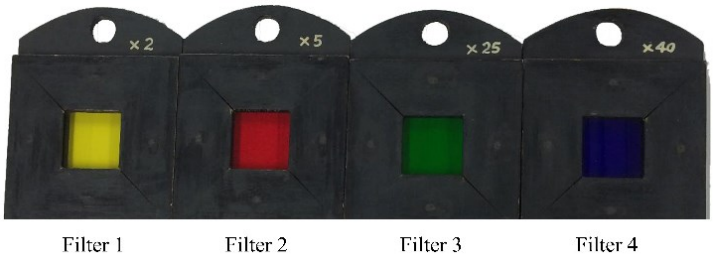

Fig. 4.3. Filters used for four color separation: corresponding to glass dry plate K, C, M and Y from the left. CMYK color is a subtractive color model commonly used in color printing. Such a model is called subtractive because inks subtract the colors red, green, blue from white light. After photographing with the four color filters, the color of object is separated into cyan, magenta, yellow and black. These four colors' components are recorded on the glass dry plates. The black glass dry plate is used to produce deeper black tones.

The calculation of the filter coefficient needs color information of the color filters, which includes spectral transmittance, XYZ value and RGB value of each filter. A spectrophotometer was used to measure the spectral transmittance of four-color filters. The spectrophotometer is C10083M manufactured by Hamamatsu, which is capable of measuring the wavelength of 320 nm to 1000nm. The light source is a halogen lamp manufactured by Sumita. The measured spectral transmittances of the filters are shown in Fig. 4.4.

The CIE 1931XYZ color space[13] was established by the International Commission on Illumination (CIE) in 1931, which defined 3 standard primaries named X, Y and Z. The color space can be a quantitative link between distributions of wavelength in the electromagnetic visible spectrum, and physiologically perceived colors in human color vision. Notably, the XYZ color space is an independent color space, and the related mathematical relationships are useful tools when encountering color issue in many applications such as using digital cameras, displays and scanners[14].

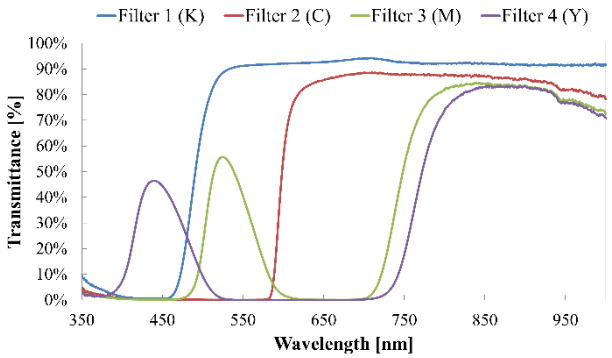

Fig. 4.4. The measured spectral transmittance of four-color filters.

Once the spectral information of the filters are obtained, according to the CIE's color matching functions $\bar{x}(\lambda), \bar{y}(\lambda), \bar{z}(\lambda)$, the XYZ values can be calculated by the following equation. The wavelength range is 400 nm to 700 nm named visible range.

$$\begin{aligned} X &= k\sum_{400}^{700} S(\lambda)\bar{x}(\lambda)T(\lambda)\Delta\lambda \\ Y &= k\sum_{400}^{700} S(\lambda)\bar{y}(\lambda)T(\lambda)\Delta\lambda \\ Z &= k\sum_{400}^{700} S(\lambda)\bar{z}(\lambda)T(\lambda)\Delta\lambda \end{aligned} \tag{4.1}$$

Where k is a constant and can be expressed by the following equation.

$$k = \frac{100}{\sum_{400}^{700} S(\lambda)\bar{y}(\lambda)\Delta\lambda} \tag{4.2}$$

In Eq. 4.1, $S(\lambda)$ denotes the spectral radiance of the illumination, $\bar{x}(\lambda), \bar{y}(\lambda), \bar{z}(\lambda)$ is the CIE's color matching functions, $T(\lambda)$ denotes the spectral transmittance, $\Delta\lambda$ denotes the wavelength interval for calculation of tristimulus values. In this paper, the D_{65} standard light source is employed; the viewing angle of the observer is 2 degrees; the wavelength interval is 10 nm. $S(\lambda)\bar{x}(\lambda), S(\lambda)\bar{y}(\lambda), S(\lambda)\bar{z}(\lambda)$ are weight factors, and the value specified in JIS Z8722[15] is used.

In this study, we assume that output devices are compliant with sRGB[16], which is generally used for many common electronic output devices. Then, to transform from XYZ to sRGB (with D_{65} white point), the matrix transform is used as shown in Eq. 4.3.

$$\begin{bmatrix} R_{sRGB} \\ G_{sRGB} \\ B_{sRGB} \end{bmatrix} = \begin{bmatrix} 3.2406 & -1.5372 & -0.4986 \\ -0.9689 & 1.8758 & 0.0415 \\ 0.0557 & -0.2040 & 1.0570 \end{bmatrix} \begin{bmatrix} X \\ \mathrm{Y} \\ \mathrm{Z} \end{bmatrix} \tag{4.3}$$

After converting from XYZ to sRGB, gamma correction is applied using the following Eq. (4) and output in 8-bit values. $\gamma = 2.4$ is applied to Eq. 4.4.

$$\begin{aligned} R_{8bit} &= floor\left[\left(1.055 \times {R_{sRGB}}^{1/\gamma} - 0.055\right) \times 255 + 0.5\right] \\ G_{8bit} &= floor\left[\left(1.055 \times {G_{sRGB}}^{1/\gamma} - 0.055\right) \times 255 + 0.5\right] \\ B_{8bit} &= floor\left[\left(1.055 \times {B_{sRGB}}^{1/\gamma} - 0.055\right) \times 255 + 0.5\right] \end{aligned} \tag{4.4}$$

The CIE 1976 $\mathrm{L}^*a^*\mathrm{b}^*$ color space[17] was defined by the CIE in 1976. L^* indicates lightness, a^* is the red or green coordinate, and b^* is the yellow or blue coordinate. More specifically, along the a^* axis, $+a$ direction represents a shift toward red; along the b^* axis, $+\mathrm{b}$ direction represents a shift toward yellow. The center L^* axis shows $\mathrm{L}^* = 0$ (black or total absorption) at the bottom.

The XYZ value can be converted to the $\mathrm{L}^*a^*\mathrm{b}^*$ value using the equations as follows:

$$\begin{aligned} \mathrm{L}^* &= 116f(Y/Y_n) - 16 \\ a^* &= 500[f(X/X_n) - f(\mathrm{Y}/Y_n)] \\ \mathrm{b}^* &= 200[f(Y/Y_n) - f(\mathrm{Z}/Z_n)] \end{aligned} \tag{4.5}$$

where,

$$\begin{aligned} f(X/X_n) &= \begin{cases} (X/X_n)^{1/3}, & X/X_n > 0.008856 \\ 7.787(X/X_n) + 16/116, & X/X_n \le 0.008856 \end{cases} \\ f(Y/Y_n) &= \begin{cases} (Y/Y_n)^{1/3}, & Y/Y_n > 0.008856 \\ 7.787(Y/Y_n) + 16/116, & Y/Y_n \le 0.008856 \end{cases} \\ f(Z/Z_n) &= \begin{cases} (Z/Z_n)^{1/3}, & Z/Z_n > 0.008856 \\ 7.787(Z/Z_n) + 16/116, & Z/Z_n \le 0.008856 \end{cases} \end{aligned} \tag{4.6}$$

X, Y, Z describe the color stimulus considered and X_n, Y_n, Z_n represent a specified white reference illuminant condition. The equations for calculating the CIE XYZ, sRGB and CIE

1976 L*a*b* values are addressed above. The obtained color information of 4 filters is shown in Table 4.1.

Table 4.1. Color information of the filters

	Filter 1 (K)			**Filter 2 (C)**			**Filter 3 (M)**			**Filter 4 (Y)**		
XYZ	71	86	11	30	14	0	9	26	3	7	2	39
RGB	248	245	0	226	0	0	0	170	0	0	0	172
L*a*b*	94	-20	96	44	80	73	58	-89	69	17	67	-85

When the multiband imaging technique is applied to an object, m spectral images of the object can be obtained in correspondence with m filters with specific wavelength range respectively. For reproducing the color of the wall painting, in this study, we proposed a color reproduction method using filter coefficient to synthesize one color image by incorporating the color information of each filter into the multiband images.

Let $r(i), g(i), b(i)$ be the RGB value of the $i(i = 1,2,\cdots,m)$ th filter, and let $r_p(i), g_p(i), b_p(i)$ be the ratio of each channel to the total channels in RGB of each filter respectively. Then we have following equations:

$$\begin{aligned} r_p(i) &= \frac{r(i)}{r(i)+g(i)+b(i)} \\ g_p(i) &= \frac{g(i)}{r(i)+g(i)+b(i)} \\ b_p(i) &= \frac{b(i)}{r(i)+g(i)+b(i)} \end{aligned} \tag{4.7}$$

Now we know the ratio of each channel to the total channels in one filter, then we can calculate the ratio of each channel in this filter to the corresponding channel in all filters. If we define this ratio as $r_f(i), g_f(i), b_f(i)$, we can obtain:

$$\begin{aligned} r_f(i) &= \frac{r_p(i)}{\sum_i^m r_p(i)} \\ g_f(i) &= \frac{g_p(i)}{\sum_i^m g_p(i)} \\ b_f(i) &= \frac{b_p(i)}{\sum_i^m b_p(i)} \end{aligned} \tag{4.8}$$

The $r_f(i), g_f(i), b_f(i)$ here is named as filter coefficient.

The filter coefficients are used to calculate with the pixel values of the acquired multiband

monochromatic images to obtain the corresponding channel values of the wall painting. If we define the monochromatic image as $V(i)$ scanned with $i(i = 1,2,\cdots,m)$ th filter, and define the calculated corresponding channel value as V_r, V_g, and V_b, we have following equations:

$$V_r = \sum_{i}^{m} V(i) r_f(i)$$
$$V_g = \sum_{i}^{m} V(i) g_f(i) \tag{4.9}$$
$$V_b = \sum_{i}^{m} V(i) b_f(i)$$

Through the calculation in Eq. 4.9, the R, G, B components of the reconstructed color image can be obtained, and the pixel matrix for each component can be created. In a RGB image, each pixel can be represented by a vector (R, G, B) that has three values for the three primary color channels. To visualize the reconstructed color image, the three-dimensional vector is used for representing the reconstructed RGB image as $V_{recon.} = [V_r, V_g, V_b]$.

Table 4.2. Filter coefficient of the filters

	Filter 1 (K)	**Filter 2 (C)**	**Filter 3(M)**	**Filter 4 (Y)**
r	248	226	0	0
g	245	0	170	0
b	0	0	0	172
r_p	0.503	1	0	0
g_p	0.497	0	1	0
b_p	0	0	0	1
r_f	0.335	0.665	0	0
g_f	0.332	0	0.668	0
b_f	0	0	0	1

Table 4.2 shows the calculated filter's RGB value, filter's RGB ratio and filter coefficient, respectively.

4.4 Evaluation of Color Reproduction by the Proposed Method

The mechanism and the related equations for color reproduction are addressed in detail. But how do we verify that the reproduced color is correct or accurate? A reference for checking the accuracy of reconstructed result is necessary.

A color reference chart is commonly used to evaluate the color reproduction accuracy of a digitization procedure. The color chart is intended for color comparison or measurements. It is used for checking the color reproduction accuracy of and color management. Typical example charts are the IT8.7/2 and Color checker charts. These are flat physical objects with different color samples[18].

The accuracy and effectiveness of the proposed system was quantitively evaluated using an IT8.7/2 color chart. Firstly, the chart was digitized by the proposed imaging system with the same type of four-color filters used for photographing the original wall paintings. Then, the acquired chart images were processed with the proposed method to reconstruct its color. Lastly, the reconstructed color image was used to calculate the color difference to evaluate the accuracy of color reproduction.

The chart images scanned with the four-color filters were obtained using the proposed high-resolution scanner in reflective mode. Fig. 4.5 is the schematic representation of the scanner. The scanner consists of a monochromatic line CMOS camera unit as the one described in previous section, a flat-bed frame and a white LED light source which can focus the illumination at the target region using a cylindrical lens. Additionally, a UV-IR cut filter was used on the camera lens since only the visible light range is involved in this study. The scanning conditions used for acquiring the images of the reference color chart were set to mimic the conditions during the initial photographic documentation of the wall paintings taken 85 years ago.

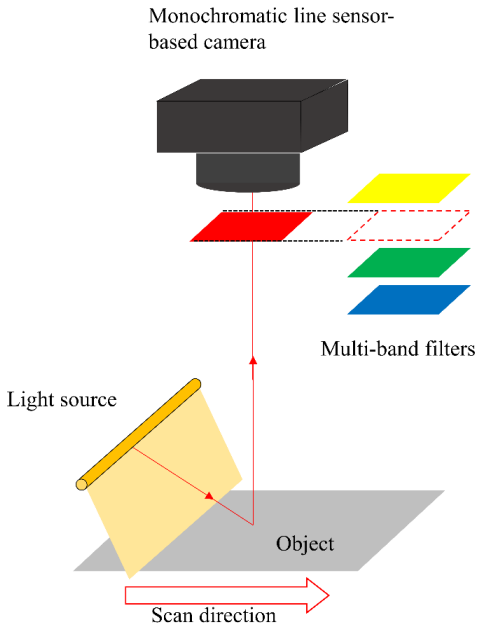

Fig. 4.5. Schematic representation of the multi-band imaging scanner.

After the image acquisition of IT8.7/2 color chart, the obtained images were used to rebuild its color using the proposed method.

Various well-known formulas for calculating color difference (Delta E) were established based on device-independent color spaces. The CIE1976 color difference formula[19] is one of the most widely used in related fields since the formula provides high accuracy and computational simplicity.

The color difference is calculated based on the CIE1976 color difference formula in Eq. 4.10:

$$\Delta E^*_{ab} = \sqrt{(\mathrm{L}^*_2 - \mathrm{L}^*_1)^2 + (a^*_2 - a^*_1)^2 + (\mathrm{b}^*_2 - \mathrm{b}^*_1)^2} \tag{4.10}$$

where the colors are represented in CIE $\mathrm{L}^*a^*\mathrm{b}^*$ color space; L^*_2, a^*_2 and b^*_2 are the actual values of the colors measured from each color patch and L^*_1, a^*_1 and b^*_1 are the reference values of the colors provided by the chart manufacture. The calculated data and detailed analysis would be discussed in Section 4.6.

Moreover, the four-color filters have different light transmittance attributes, which can cause the acquired images to show different brightness. Therefore, it is necessary to adjust all the images to be at same level. However, if the images are acquired under low light conditions, the adjustment may cause a lot of image noise that affects the color reproduction. An experiment was conducted to investigate the effect on color reproducibility due to the difference in exposure adjustment for each filter in the imaging procedure. Table 4.3 shows the lighting conditions and setting methods used in the experiment. When the scanning of the color chart was conducted as shown in Fig. 4.5, the filters were changed in order depicted in the figure. There were three methods employed in adjusting the amount of light for each filter: 1) changing light intensity; 2) changing lens aperture; and 3) changing camera sensitivity. Before any actual scanning, all devices were set to factory settings. These three methods were used individually or in combination to create three different conditions for adjusting the light intensity. For condition 1, the light amount of filter 1 was adjusted by changing light intensity only. When the value of sensor response comes to the reference value shown in Table 4.3, the adjustment would be accomplished. The scan with the rest of filters would follow the above setting without any adjustment. For condition 2, the adjustment for each scan with each filter were performed as what was described in condition 1 at first. During the adjustment, if the value of sensor response cannot fit the reference value, then the lens aperture would be changed to match the reference value. For condition 3, the light amount of each filter was adjusted by changing the camera sensitivity only.

Table 4.3. Light amount setting for each filter

	Condition 1	Condition 2	Condition 3
Light amount of each filter	Constant	Adjust each filter	Adjust each filter
Reference value for sensor response (Range from 0~255)	Filter1: 220 Filter2~4: Auto	Filter1~4: 220	Filter1~4: 220
Adjustment method	Light intensity	Light intensity and aperture	Camera sensitivity

4.5 Image Registration

For restoring the color image of the wall painting in the case of this study, the initial step is digitizing the four glass-based dry plates. Then, the image registration was performed on the images which is processed and ready to be overlapped into a color image. In order to accomplish the image registration, feature point detection and feature matching is necessary. Various feature detection techniques and algorithms have been developed in the field of computer vision[20]. In addition to some widely used feature detection methods such as Scale-Invariant Feature Transform (SIFT)[21], there are many methods for specifical application and scenario. For instance, Damon M. Conover showed a technique for automatic registration and mosaicking of technical images of old master paintings[22]. The technique can provide accurate alignment of a variety of types of images, even when content differences are present.

However, for the registration of the images of the wall painting in this study, it is hard to make use of such technique. On one hand, the lack of equivalent information in each monochromatic image or channel complicates the registration process; on the other hand, the test samples used in the literature all have a standard or a color image of the original object, which makes the point-based registration algorithms can be accomplished easily. While the wall paintings of Kondo Horyuji Temple are no longer exists due to the fire, it is impossible to acquire any type of image of the original objects.

Hence, we decided to fulfill this process by making use of the proposed imaging system. With support of the high-resolution imaging system used in this study, the acquired images are detailed enough to find feature points manually. So, a total of 11 feature point pairs is selected from the entire image area. Then, the affine transformation is conducted to accomplish the image registration.

Affine transformation is composed of translation, scaling, homothety, similarity transformation, reflection, rotation, shear mapping, and compositions of them in any combination and sequence[23]. If we set $\boldsymbol{X}$ and $\boldsymbol{Y}$ as affine spaces, since the combination of several transformations is obtained as one linear transformation, then every affine transformation $\boldsymbol{f}: \boldsymbol{X} \rightarrow \boldsymbol{Y}$ can be represented as $\boldsymbol{x} \rightarrow \boldsymbol{A}\boldsymbol{x} + \boldsymbol{b}$, where $\boldsymbol{A}$ is a linear transformation on $\boldsymbol{X}$ and $\boldsymbol{b}$ is a vector in $\boldsymbol{Y}$. Then affine transformation can be described as shown in Eq. 4.11:

$$\begin{bmatrix} y \\ 1 \end{bmatrix} = \begin{bmatrix} \boldsymbol{A} & \boldsymbol{b} \\ 0, \cdots, 0 & 1 \end{bmatrix} \begin{bmatrix} x \\ 1 \end{bmatrix} \tag{4.11}$$

Since it is a transformation matrix, the equation is equivalent to the following:

$$\boldsymbol{y} = \boldsymbol{A}\boldsymbol{x} + \boldsymbol{b} \tag{4.12}$$

which is called affine transformation matrix.

4.6 Experimental Results and Discussion

4.6.1 Color Reproduction Accuracy

The color reproduction of the IT8.7/2 color chart based on the proposed method with three scan settings as shown in Fig. 4.6. Basically, the allowance for color difference should be judged by the agreement between the relevant parties, and acceptable Delta E values may vary greatly depending on the exact applications and environment; the Delta E values listed in 'Example of the allowance by color' are valid universally at ISO regulation or in a variety of industries[24]. According to the Delta E values and its corresponding description, the Delta E of condition 1 and condition 2 belong to Grade A color tolerance, which can be considered as the same color in general; while condition 3 is a Grade B color tolerance, it means the color difference of this level may catch the attention of relevant skilled practitioners.

Condition 1 (ΔE^*_{ab}=2.32)

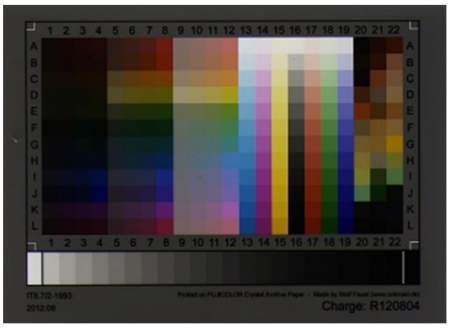

Condition 2 (ΔE^*_{ab}=2.22)

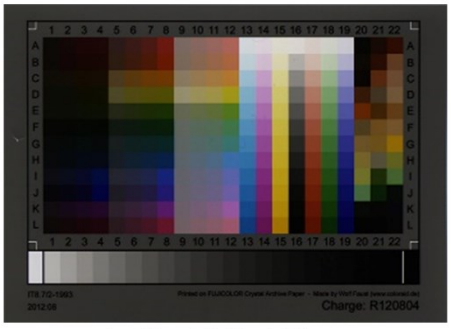

Condition 3 (ΔE^*_{ab}=4.73)

Fig. 4.6. Color reproduction results under the three scanning conditions.

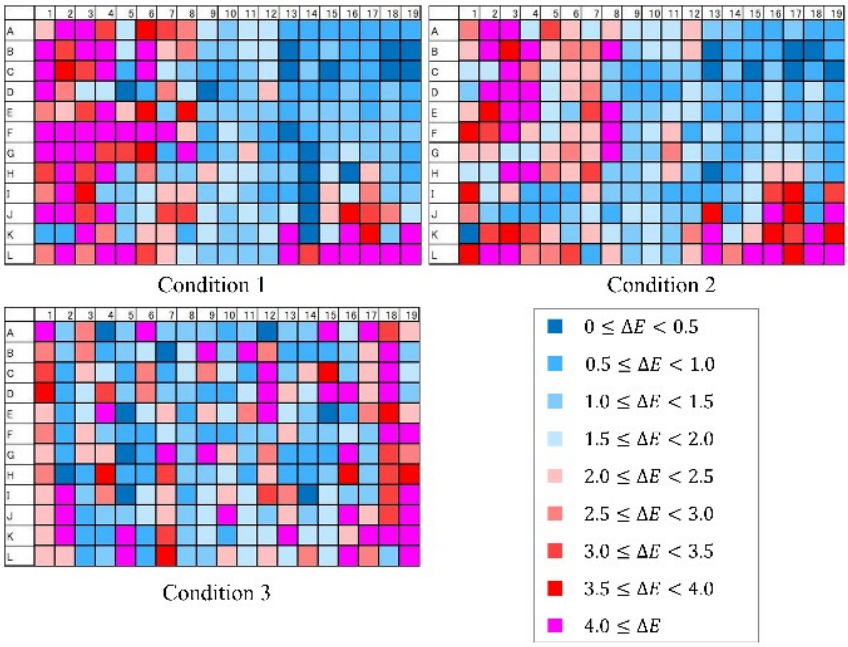

Fig. 4.7. Distribution of color difference for each patch. The coverage of the patch with good reproduction result in condition 1 and 2 are similar, which indicates that the adjustment of light amount for each filter cannot affect the result of color reproduction significantly. While comparing condition 2 and 3, both were adjusted to make the light amount of each filter uniform but in different ways. The adjustment of the sensitivity of camera sensor leads to a larger color difference.

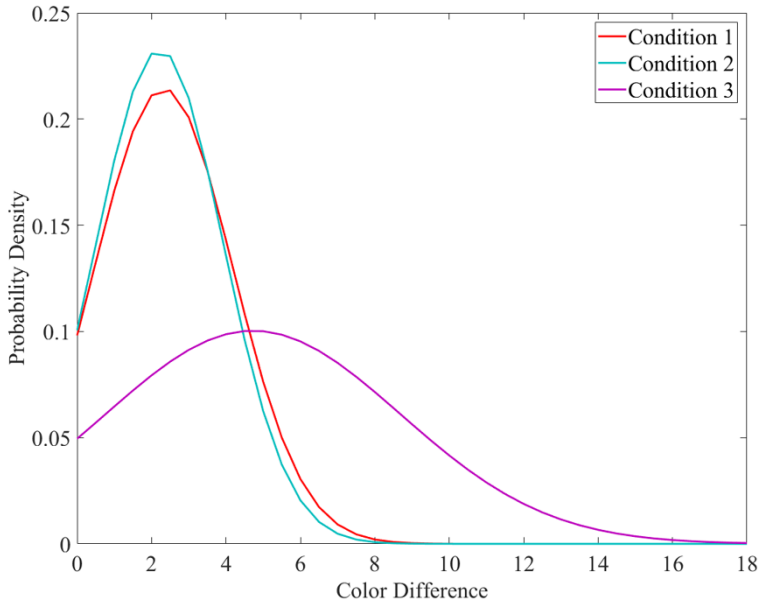

Fig. 4.8. Probability density distribution of color difference of color patches with respect to three scanning conditions.

Comparing the results of condition 1 and 2 in Fig. 4.7, it can be found that the coverage of the patch with good reproduction result is similar. This indicates that the adjustment of light amount for each filter cannot affect the result of color reproduction significantly. While comparing condition 2 and 3, both of them were adjusted to make the light amount of each filter uniform but in different ways. The adjustment of the sensitivity of camera sensor leads to a larger color difference.

Based on this analysis, it was found that the way of adjusting the light amount in correspondence with each filter can affect the accuracy of color reproduction using the proposed method. Among three adjustment methods, condition 2 gives the best result of color reproduction.

4.6.2 Color Reproduction Result of the Wall Painting

The proposed method is used to digitize the dry glass plate negatives of the Horyuji Kondo wall painting, which belongs to UNESCO World Heritage Site under the name Buddhist Monuments in the Horyuji Area. The digital archiving of the plates was performed by the Advanced Imaging Technology Lab at Kyoto University in Japan in 2015. Since Horyuji Kondo wall painting no longer exists and there is less authoritative literature for quantitatively evaluating the quality of the reproduction, in this study we just list the reconstructed color image (Fig. 4.9(b)) and a photo of a replica of the wall painting drawn by a professional painter before it was burned down (Fig. 4.9(c)), and then have a rough visual comparison of the reconstruction result. On one hand, it is difficult to draw a conclusion that the color information of the replica is correct or close to the original wall painting, since the process of making replica is dependent on the experience of the professional, which is highly subjective. On the other hand, both the wall painting and the replica would deteriorate over time, making it even more difficult to confirm if the color is correct or not. In the experiment for evaluating the proposed method, the scanning conditions used for acquiring the images of the reference color chart were set to mimic the conditions during the initial photographic documentation of the wall paintings taken 85 years ago. Especially, the filters used for photographing the original wall paintings was employed in this experiment. The experimental results show that the effectiveness of the proposed method. Hence, the color of the glass plate of the wall painting reproduced by the proposed method should be closer to the original wall painting and more accurate.

As mentioned previously, the light amount in correspondence with each filter can affect the accuracy of color reproduction, so it is necessary to adjust the brightness of multiband images properly before applying the proposed color reproduction method. Fig. 4.9(a) shows the positives of the negatives shown in Fig. 4.2, which are adjusted with proper brightness setting and available for reproducing color with the calculated filter coefficient. In his study, the negative-positive process was accomplished by the Photoshop software. Fig. 4.9(b) shows the reproduced color image of the wall painting using the proposed method. Finally, Fig. 4.10(a) shows the stitched image of the wall painting.

Fig. 4.9. Positives of the glass dry plates and comparison of the reconstructed color image and replica artwork. (a) shows the positives of the glass dry plates adjusted with proper brightness setting; (b) shows the color-reconstructed image of the wall painting with the proposed method; (c) shows the wall painting drawn by a professional painter before the fire.

Several regions of interests (ROI) shown in Fig. 4.10(b)-(d)were enlarged show the level of detail that can be achieved from the high-resolution scans and the color reproduction of details. A comparison between the 2400 dpi image acquired in this study and the 300 dpi image acquired by conventional commercial scanner is conducted (Fig. 4.10(b')-(d')). The size of each ROI is approximately 5mm x 5mm. It can be observed that the 2400 dpi images can represent fine outlines and colors even with a magnified view of more than 10 times larger than its actual size. The enlarged images also demonstrate that the color reproduction is well accomplished without misalignment or displacement issue.

From the above results, the high-definition color reproduction for Horyuji Kondo wall painting is accomplished. However, it is difficult to set a conclusion that the color reproduction result is completely accurate. Because all the conditions and settings for the photograph used in this study are based on the limited amount of relevant literature found in historical records. The attempt for estimating and representing the photographing condition of such a precious cultural

heritage could be a subject of research in the future.

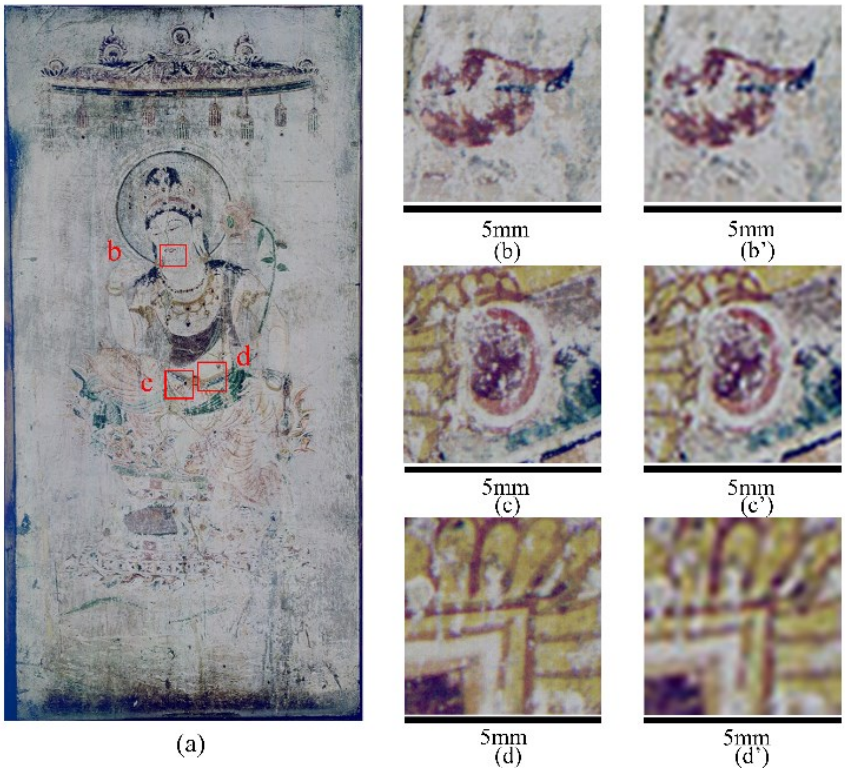

Fig. 4.10. Stitched image of the wall painting and selected details of the reconstructed results. (a) gives the stitched image of the wall painting from different glass dry plates; (b), (c), (d) shows the magnified view of selected ROI with 2400 dpi; (b'), (c'), (d') shows the magnified view of selected ROI with 300 dpi.

4.7 Conclusion

In this chapter, a line sensor camera-based digital archiving method for high-precision color reproduction of traditional glass dry plate is proposed and experimentally verified. The experimental equipment used in this study, a high-resolution scanner for digitizing large format transmissive object, was carefully designed and implemented. The acquired images demonstrate that the imaging system is capable of high-precision image acquisition. With support of high-resolution imaging system, image registration can be accomplished simply. Because the glass dry plates were scanned at a very high-resolution of 2400 dpi, even though the acquired images are monochromatic, feature points can be selected by the naked eye. As a result, it is possible to perform accurate alignment and to eliminate misalignment and color blur. An approach for recovering color information of Horyuji Kondo wall painting using the filter coefficient is addressed in detail. A spectrophotometer is employed to measure the spectral transmittance of the filters that is used to acquire further color information including XYZ value and RGB value of each filter. These acquired color information are then utilized to calculate

the filter coefficient used in the color reproduction of the wall painting. On the other hand, to verify that the proposed method is correct and effective is also a vital issue. A standard IT8.7/2 color chart with known color information was used as a scan object in the experiment to verify the correctness of reproduced color. The results showed that the proposed method can provide good accuracy in color reproduction that belongs to grade A color tolerance. The color reproduction result of the wall painting also indicates that the proposed method is capable of high-quality image acquisition and color reproduction even in image details. The application to the real cultural heritage indicates the great potential of the proposed method to reconstruct color information of similar kinds of precious documentation material. Using the method presented in this study, it is possible to archive them with high resolution, high color fidelity and less geometric distortion issue.

4.8 References

1) Y. Lusenet: “Tending the garden or harvesting the fields: digital preservation and the UNESCO charter on the preservation of the digital heritage”, Library Trends, 56, pp. 164-182 (2007)

2) C. Karp: “Digital Heritage in Digital Museums”, Museum International, 66, pp. 157-162 (2014)

3) S. Nishimura: “Photography of Cultural assets – A Century of Photographs by Benrido – “, Jpn. Photographic Soc., J75, pp. 489-492 (2012)

4) H. Gernsheim, “A concise history of photography. No. 10”, Dover publications, Inc., New York, pp. 16-22 (1986)

5) M. Jones: “The Burned Murals of Hōryū-Ji: A Transformation of the Gods”, Art Journal, 25, pp. 238-240 (1966)

6) D. Defibaugh: “The Collotype: History, process & photographic documentation. (Master’s degree thesis)”, Rochester Institute of Technology, New York (1997)

7) J. A. Toque: “Multispectral Imaging: the influence of lighting condition on spectral reflectance reconstruction and image stitching of traditional Japanese paintings”, International Joint Conference on Computer Vision, (Imaging and Computer Graphics Theory and Applications (VISIGRAPP)), pp. 13-20 (Feb. 2009)

8) J. A. Toque, Y. Sakatoku, and A. Ide-Ektessabi: “Analytical imaging of cultural heritage paintings using digitally archived images”, Computer Vision and Image Analysis of Art, 7531, pp. 75310N (Feb. 2010)

9) J. A. Toque, Y. Murayama, Y. Matsumoto, A. Ide-Ektessabi: “Polarized light scanning for cultural heritage investigation”, Computer Vision and Image Analysis of Art II, 7869, pp. 78690N (Mar. 2011)

10) A. Sharma: “Understanding color management”, John Wiley & Sons, Hoboken (2018)

11) J. Y. Hardeberg: “Acquisition and reproduction of color images: colorimetric and

multispectral approaches", Universal-Publishers, USA, pp. 50-51 (2001)

12) J. R. Mansfield, M. Attas, C. Majzels, E. Cloutis, C. Collins, and H. H. Mantsch: "Near infrared spectroscopic reflectance imaging: a new tool in art conservation", Vibrational Spectroscopy, 28, pp. 59-66 (2002).

13) J. Schanda: "Colorimetry: understanding the CIE system", John Wiley & Sons, Hoboken, pp.61-62 (2007)

14) L. Busin, N. Vandenbroucke, and L. Macaire: "Color spaces and image segmentation", Advances in imaging and electron physics, 151, 1 (2008)

15) Japanese Standards Association: "JIS Z8722 Methods of color measurement – reflecting and transmitting objects", www.jisc.go.jp, accessed 09/02/2021

16) H. Murata, K. Saitoh, and Y. Sumida: "True color imagery rendering for Himawari-8 with a color reproduction approach based on the CIE XYZ color system", Journal of the Meteorological Society of Japan. Ser. II, 96B, pp. 211-238 (2018)

17) CIE S014-4:2007 Colorimetry: "Part 4 CIE 1976 L*a*b* color space, 2nd Edition (CIE, Vienna) ", www.cie.co.at, accessed 25/03/2021

18) D. Q. McDowell: "Summary of IT8/SC4 color activities", Device-Independent Color Imaging and Imaging Systems Integration, 1909, pp. 229-235 (1993)

19) L. Mandic, S. Grgic, and M. Grgic: "Comparison of Color Difference Equations", Proceedings ELMAR 2006, pp. 107-110 (2006)

20) B. Zitová, and J. Flusser: "Image registration methods: a survey", Image and vision computing, 21, pp. 977-1000 (2003)

21) D. G. Lowe: "Object recognition from local scale-invariant features", Proceedings of the Seventh IEEE International Conference on Computer Vision, pp. 1150-1157 (1999)

22) D. M. Conover, J. K. Delaney and M. H. Loew: "Automatic registration and mosaicking of technical images of Old Master paintings", Appl. Phys. A, 119, pp. 1567–1575 (2015)

23) L. Gottesfeld Brown: "A survey of image registration techniques", ACM computing surveys (CSUR), 24, pp. 325-376 (1992)

24) Nippon Denshoku Industries Co., LTD: "Example of the allowance by color", https://www.nippondenshoku.co.jp/web/84nglish/colorstory/08_allowance_by_color.htm, accessed 02/12/2020

Chapter 5

2.5D Fine Surface Structure Reconstruction

5.1 Introduction

Digitization of cultural heritage has been highly developed for the last decade. Various high-precision image acquisition systems and methods have been developed for 2D objects, which can be digitized with high resolution and exceptional color reproduction. However, digital archiving remains a challenging problem for researchers. Especially, when we try to scan a 2.5D object that has complex texture or uneven surface, it is not easy to acquire a result combined with good-quality image and object's surface shape. In an on-the-site digitization environment, an applicable and efficient imaging system that can acquire high-resolution image with surface information is very helpful to inspect the quality of digitization work and provide more useful information to related researchers. Moreover, most of the conventional methods and recent studies focused on area sensor-based camera and laser ranger for image acquisition or shape reconstruction process[1-3].

Laser-based methods and image-based methods are two leading technologies used for shape reconstruction of cultural heritage digitization[4]. The former has a high accuracy of shape reconstruction but corresponding high cost, while the latter has relatively lower accuracy and lower cost. Both have merits and drawbacks for corresponding applications, and the practicality of both are also gradually being improved with the development of computing technology[5,6]. Among the image-based methods, photometric stereo method and stereovision method are widely used in the field. Compared with stereovision method, whose 3D reconstruction accuracy and efficiency still cannot meet the growing requirements, the photometric stereo method is capable of extracting more details of the object surface, and its accuracy depends on the resolution of the acquired image[7-9]. Because the objective is to rebuild the surface shape of a flat object with slightly textured surface, the photometric stereo method is employed in this study.

The photometric stereo method is generally used with area sensor-based camera, but it has some demerits that commonly manifested as geometric image distortion and insufficient resolution. Moreover, since the light projected onto the object heavily affects the accuracy of the surface reconstruction results, the light source setting and its calibration need to be prepared very carefully in practice. Based on its imaging mechanism and structure feature, a line sensor-based camera has higher detail of expressiveness and higher spatial resolving capability than an area sensor-based one, which makes it more suitable for resolving fine details of cultural heritages. In addition, a line sensor-based camera is a better choice for recording color of cultural heritage with higher color fidelity. The most crucial point is that the line sensor-based camera has a less geometrical optic problem for imaging[10,11].

Therefore, in this study, we employed an image acquisition system that can obtain the object surface shape and color image at the same time by photometric stereo using a line sensor-based camera. In addition, a method for estimating the light source incident angle is proposed. A

selected reference object can be scanned with the target object at the same time, which is more efficient.

5.2 A Photometric Stereo Method based on Line-sensor Scanner

As the first step to reconstruct object surface shape, the derivation of the normal vector based on the photometric stereo method is addressed in this section. Photometric stereo, which was introduced by Woodham in 1980, reconstructs surface normal using multiple illuminations[12]. Firstly, a coordinate system of scanner can be set as shown in Fig. 5.1 (a). Angle θ refers to the incident angle of the light source. $\mathrm{r}(x, y, \mathrm{Z}(x, y))$ is a coordinate of the object surface, and $p(x, y)$, $q(x, y)$ represent components in the x-axis direction and y-axis direction, respectively. Then, the normal vector $\boldsymbol{n}$ of the object surface satisfies Eq. 5.1.

$$\boldsymbol{n} = \frac{(-p, -q, 1)}{\sqrt{1^2 + p^2 + q^2}} \tag{5.1}$$

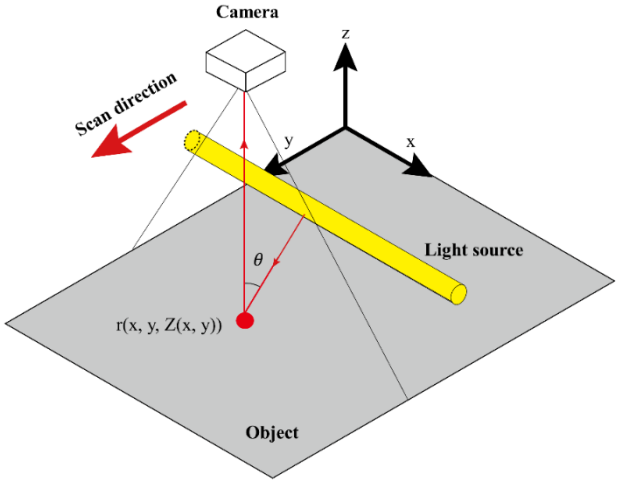

(a)

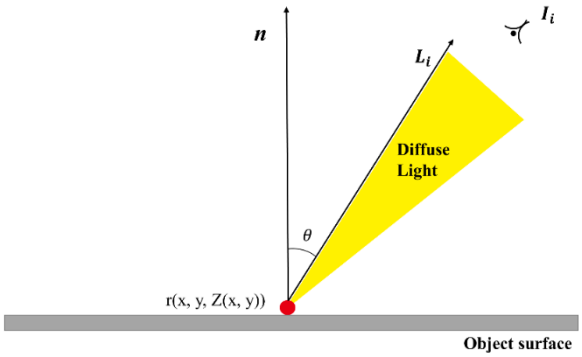

(b)

Fig. 5.1. Basic concept diagram and mathematical model of the proposed method. (a) shows the schematic representation of the line sensor-based scanner; (b) shows the Lambertian reflectance model used in this study.

Since a bar-type LED light source is arranged in a linear array, each individual unit can be treated as a point source. The units are oriented in the same direction so we can assume uniformity in light distribution and light incidence. For simplicity, we assume Lambertian for all surfaces of the object, and the light sources are point light sources with respect to the textured surface. According to the Lambertian reflectance model[13], which models a perfectly diffused surface that scatters incident illumination equally in all directions[14], when the unit lighting direction vector of i th light source is $L_i(L_{ix}, L_{iy}, L_{iz})$ that is observed from an object surface point $\mathrm{r}(x, y, \mathrm{Z}(x, y))$ as shown in Fig.5.1 (b), the diffuse reflection of i th light source can be represented as shown in Eq. 5.2:

$$\begin{aligned} I_i &= E_{\text{incident}} K_{\text{diffuse}} \cos\theta_{\mathrm{d}} \\ &= E_{\text{incident}} K_{\text{diffuse}} \boldsymbol{n} \cdot \boldsymbol{L}_i \\ &= E_{\text{incident}} K_{\text{diffuse}} \frac{(-pL_{ix}, -qL_{iy}, L_{iz})}{\sqrt{1^2+p^2+q^2}} \end{aligned} \tag{5.2}$$

where I_i denotes a known vector of observed intensity, E_{incident} denotes the intensity of the incident light, K_{diffuse} denotes diffuse reflection coefficient, θ_{d} denotes the angle between the light direction and the normal direction, and $\boldsymbol{L}_i$ denotes a known matrix of normalized light directions, considering the product $E_{\text{incident}} K_{\text{diffuse}}$ as one variable, when the normalized light direction vector $\boldsymbol{L}_i(L_{\mathrm{ix}}, L_{\mathrm{iy}}, L_{\mathrm{iz}})$ is known, the unknown variables of the equation are $E_{\text{incident}} K_{\text{diffuse}}$, p, q. Therefore, if there are three images taken while changing the incident angle of the light source, the normal vector can be obtained. However, since the accuracy of the normal vector can be affected by various factors, such as the noise of the captured image and the lighting direction vector for each light source, it is possible to obtain a more accurate result from at least three or more images[15-17].

The following shows how to determine the normal vector from multi-images taken with different lighting angle.

$$\tilde{\boldsymbol{L}} = \begin{bmatrix} L_{1x} & L_{2x} & \cdots & L_{nx} \\ L_{1y} & L_{2y} & \cdots & L_{ny} \\ L_{1z} & L_{2z} & \cdots & L_{nz} \end{bmatrix} \tag{5.3}$$

$$\boldsymbol{I} = [I_1 \quad I_2 \quad \cdots \quad I_n] \tag{5.4}$$

With the lighting condition shown in Eq. 5.3, the intensity of the incident light or diffuse reflection shown in Eq. 5.4 can be written as following:

$$\boldsymbol{I} = E_{\text{incident}} K_{\text{diffuse}} \boldsymbol{n} \cdot \tilde{\boldsymbol{L}} \tag{5.5}$$

Using the generalized inverse $\tilde{\boldsymbol{L}}^+$ of the matrix $\tilde{\boldsymbol{L}}$ to transform Eq. 5.5, we can obtain the surface normals as shown in Eq. 5.6:

$$\boldsymbol{n} = \frac{\boldsymbol{I} \cdot \tilde{\boldsymbol{L}}^+}{E_{\text{incident}} K_{\text{diffuse}}} \tag{5.6}$$

5.3 2.5D Reconstruction from Surface Normal Vector

The recovery of the surface of a 2.5D object is addressed in this section. Many methods have been developed to solve the problem of surface normal integration for several decades, and generally the methods can be classified into two categories: local techniques and global methods[18,19]. Two classic methods to reconstruct depth map are described as following.

5.3.1 Local Techniques

Local Techniques refer to a direct line-integration scheme, which is based on the fact that the integral of a closed path on a continuous surface should be zero. Using this technique, the height information can be estimated by integrating the gradient components in different directions. Specifically, denoting the surface height by $\mathrm{Z}(x, y)$, and denote the partial derivatives of Z with respect to x and y respectively, which are introduced by the short-hand notation shown in Eq. 5.7 and Eq. 5.8:

$$\frac{\partial \mathrm{Z}(x,y)}{\partial x} = p(x,y) \tag{5.7}$$

$$\frac{\partial \mathrm{Z}(x,y)}{\partial y} = q(x,y) \tag{5.8}$$

So, the surface height information can be written as:

$$\mathrm{Z}(x,y) = \mathrm{Z}(\mathrm{x}_0,\mathrm{y}_0) + \int_{\gamma} \{p(x,y)\mathrm{d}x + q(x,y)\mathrm{d}y\} \tag{5.9}$$

where γ is the integration path from $r(x_0, y_0)$ to $r(x, y)$.

Although this method has the advantage of short computational time, due to their local nature, the reconstruction highly depends on the integration path, and sensitive to noise and discontinuities[20], which lead to error accumulation during the reconstruction. In the case of calculating the normal vector from images, an error occurs because the noise and the specular reflection component contained in the image cannot be removed entirely.

5.3.2 Global Optimization

In order to eliminate error accumulation as much as possible, a global method based on the calculus of variations is a preferred choice for surface reconstruction. One of the most natural and classic variational method proposed by Horn and Brooks solved this problem by casting the corresponding function in a form that results in a least-squares approximation[21]. Many global methods are formulated in an energy-minimization framework, and the objective is to find a disparity function that minimizes a global energy[22,23].

In the case of Global Optimization, $\mathrm{Z}(x, y)$ can be derived when the evaluation function W is minimized (Eq. 5.10). The minimization of the function can be solved by Variational Method.

In general, when the independent variables x and y are defined as dependent variables $u(x, y)$, the Euler equation of a two-dimensional function Eq. 5.11 can be written as Eq. 5.12.

$$\mathrm{W} = \iint \left\{ \left(\frac{\partial \mathrm{Z}(x,y)}{\partial x} - \mathrm{p}(x,y) \right)^2 + \left(\frac{\partial \mathrm{Z}(x,y)}{\partial y} - \mathrm{q}(x,y) \right)^2 \right\} \mathrm{d}x\mathrm{d}y \tag{5.10}$$

$$\mathrm{J}[u] = \iint f\left(x, y, u, u_x, u_y\right) dxdy \tag{5.11}$$

$$\begin{aligned} &\frac{\partial^2 f}{\partial u_x \partial x} + \frac{\partial u}{\partial x}\frac{\partial^2 f}{\partial u_x \partial u} + \frac{\partial^2 u}{\partial x^2}\frac{\partial^2 f}{\partial {u_x}^2} + \frac{\partial^2 u}{\partial x \partial y}\frac{\partial^2 f}{\partial u_x \partial u_y} + \frac{\partial^2 f}{\partial u_y \partial y} + \frac{du}{dy}\frac{\partial^2 f}{\partial u_y \partial u} \\ &\quad + \frac{\partial^2 u}{\partial y}\frac{\partial^2 f}{\partial {u_y}^2} + \frac{\partial^2 u}{\partial x \partial y}\frac{\partial^2 f}{\partial u_y \partial u_x} - \frac{\partial f}{\partial u} = 0 \end{aligned} \tag{5.12}$$

By plugging Eq. 5.13 and 5.14 into Eq. 5.12, we can obtain Eq. 5.15, which is also known as the Poisson equation.

$$u_x = \frac{\partial u}{\partial x} \tag{5.13}$$

$$u_y = \frac{\partial u}{\partial y} \tag{5.14}$$

$$\frac{\partial^2 \mathrm{Z}(x,y)}{\partial x^2} + \frac{\partial^2 \mathrm{Z}(x,y)}{\partial y^2} = \frac{\partial \mathrm{p}(x,y)}{\partial x} + \frac{\partial \mathrm{q}(x,y)}{\partial y} \tag{5.15}$$

Discretizing this Poisson equation into a difference equation, Eq. 5.16 can be obtained.

$$\begin{aligned} &\frac{\mathrm{Z}(x+1,y) - 2\mathrm{Z}(x,y) + \mathrm{Z}(x-1,y)}{\Delta x^2} + \frac{\mathrm{Z}(x,y+1) - 2\mathrm{Z}(x,y) + \mathrm{Z}(x,y-1)}{\Delta y^2} \\ &\quad = \frac{\mathrm{p}(x+1,y) - \mathrm{p}(x,y)}{\Delta x} + \frac{\mathrm{q}(x,y+1) - \mathrm{q}(x,y)}{\Delta y} \end{aligned} \tag{5.16}$$

Substituting $\Delta x = \Delta y = 1$ into Eq. 5.16, then Eq. 5.17 can be derived.

$$\mathrm{Z}(x,y) = \frac{\mathrm{Z}(x+1,y) + \mathrm{Z}(x-1,y) + \mathrm{Z}(x,y+1) + \mathrm{Z}(x,y-1)}{4} - \frac{\eta(x,y)}{4} \tag{5.17}$$

Where, $\eta(x,y) = \mathrm{p}(x+1,y) - \mathrm{p}(x,y) + \mathrm{q}(x,y+1) - \mathrm{q}(x,y)$ (5.18)

To solve Eq. 5.17, we will use iterative methods, mainly including the Jacobi method, Gauss-Seidel method, and SOR (Successive Over Relaxation) method.

In the Jacobi method, assuming that in $\mathrm{Z}_n(x,y)$ is the $\boldsymbol{n}$ th step iteration of $\mathrm{Z}(x,y)$, the method repeatedly calculates an iterative expression as shown in Eq. 5.19. The Gauss-Seidel method uses the latest value when updating the value in the Jacobi method, and improves the

convergence to be faster. In the Gauss-Seidel method, the method repeatedly calculates an expression as shown in Eq. 5.20.

$$\mathrm{Z}_{n+1}(x,y) = \frac{\mathrm{Z}_n(x+1,y) + \mathrm{Z}_n(x-1,y) + \mathrm{Z}_n(x,y+1) + \mathrm{Z}_n(x,y-1)}{4} - \frac{\eta(x,y)}{4} \tag{5.19}$$

$$\mathrm{Z}_{n+1}(x,y) = \frac{\mathrm{Z}_n(x+1,y) + \mathrm{Z}_{n+1}(x-1,y) + \mathrm{Z}_n(x,y+1) + \mathrm{Z}_{n+1}(x,y-1)}{4} - \frac{\eta(x,y)}{4} \tag{5.20}$$

The SOR method is a method devised to make convergence faster by using the acceleration coefficient ω. (Eq. 5.21)

$$\mathrm{Z}_{n+1}(x,y) = (1-\omega)\mathrm{Z}_n(x,y) + \omega\left\{\frac{\mathrm{Z}_n(x+1,y) + \mathrm{Z}_{n+1}(x-1,y) + \mathrm{Z}_n(x,y+1) + \mathrm{Z}_{n+1}(x,y-1)}{4} - \frac{\eta(x,y)}{4}\right\} \tag{5.21}$$

When $0 \le x \le \mathrm{J}-1,\ 0 \le y \le \mathrm{J}-1$, we have:

$$\omega = \frac{2}{1+\pi/\mathrm{J}} \tag{5.22}$$

In this study, the height information is reconstructed by calculating $\mathrm{Z}(x,y)$ obtained from iterative calculation until the SOR Eq. 5.21 converges.

In terms of the imaging mechanism of the line sensor, where the light source is fixed to illuminate from one direction for one scan, the normal vector can only be calculated in one direction. In general, the issue mentioned above can be solved by either of rotating the object, placing the light source at several angles, or applying constraints to estimate the normal vector. However, the method of rotating the object is not an efficient way to acquire image and require image correspondence after image acquisition. The method of using several angled light source may cause uneven illumination. In this study, we estimate the normal vector in the x-axis direction by optimizing the calculated normal vector in the y-axis direction using a constraint.

From Eq. 5.7 and 5.8, we have:

$$\frac{q(x,y)}{\partial x} = \frac{p(x,y)}{\partial y} \tag{5.23}$$

When we redefine $p(x,y)$ in the form of a sum with a function $\mathrm{C}(x)$, we have following equation:

$$p(x,y) = p'(x,y) + \mathrm{C}(x) \tag{5.24}$$

Substituting Eq. 5.24 to Eq. 5.23 would cause the term $\mathrm{C}(x)$ to be eliminated. This means that $p(x,y)$ is arbitrary with respect to x and is not uniquely determined. As a new constraint, we assume that the height of the object's surface $Z(x,y)$ changes smoothly, and therefore $p(x,y)$ also changes smoothly. Based on the above constraint, the evaluation function W_2 can be set as

following equation:

$$\mathrm{W}_2 = \iint \left(\frac{q(x,y)}{\partial x} - \frac{p(x,y)}{\partial y} \right)^2 dxdy + \lambda \iint \left(\frac{p(x,y)}{\partial x} \right)^2 dxdy \tag{5.25}$$

where the first term on the right side reflects the constraint in the y-direction of $p(x,y)$, and the second term reflects the constraint in the x-direction of $p(x,y)$. λ is a parameter that determines the weight of each term. When λ is small, the influence of the first term is increased, and when λ is large, the influence of the second term is increased. In this study, the calculations were performed with $\lambda = 0.5$. Then, $p(x,y)$ can be calculated by minimizing the evaluation function W_2. The optimal solution in the above equation can be derived by the variational method. Eq. 5.25 can be written in the following form:

$$\frac{\partial^2 p(x,y)}{\partial y^2} + \lambda \frac{\partial^2 p(x,y)}{\partial x^2} = \frac{\partial^2 q(x,y)}{\partial x \, \partial y} \tag{5.26}$$

By applying Newton's method to equation (5.26) and performing iterative calculations, we can obtain $p(x,y)$, the component of the normal vector in the x-axis direction.

5.4 Estimation of the Light Source Incident Angle

The accuracy of the photometric stereo method depends highly on the measurement of light source incident angle or direction. However, it is difficult to measure the lighting direction manually, which is also error-prone and time-consuming. Regarding the issues above, a method to automatically estimate the lighting direction using a reference object is proposed. The proposed method only needs to scan a small reference object simultaneously at the time of scanning, which is not a time-consuming procedure. Since the processing after scanning can also be accomplished automatically, the working time can be shortened, and stable measurement values can be acquired compared to the manual measurement. Furthermore, it is flexible to apply different lighting directions or even different light source to an experiment for testing any lighting condition.

A reference object with a known surface normal vector was scanned in the experiment, and its brightness value of each pixel was extracted from a scanned image. Then, comparing the theoretical value of brightness with extracted one to estimate the vector of the light source direction.

We apply the same assumptions described in section 5.2, that is Lambertian for all surfaces of the object; the light sources are point light sources. According to the Lambertian reflectance model presented in Eq. 5.2, we obtain:

$$\begin{aligned} \mathrm{W}_{\mathrm{light}} &= \boldsymbol{I} - E_{\mathrm{incident}} K_{\mathrm{diffuse}} \boldsymbol{n} \cdot \tilde{\boldsymbol{L}} \\ \text{where, } \tilde{\boldsymbol{L}} &= \begin{pmatrix} a \\ b \\ c \end{pmatrix}, a^2 + b^2 + c^2 = 1 \end{aligned} \tag{5.27}$$

then the lighting direction vector can be obtained by minimizing function W_{light}.

The reference object used in the experiment is shown in Fig. 5.2. Since the object is a hemisphere, its surface normals change along the hemispherical surface continuously, and the brightness values of surface normals can be easily acquired. And it is also easy to calculate surface normals from the coordinates on the image. We assume that an equation of a spherical surface in 3-space as following:

$$f(x, y, z) = x^2 + y^2 + z^2 - \mathrm{r}^2 = 0 \tag{5.28}$$

Thus, the gradient of the function is

$$\nabla \boldsymbol{f} = 2x\boldsymbol{i} + 2y\boldsymbol{j} + 2z\boldsymbol{k} \tag{5.29}$$

And so, $\nabla \boldsymbol{f}$ is the surface normal vector.

Hence, the unit normal vector can be derived as:

$$\boldsymbol{n}(x, y, z) = \frac{x\boldsymbol{i} + y\boldsymbol{j} + z\boldsymbol{k}}{\sqrt{x^2 + y^2 + z^2}} \tag{5.30}$$

Since the reference object was scanned from the top side, where $z = \sqrt{r^2 - x^2 - y}$, we have:

$$\boldsymbol{n}(x, y) = \frac{x\boldsymbol{i} + y\boldsymbol{j} + \sqrt{r^2 - x^2 - y^2}\boldsymbol{k}}{r^2} \tag{5.31}$$

From Eq. 5.31 and the coordinates on the image, the surface normal vectors can be obtained.

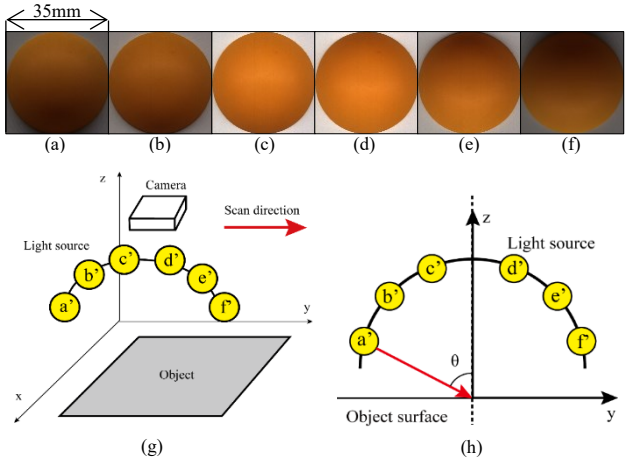

Fig. 5.2. Image of reference object scanned with 6 lighting directions used for surface reconstruction and the positional relationship of 6-pattern light sources. (a)-(f) shows the reference object scanned with 6-pattern light sources; (g), (h) shows the positional relationship of 6-pattern light sources.

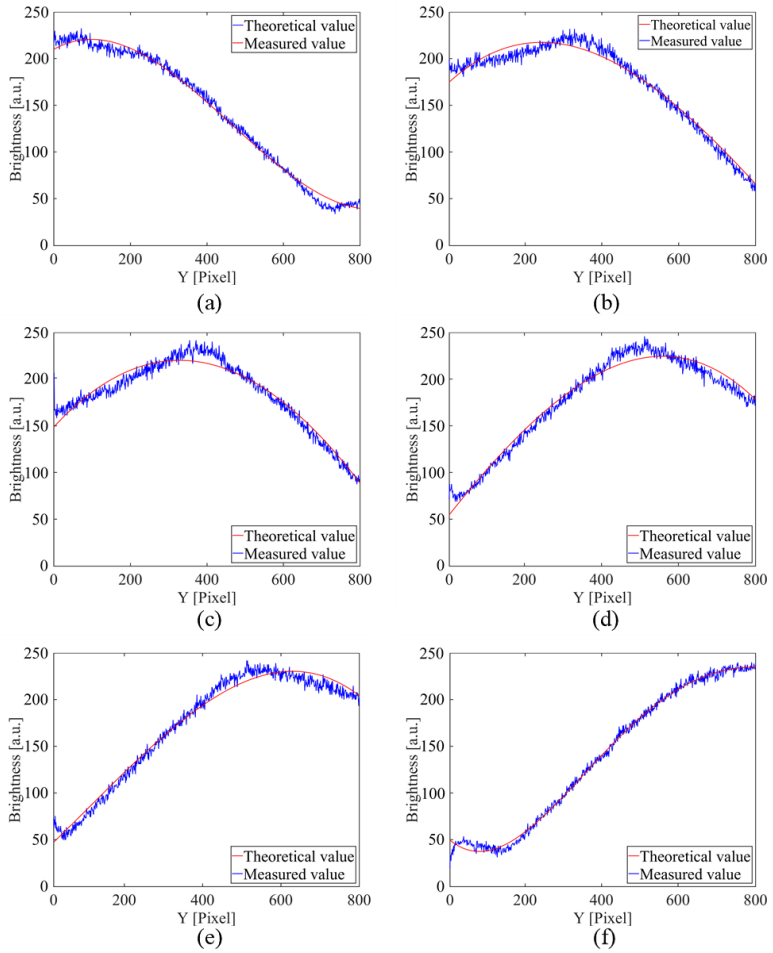

Fig. 5.3. Comparison of theoretical value and measured value of the reference object image brightness. (a)-(f) show the brightness distribution of the reference object scanned with 6-pattern light sources, respectively. The measured values denote the brightness measured from the scanned images, and the theoretical values denote the corresponding fitting results.

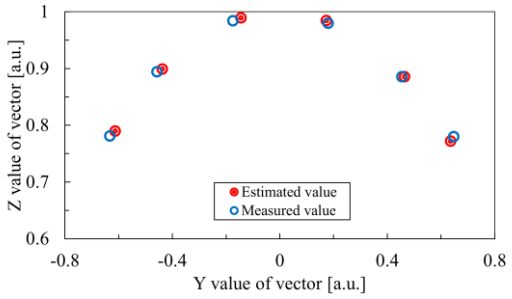

Fig. 5.4. Comparison of estimated value and the measured value of the light source vector.

A total of 6 patterns of lighting positions were tested. The scanned images of the reference object with 6-pattern light sources are shown in Fig. 5.2 (a)-(f), which shows that the incident light is changing along the surface of the object continuously. The positional relationship between each pattern is shown in Fig. 5.2 (g)(h). The light source incident angles are selected as 30°, 45° and 60°, approximately. Fig.5.3 shows the comparison of theoretical brightness

value and the measured brightness value of the object image. Fig. 5.4 shows the comparison of estimated vector data and measured data, which also demonstrates the lighting direction of the light source. When the light source vector is normalized, the error between the measured value and the estimated value is very small at 0.01 or less.

5.5 Experimental Results and Discussion

In this section, the experiment is conducted to reconstruct the surface shape of an object with the proposed method. A commercial laser ranger is also employed to evaluate the reconstruction result. Lastly, the practical application to a clay tablet engraved with cuneiform indicates the significant effectiveness of the method.

A high-precision large flatbed scanner shown in Fig. 5.5 was designed for the experiment, which mainly includes a line sensor-based camera module, a stepping motor, an LED-light source group which is well designed for high color fidelity and minimum light irradiation, and a scanner frame structure. The line sensor-based camera module consists of a color CCD camera TLC-7500CLD manufactured by Takenaka which has 7500 pixels for each of RGB channels, and an Apo Rodagon-N 105mm lens.

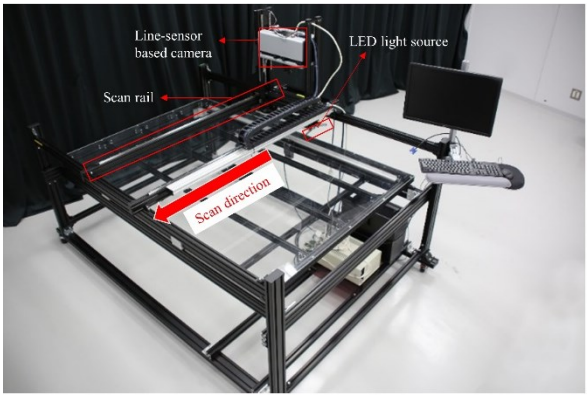

Fig. 5.5. The High-precision flatbed scanner used for the experiment.

An oil painting stroke sample with a height of approximately 2mm (the thickness of paints layer) was employed as a target object, which was scanned by the scanner with 6 LED bars attached in 6 different directions. Thus, 6 images are captured in total in 1109 dpi.

(a) (b)

Fig. 5.6. The oil paints sample swatch used in the experiment. (a) oil paints sample swatch; (b) exact oil paints sample used in the experiment.

To evaluate the reconstruction result of the proposed method, a laser ranger manufactured by KEYENCE (Model: LG_G200) was employed as the reference for the accuracy comparison. The actual experimental equipment and its related dimension information is shown in Fig. 5.7. The laser is emitted to the object surface, then the reflected diffuse light would be collected on a CMOS sensor of the laser ranger to form an image. This image is used to detect the position and measure the shape of object surface. The measurement is based on the principle of triangulation. The laser ranger is capable of measurement with a repeat accuracy of 2μm in the height direction and 20μm in the width, which is considered higher accuracy than the proposed method theoretically. Since the sensor shape is two dimensional, it cannot be used to measure the object in three dimensional directly. It was attached on the scanner and sampled while simultaneously moving in the scanning direction to obtain three dimensional shape.

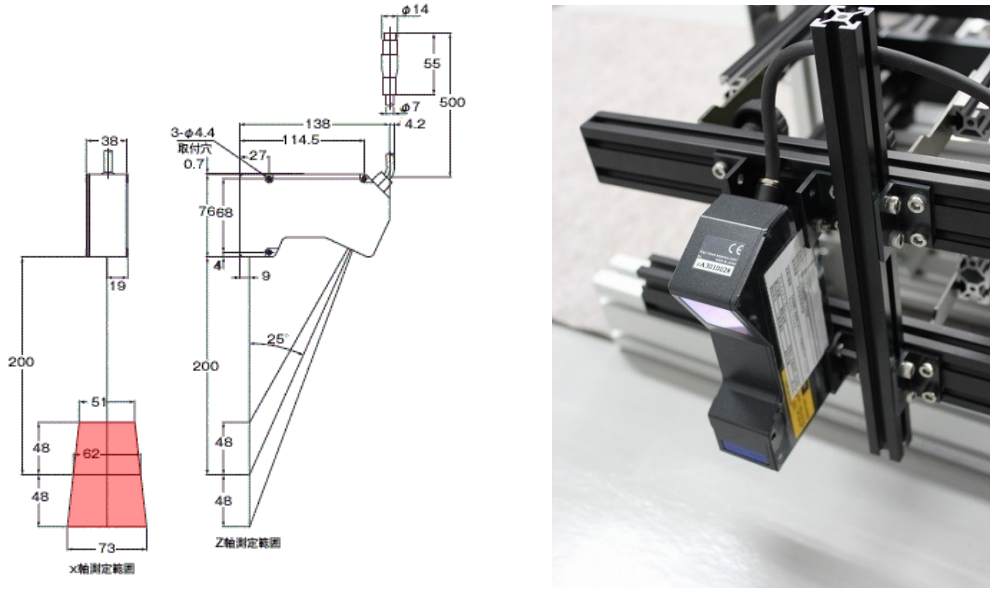

(a) (b)

Fig. 5.7. The laser ranger used in the experiment. KEYENCE (Model: LG_G200). (a) the red area on the drawing shows its measurable field; (b) is a photograph of the actual experimental equipment.

Fig. 5.8(a) is the normal vector map of the target object estimated by the proposed method. It is an image in which the components of the normal vector at each pixel are visualized in correspondence with the RGB channels. This normal vector map reflects the shape characteristics of the surface, which also indicates the shape characteristics shown in Fig. 5.8 (c) is correct. The reconstructed depth maps of the target object by the laser and the proposed method are shown in Fig. 5.8 (b)(c). From Fig. 5.8 (c), it demonstrates very good surface shape of the painting stroke, while the laser result shown in Fig. 5.7(b) is obviously not clear enough. Due to the condition of experimental instrument settings, we only had 500 dpi resolution setting for recording the data by the laser. However, the proposed method also indicates its potential to present such accuracy with the proposed imaging system.

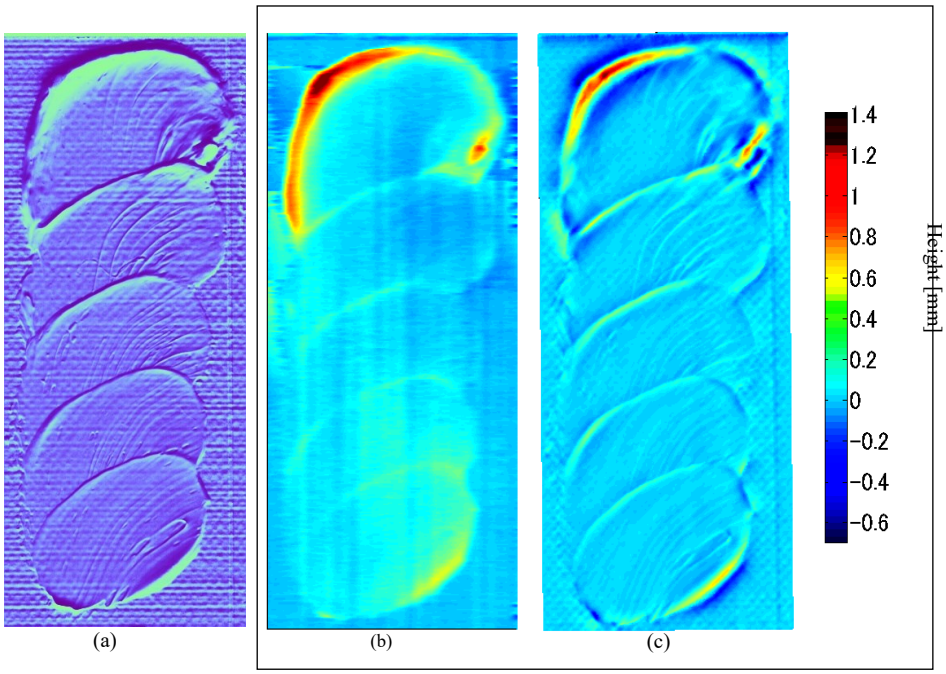

Fig. 5.8. Normal vector map and comparison of reconstructed depth maps. (a) shows the normal vector map; (b) and (c) present the depth map obtained by the laser ranger and the proposed method, respectively.

Fig. 5.9 shows the depth map comparison of the results from laser and the proposed method. Fig. 5.9 (a) is the selected area denoted by AA' and BB' for the comparison. Two lines are selected to compare the accuracy of the reconstructed 2.5D surface shape that was accomplished by the proposed method and the laser ranger. Fig. 5.9 (b) and (c) present the result of the comparison. It is observed that in some parts of the sample, the results of the proposed method and the laser are deviated due to the influence of strong specular reflection on the surface of the object, which is also a subject for future work. Nevertheless, the RMSE is considerably small, which indicates reconstructed result of the proposed method is comparable with the accuracy of the laser ranger, and the outliers in correspondence with the specular parts do not affect overall data.

The experimental results above show that the proposed method can recover the depth map with such accuracy though, there are still some limitations. In this study, the selected object basically has a flat base and slight uneven surface with a range of ±2mm approximately. This is because if the surface is uneven and undulates too far beyond the depth of field set by the current resolution, the image would be blurred, which is possible to affect the reconstruction accuracy.

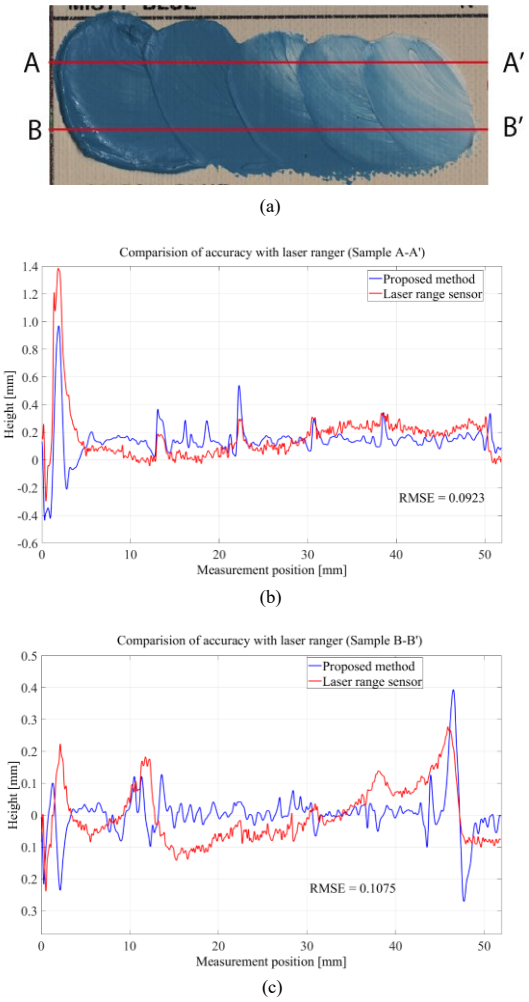

Fig. 5.9. Comparison of the 2.5D reconstruction results of the proposed method and laser. (a) gives the selected lines for reconstruction accuracy comparison; (b) gives the depth curve of line AA with RMSE of 0.0923; (c) shows the depth curve of line BB with RMSE of 0.1075.

The proposed method was applied to reconstruct the surface shape of several clay tablets engraved with cuneiform which records an administrative-economic document about 800 years ago. The length of the clay tablet ranges from 7.0 cm to 9.7 cm, width from 4.6 cm to 12.3 cm and thickness from 1.3 cm to 2.2 cm. The experiment was conducted by the Advanced Imaging Technology Laboratory at Kyoto University. The scanning resolution for image acquisition is 700 dpi. This resolution was selected based on the request of the owner of the object. Surface reconstruction is achieved by the photometric stereo method proposed in the paper. The relevant image processing program was developed by the Advanced Imaging Technology Laboratory using MATLAB R2016a version and Visual Studio 2011 64-bit version. A computer equipped with Windows 7 and Intel i7-6700 processor was used for processing all the images and the data. The operator only needs to import the object images to the program if the light source calibration is accomplished, and the program can process the data to output the corresponding

reconstructed result automatically, which includes a color image, a normal vector map, and reconstructed surface shape of the object. The generated images can be saved in any image format, and the reconstructed surface data can be observed on the MATLAB program.

One of the clay tablets is shown in this paper to demonstrate the performance of the proposed method. This clay tablet is engraved with ancient cuneiform letters that record some administrative documents published about 800 years ago. The letters on the surface are hollow like intaglio, and their depth is about 2 mm. It has depth range that is similar to the oil paint samples, so it can be inferred that the same reconstruction accuracy would be expected. Fig. 5.10 shows the processing results of both sides of the clay tablet images, including a color image, a normal vector map and surface reconstructed image, respectively. Furthermore, the data can be also observed by various 3D visualization tools inside MATLAB software. For instance, the reconstructed surface data is visualized with a plot tool inside the plot catalog named '3-D Surface' 'mesh (Z-map)' using gray color map as shown in Fig. 5.11 (a)(b); another one (Fig. 5.11 (a') (b')) is plotted by 'Image Tool' and the contrast is adjusted with a range from -5 to +5.

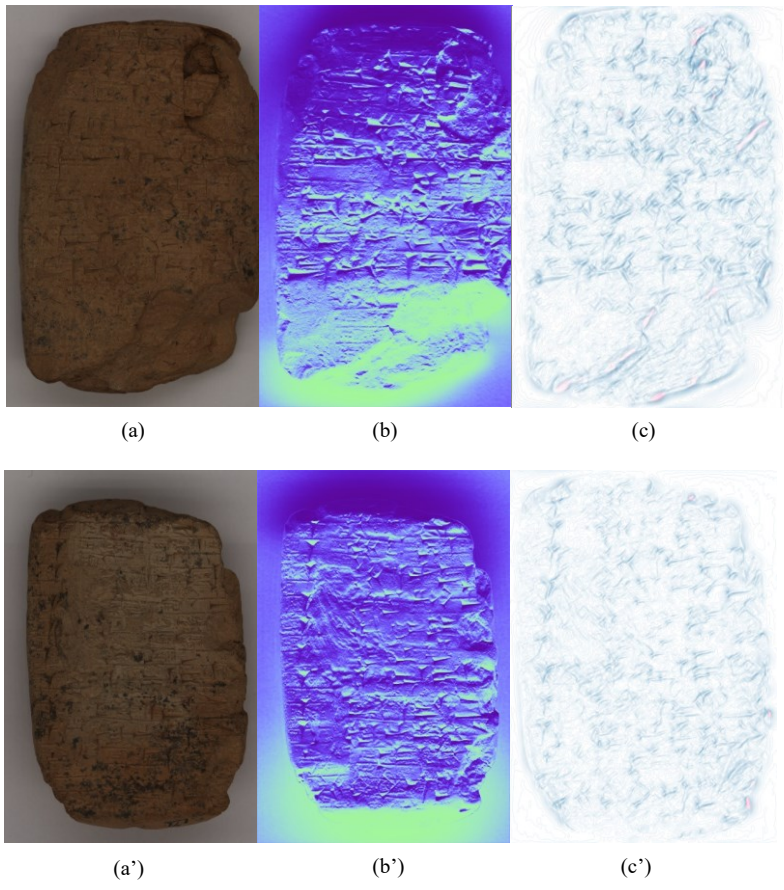

Fig. 5.10. Processed images from the program. (a), (b), (c) gives the color image, normal vector map, and surface reconstructed result of the clay tablet front side, respectively; (a'), (b'), (c') gives the color image, normal vector map, and surface reconstructed result of the clay tablet reverse side, respectively.

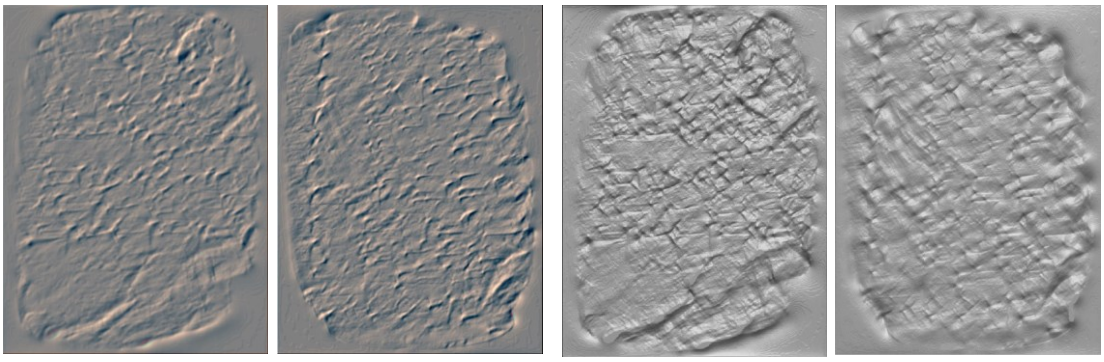

Fig. 5.11. Visualization of the surface information via two tools in MATLAB software. (a), (a') gives the surface reconstructed result of the clay tablet front side in '3D Surface' 'mesh (Z-map)' and 'Image Tool', respectively; (b), (b') gives the surface reconstructed result of the clay tablet reverse side in '3D Surface' 'mesh (Z-map)' and 'Image Tool', respectively.

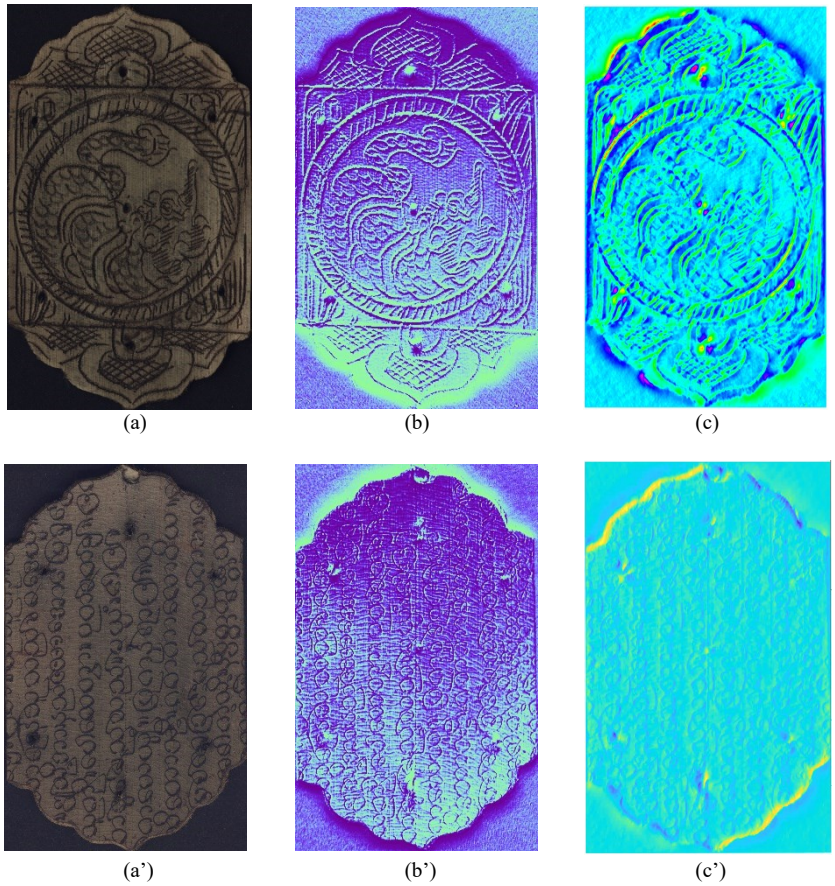

Fig. 5.12. Processed images of selected sample: two piece of booklet. (a), (b), (c) gives the color image, normal vector map, and surface reconstructed result of the piece of booklet engrave with traditional Myanmar cultural totems, respectively; (a'), (b'), (c') gives the color image, normal vector map, and surface reconstructed result of the piece of booklet engrave with Myanmar characters, respectively

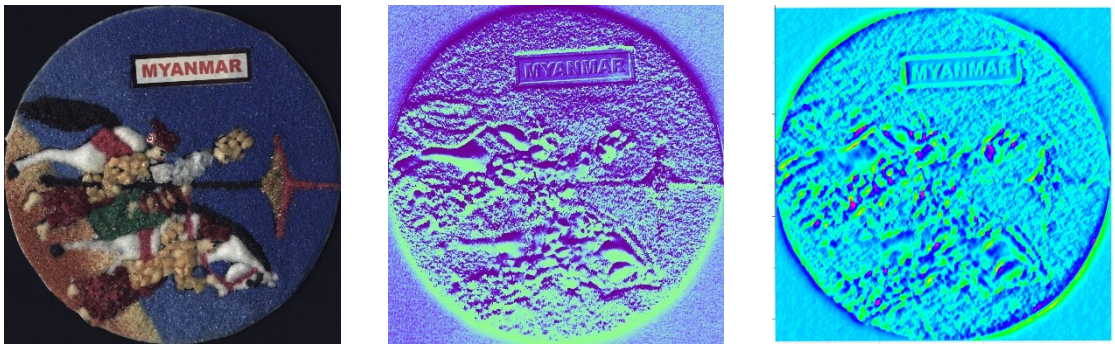

(a) (b) (c)

Fig. 5.13. Processed images of selected sample: a traditional handicraft from Myanmar decorated with sandstone of different coarseness. (a), (b), (c) gives the color image, normal vector map, and surface reconstructed result of the handicraft, respectively.

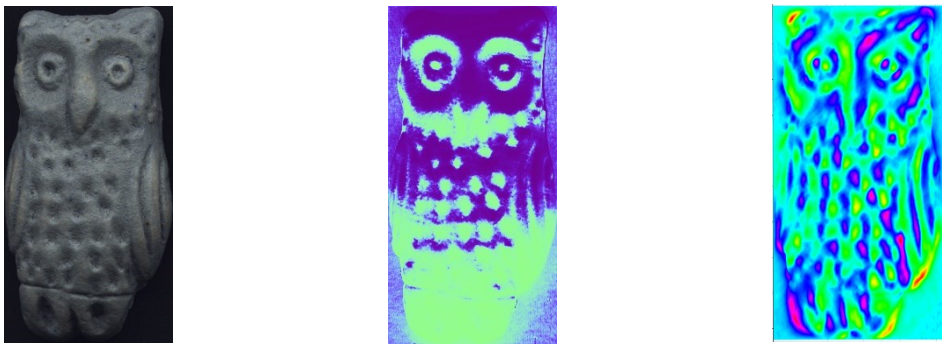

(a) (b) (c)

Fig. 5.14. Processed images of selected sample: a chopsticks stand in the shape of an owl. (a), (b), (c) gives the color image, normal vector map, and surface reconstructed result of the chopsticks stand, respectively.

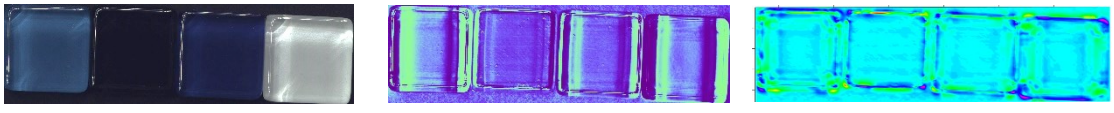

(a) (b) (c)

Fig. 5.15. Processed images of selected sample: a group of tile. (a), (b), (c) gives the color image, normal vector map, and surface reconstructed result of the group of tile, respectively.

Fig. 5.12-5.15 shows some other selected samples that processed by the program. Each figure demonstrates the color image, normal vector map, and surface reconstructed image of each selected sample from left to right respectively. All the samples were scanned with the image

resolution setting of 1023dpi. The objects in Fig. 5.12 are two pieces of a handicraft booklet. The surface of the object is engraved with traditional Myanmar cultural totems and Myanmar characters. The size of the booklet piece is 4.68cm by 7.45cm approximately, and the thickness is about 1mm. The depth of the engraved parts is close but less than 1mm, since it is coated by black ink. Due to the deformation of the wooden material by moisture, the whole object is not complete flat. The object in Fig. 5.13 is a traditional handicraft from Myanmar, which is decorated with sandstone of different coarseness. The size of it is 4cm by 4cm (image size) approximately and the thickness is about 2.5mm. This disc-shaped sample has more complex surface condition compared with the objects shown in the last figure. The sandstone of different coarseness results in extremely uneven surface and strong specular reflection in some parts, which raises great challenge for surface reconstruction. The object in Fig. 5.14 is a chopsticks holder in the shape of an owl, and the size of it is 2.32cm by 4.66cm approximately. The surface of this object is not complicated as the disc-shape sample, but its curved surface is also a challenge for the surface reconstruction. The thickest part reaches nearly 1cm. The last sample is a group of tile with the dimension of 2cm by 2cm, and the thickness of each tile is about 0.6cm. This object basically has a flat surface though, the manufacturing material is transparent, which makes it hard to reconstruct the correct surface. From the results of surface reconstruction of each samples, it can be observed that the result of the booklet is the best, while the other samples are problematic either because of the complex surface structure, or because of the too much thickness and the special material. One the other hand, the surface condition of the booklet matches to the range of applicability described in previous, that is a flat base and slight uneven surface with a range of ±2mm approximately. The proposed method can accomplish surface reconstruction well, when the object is within the range of applicability. For the issue that occur on other samples will be the subject of future research.

5.6 Conclusion

A surface shape reconstruction method based on a line-sensor scanner is proposed. The motivation is to extract more usable information from the images acquired by the image acquisition system and making use of high-quality images. Especially for 2.5D cultural heritage objects that have flat base and uneven surface with a range of ±2mm approximately, the method could be used in the investigation of surface structure, conservation, and restoration, etc., which also makes the digital archiving of precious artifacts more detailed and stereoscopic.

The mechanism of the proposed method is discussed in detail, including the derivation of the surface normal, integration of the normal vectors and the process of light direction estimation. Notably, the approach and the experiment for acquiring the lighting direction is described in detail. Unlike manual measurement method that is time-consuming and error-prone, the proposed one can be accomplished when a scanning job is conducted, which is more concise and efficient. The experimental equipment employed in this study is well-designed and accomplished, which enables the line sensor-based camera to exert its features of high detail expressiveness and high spatial resolving capability. Two sets of objects were used to test the proposed 2.5D reconstruction method in the experiment of this study: 1) The first one is a swatch of oil paint samples. This object was scanned using a high-resolution scanner as well as a laser ranger to verify the reconstruction accuracy.; 2) The second object was an ancient clay

tablet containing cuneiform. This was selected a test case for an actual cultural heritage object. The reconstructed results of the cuneiform clay tablet imply the possibility and potential that the data can be widely used in various scenarios, such as education, museum exhibition, replication of 2.5D printing, etc. Moreover, in the future, the focus will be given to improve its robustness and the ability to deal with objects with more complex surfaces, large dimension, and excessive specular reflection.

5.7 References

1) C. K. Yeh, N. Matsuda, X. Huang, F. Li, M. Walton, O. Cossairt: “A Streamlined Photometric Stereo Framework for Cultural Heritage”, European Conference on Computer Vision (ECCV 2016), 9913, pp.738-752 (Sep. 18, 2016)

2) F. Li, P. Ruiz, O. Cossairt, A. K. Katsaggelos: “Multi-frame Super-resolution for Time-of-flight Imaging”, ICASSP 2019-2019 IEEE International Conference on Acoustics, Speech and Signal Processing (ICASSP), pp. 2327-2331(May. 2019)

3) Y. Quéau, B. Durix, T. Wu, D. Cremers, F. Lauze, J. D. Durou: “LED-Based Photometric Stereo: Modeling, Calibration and Numerical Solution”, Journal of Mathematical Imaging and Vision, 60, 3, pp. 313-340 (2018)

4) D. Akca: “3D Modeling of Cultural Heritage Objects with A Structured Light System”, Mediterranean Archaeology and Archaeometry, 12, 1, pp. 139-152 (2012)

5) M. Schreiner, M. Strlič, R. Salimbeni: “Handbook on the use of laser in conservation and conservation science”, http://www.science4heritage.org/COSTG7/booklet/, accessed 09/04/2019, COST office, Brussels (2008)

6) F. Remondino: “Heritage Recording and 3D Modeling with Photogrammetry and 3D Scanning”, Remote sensing, 3, 6, pp. 1104-1138 (2011)

7) G. Pavlidis, A. Koutsoudis, F. Arnaoutoglou, V. Tsioukas, C. Chamzas: “Methods for 3D digitization of cultural heritage”, Journal of cultural heritage, 8, 1, pp. 93-98 (2007)

8) G. Earl, K. Martinez, T. Malzbender: “Archaeological Applications of Polynomial Texture Mapping: Analysis, Conservation and Representation”, Journal of Archaeological Science, 37, 8, pp. 2040-2050 (2010)

9) L. Gomes, O. R. P. Bellon, L. Silva: “3D Reconstruction Methods for Digital Preservation of Cultural Heritage: A Survey”, Pattern Recognition Letters, 50, pp. 3-14 (2014)

10) J. A. Toque, Y. Sakatoku, A. Ide-Ektessabi: "Analytical Imaging of Cultural Heritage Paintings Using Digitally Archived Images", Computer Vision and Image Analysis of Art, 7531, pp. 75310N (Feb. 2010)

11) J. A. Toque, Y. Murayama, Y. Matsumoto, A. Ide-Ektessabi: “Polarized Light Scanning for Cultural Heritage Investigation”, Computer Vision and Image Analysis of Art II, 7869, pp. 78690N (Mar. 2011)

12) R. J. Woodham: “Photometric Method for Determining Surface Orientation from Multiple Images”, Optical Eng., 19, 1, pp. 139-144 (1980)

13) O. Drbohlay and M. Chantler: “On optimal light configurations in photometric stereo”, Tenth IEEE International Conference on Computer Vision (ICCV'05) Volume 1, 2, pp. 1707-1712 (2005)

14) Y. Mukaigawa, S. Mihashi, T. Shakunaga: “Photometric Image-based Rendering for Virtual Lighting Image Synthesis”, Proceedings 2nd IEEE and ACM International Workshop on Augmented Reality (IWAR'99), pp. 115-124 (1999)

15) T. Papadhimitri and P. Favaro: “Uncalibrated Near-Light Photometric Stereo,” Proceedings of the British Machine Vision Conference, pp. 127-128 (Sep. 2014)

16) M. Breuss, Y. Quéau, M. Bähr, J. D. Durou: “Highly Efficient Surface Normal Integration”, Conference Algoritmy 2016 (ALGORITMY 2016), pp. 204-213 (Mar. 2016)

17) D. Antensteiner, S. Štolc, R. Huber-Mörk: “Depth Estimation with Light Field and Photometric Stereo Data Using Energy Minimization”, Iberoamerican Congress on Pattern Recognition, 10125, pp. 175-183 (2016)

18) R. Klette and K. Schluens: “Height Data from Gradient Maps”, Machine Vision Applications, Architectures, and Systems Integration V, 2908, pp. 204-215 (Oct. 1996)

19) Y. Quéau, J. D. Durou, J. F. Aujol: “Normal Integration: A Survey”, Journal of Mathematical Imaging and Vision, 60, 4, pp. 576-593 (2018)

20) M. Bähr, M. Breuß, Y. Quéau, A. S. Boroujerdi, J. D. Durou: “Fast and Accurate Surface Normal Integration on Non-rectangular Domains”, Computational Visual Media, 3, 2, pp. 107-129 (2017)

21) B. K. P. Horn and M. J. Brooks: “The Variational Approach to Shape from Shading”, Computer Vision, Graphics, and Image Processing, 33, 2, pp. 174-208 (1986)

22) D. Scharstein and R. Szeliski: "A Taxonomy and Evaluation of Dense Two-frame Stereo Correspondence Algorithms”, International Journal of Computer Vision, 47, 1, pp. 7-42 (2002)

23) G. Radow, L. Hoeltgen, Y. Quéau: “Optimisation of Classic Photometric Stereo by Non-convex Variational Minimisation”, Journal of Mathematical Imaging and Vision, 61, pp. 84–105 (2019)

Chapter 6

Concluding Remarks and Future Outlooks

6.1 Closing Remarks

Archiving can be considered as a typical activity that has always existed throughout human history. An archive is an accumulation of historical records. A typical usage example of archives is that researchers learned about ancient alphabets, languages, literature, and politics by studying the clay tablets found during archaeology. It shows that the archives could be the basic tool for historical research. Through the development and changes over time, modern science such as digital technology, imaging technology has offered new frontiers for archiving which is now known as digital archiving. As the main body of digital archiving, images and the application of images have greatly broadened the depth and breadth of its application scenarios. The advancement of imaging device and computing have led researchers to explore the usage beyond conventional visualization and to acquire more useful information for further applications. This information can be used to interpret the shapes, spectral characteristics, colors, and dimensions by processing or quantifying the interaction between light and matter. The results of the interpretation and analysis could be a part of the digital archives, which enriches digital archiving to become more comprehensive and useful in related research, display for research purposes, material investigation etc.

In this dissertation, a high resolution image acquisition system using line sensor was developed, which is a preliminary model for image acquisition in the other three applications. Each application has its corresponding set of modules, including image acquisition, image processing, and data extraction and analysis to obtain three types of information including spectral, color and spatial. The image acquisition module in each application has the same mechanism for imaging, and the preliminary model would be adjusted with the corresponding setting for the requirements of each application. Each of them has been carefully studied and tested. Multispectral imaging, color reproduction, surface reconstruction are very common topics in the research field, and a dozen of successful relevant applications and methods have been reported as so far. However, if the components that make up the image acquisition system are listed individually, each of them is nothing special, but the strategy of combining them according to the intended applications is quite innovative and well-designed. Several practical cases shown in this dissertation demonstrates that the proposed system is capable of providing a comprehensive result of digital archiving and making contribution to wider application fields.

6.2 Achievements and Significant Results

This study provides the first comprehensive digital archiving method through high resolution imaging system with linear imagers. All aspects of image acquisition of each application were carefully studied and examined in the laboratory. All the algorithms and software for image

processing and data extraction are implemented and tested by numerous experiments. Specific achievements and significant results are listed as follows:

(1) A high resolution imaging system using linear imagers was developed, which is a preliminary model for the other applications presented in the dissertation. Several crucial points of the system were addressed in detail including the image sensor, imaging mechanism of the proposed system, shading correction, image noise and common color calibration routine. For general digital archiving, the system is capable of high resolution imaging with high color fidelity and less geometric distortion. Notably, it can easily deal with objects with large size and it is a non-contact and non-destructive technique for image acquisition. In terms of the intended applications of images, the system can be adjusted with corresponding settings.

(2) To develop a more efficient multispectral imaging system, a concept of rotating filter scanning system is proposed. Compared to the conventional method that needs several scans to acquire relevant multispectral images, the proposed method can acquire the multispectral images with only one scan. Through a series of image processing, including image separation and interpolation processing, the processed images can be used in the estimation of spectral reflectance. An indirect method (learning sample based method) was employed in spectral reflectance estimation. To find the best filter combination, a simulation was conducted to optimize the filter selection, so that the accuracy of spectral reflectance estimation can be maximized as much as possible. Based on the experimental results, The accuracy of the estimated spectral reflectance by the proposed method is comparable to the results acquired by the conventional method, especially when efficiency issue is considered.

(3) A method for color reproduction of old glass dry plates is proposed. The image acquisition for such transmissive object was achieved by the system based on the preliminary model mentioned in previous. The line sensor based-camera and the light source are optimized for this object. The color reproduction uses filter coefficient calculated from color information of multiband filters. An approach for the calculation of filter coefficient used for color reproduction is addressed in detail. The method was applied to the digitization and color reproduction of a wall painting belonging to World Cultural Heritage Horyuji Kondo, Japan. A verification experiment was conducted to evaluate the accuracy of color reproduction results. Experimental results show that the proposed method is capable of high-quality color reproduction of image details, and there is merit to using this high-resolution digitization techniques for cultural heritage.

(4) A line-sensor camera based photometric stereo method for high-resolution 2.5D surface shape reconstruction is proposed. Compared to using an area sensor-based camera, a line sensor-based one can acquire higher resolution images with less geometric distortion, which can yield more accurate depth map results. A technique for estimating the lighting direction based on such system was addressed in detail for high-resolution surface shape reconstruction with improved efficiency. Experimental results yielded reconstructed depth maps comparable with the accuracy of conventional method like a laser ranger. In addition to surface reconstruction, the images acquired are colorimetrically accurate. This means that the method can produce both stereoscopic and spectroscopic information for digitizing object with textured surfaces.

6.3 Future Works

Many efforts have been made to provide more comprehensive results of digital archiving through high resolution imaging system. However, there are still many possibilities to further improve the solution and enrich the information extracted from images. Because the individual components and related techniques of the imaging system are constantly being advanced and improved, the advancements would deliver improved image quality and improved efficiency in image acquisition. New imaging technology may be able to further broaden the boundaries of applications to obtain more useful information from images. For example, as image sensor manufacturing process continues to advance, image sensor with finer pixel size would be developed, which would also provide higher spatial resolution for image acquisition. For light source, nowadays LED technology has been used extensively for commercial, industrial, and residential applications. The capabilities of LEDs have increased across the board: increases in lifespan, increases in performance(brightness) and increases in energy efficiency. In addition to the above, some new LEDs that can control the wavelength of the light source have been developed, known as narrow-band LED light sources. As the name implies, narrow-band light sources can produce a specific wavelength of light. With the development of semiconductor materials, the spectral coverage of LEDs would be extended further, although the current coverage is quite broad than before including ultraviolet, visible and infrared region.

For multispectral imaging, image acquisition could be simplified by using the narrow-band LED light source mentioned above. Using such kind of light source instead of using spectral absorbing filters, the light emitted from the light source would go to the camera directly, which would reduce the loss of light caused by passing through the filters. Besides, it can also avoid the degradation of image quality due to non-uniform filter material. This would also improve the accuracy of reconstructing spectral reflectance. For color reproduction of traditional glass plates, new image sensor developed in future with higher spatial resolution would improve image quality of the scanned glass dry plates. It is worth trying to develop a method for color reproduction based on the pigments used in the wall painting and make deep investigation of the material of the original glass dry plates and analyze its imaging characteristics if it is possible. For 2.5D surface structure reconstruction, the surface structure of objects in 2.5D have much more complex forms than in the case of 2D circumstance, methods for reconstructing accurate and complete 2.5D surface structure should be further studied. The proposed system and method in this study should be applied to a wider range of surface materials. Moreover, new algorithms to better reconstruct surface structure would need to be invented and explored. With the development and advancement of imaging technology including relevant hardware and software, the applications would not be limited in the field of digital archiving, but more new applications would be discovered.

List of Publications

1) Peng Wang, Jay Arre Toque, and Ari Ide-Ektessabi: “Color Reproduction of Glass Dry Plate Scanned by a Linear Sensor Camera Using Filter Coefficient”, ITE Transactions on Media Technology and Applications, 9, 4, pp. 287-296 (2021)

2) Peng Wang, Jay Arre Toque, and Ari Ide-Ektessabi: “A 2.5D Surface Structure Reconstruction Method using an Imaging System with Linear Sensor”, ITE Transactions on Media Technology and Applications, 9, 1, pp. 71-79 (2021)

3) Kyohei Yoshida, Peng Wang, Jay Arre Toque, Masahiro Toiya, and Ari Ide-Ektessabi: “A Simple Scanner for High Resolution Imaging of Wall Paintings”, Computational Color Imaging. CCIW 2017. Lecture Notes in Computer Science, 10213, pp. 135-143 (Mar. 2017)

4) Ryo Kanai, Yoshiharu Kowada, Peng Wang, Masahiro Toiya, Jay Arre Toque, and Ari Ide-Ektessabi: “A Novel Scanning Technique for Imaging of Gold and Silver Foils Used in Art Works”, Computational Color Imaging. CCIW 2017. Lecture Notes in Computer Science, 10213, pp. 150-162 (Mar. 2017)

5) Tatsuya Komiyama, Daichi Tsunemichi, Peng Wang, Yusuke Isobe, and Ari Ide-Ektessabi: “A Transmission Type Scanning System for Ultra High Resolution Scanning”, Computational Color Imaging. CCIW 2017. Lecture Notes in Computer Science, 10213, pp. 163-174 (Mar. 2017)

6) Jay Arre Toque, Pengchang Zhang, Peng Wang, and, and Ari Ide-Ektessabi: “High-Resolution Multispectral Scanning for Mesoscopic Investigation of Discoloration of Traditional Japanese Pigments”, Computational Color Imaging. CCIW 2015. Lecture Notes in Computer Science, 9016, pp. 195-207 (Feb. 2015)

7) Pengchang Zhang, Jay Arre Toque, Peng Wang, and Ari Ide-Ektessabi: “Identification, Analysis and Elimination of Craquelures in Old Oil Painting Images”, Proc. IS&T Archiving, 2015, 1, pp.83-86 (May 2015)